Chapter 3

Structural Studies of the Diiron Center in Methane Monooxygenase in the Presence of Substrate and the Regulatory Protein of the MMO Enzyme System

3.1. Introduction

Soluble methane monooxygenase (MMO) is a multi-component enzyme system which catalyzes the NAD(P)H- and O_2- dependent hydroxylation of methane to methanol in methane-metabolizing bacteria.[1] MMO from Type I methanotroph *Methylococcus capsulatus* (Bath)[2] and Type II methanotroph *Methylosinus trichosporium* (OB3b)[3] has been resolved into three components. The enzyme system from *M. capsulatus* (Bath) has been the most well-characterized and consists of a dinuclear non-heme iron enzyme[4] (hydroxylase, M_r 250 kDa), an Fe_2S_2-FAD electron transport protein[5] (reductase, M_r 39 kDa) which mediates the transfer of electrons from NAD(P)H to the hydroxylase, and a small regulatory protein (component B, M_r 16 kDa) which contains no metals or prosthetic groups.[6] The soluble enzyme system is not methane-specific and catalyzes the oxidation of a wide variety of alkanes, alkenes and alicyclic, aromatic and heterocyclic compounds.[7] The three components of the *M. trichosporium* (OB3b) MMO system are analagous to those of the *M. capsulatus* (Bath) system,[8] and demonstrate the same lack of substrate-specificity.[9]

The hydroxylase component from *M. trichosporium* (Ob3b) can oxidize methane to methanol in its chemically mediated fully reduced form in the presence of O_2, or in the presence of H_2O_2 when fully oxidized[10] confirming that it is at the hydroxylase component that both substrate binding and oxygen activation occurs. Neither the reductase nor component B are catalytically competent, and all three components of the MMO enzyme system are required for efficient oxidation of substrate.[10,11] EPR, Mössbauer, and X-ray absorption spectroscopy have been used to characterize the dinuclear non-heme iron active site in the MMO hydroxylase component from both *M. capsulatus* (Bath)[4,12] and *M. trichosporium* (OB3b).[8,10,12,13] These studies have shown that the hydroxylase from the two methanotrophs are spectroscopically and structurally similar to each other and to the other dinuclear non-heme iron proteins hemerythrin (Hr), ribonucleotide reductase (RR), purple acid phosphatase (PAP) and uteroferrin (Uf).[14] The oxidized Fe(III)Fe(III) form of the hydroxylase has two high-spin ferric atoms and is EPR silent. The one-electron reduced semimet Fe(III)Fe(II) form has an EPR signal with $g_{av} = 1.83$ (for *M. capsulatus* (Bath); $g_{av} = 1.85$ for *M. trichosporium* (OB3b)), characteristic of an antiferromagnetically coupled dinuclear non-heme iron center (S = 1/2 ground state). The reduced Fe(II)Fe(II) form exhibits a g = 16 EPR signal, attributed to a ferromagnetically coupled[15] integer spin system.

EXAFS studies of the hydroxylase have shown that the first coordination sphere of the iron active site in the oxidized form of the *M. capsulatus* (Bath) hydroxylase consists of

~ 6 N/O at an average distance of 2.04 Å. The photoreduced semimet form has ~ 6 N/O at 2.08 Å for the *M. capsulatus* (Bath) hydroxylase, and ~ 6 N/O at 2.06 Å for the *M. trichosporium* (OB3b) hydroxylase. The reduced hydroxylase from *M. capsulatus* (Bath) has ~ 5 N/O at 2.15 Å in its first coordination sphere. The iron-iron distance for the oxidized and semimet forms of the hydroxylase was determined to be ~ 3.4 Å, and no iron-iron interaction was seen in the EXAFS of the reduced form of the protein, although EPR verified that the dinuclear iron center was intact after exposure to the beam.

These studies have formed the basis for understanding the mechanism of oxygen activation and substrate oxidation. However, studies of the hydroxylase isolated from the other required components of the MMO enzyme system can yield only limited information, as it is known that all three components are required *in vivo*. Kinetic studies on the roles and interaction of the three components of the MMO system from *M. capsulatus* (Bath)[6,11] have suggested the formation of protein complexes during the catalytic cycle which have an effect on the oxygenase activity. Component B appears to serve a strict role in regulating the oxygenase activity of the *M. capsulatus* (Bath) system, preventing reduction of the hydroxylase by the reductase in the absence of substrate, and greatly increasing the electron transfer rate between the two components in the presence of substrate.[11] In the *M. trichosporium* (OB3b) system, electron transfer between the reductase and the hydroxylase is inhibited, but not prevented by component B in the absence of substrate, and in the presence of substrate, component B greatly increases the yield and the rate of product formation.[10]

Perturbations in the EPR spectra of the hydroxylase in the presence of component B and in the presence of small molecules have been documented, suggesting that complexation with the hydroxylase in some way affects the Fe site.[16,17] The effects of substrate, component B and the reductase on the redox potentials of the hydroxylase have also been investigated[18] and show that dramatic changes in the electron affinity of the hydroxylase core occur as a function of the presence of the other components. The change in the redox potentials and the EPR of the complexed forms of the hydroxylase implies a change in the electronic structure of the iron site which could be caused by changes in the ligation of the diiron site, or by conformational changes of the protein near or at the iron center which affect the electronic properties of the diiron core. EXAFS data analysis would be sensitive to any structural changes which occur as a result of the complex formation, and electronic perturbations would have an effect on the edge structure of the hydroxylase complexes.

We have collected Fe K-edge EXAFS data and high-resolution edge data on hydroxylase samples in the diferric and diferrous forms in the presence of component B,

bromopropene, and both component B and bromopropene to determine the nature of the change in the coordination environment of the iron atoms. These studies show that no dramatic change in the coordination of the iron atoms occurs upon formation of the various complexes. Evidence for a change in the covalency of the diiron center in its semimet form, and inhibition of the reduction of the hydroxylase component to its diferrous form in the presence of component B and bromopropene is directly seen.

3.2. Experimental

3.2.1. EXAFS Sample Preparation

The soluble hydroxylase of MMO from *M. capsulatus* (Bath) was isolated and purified as previously described.[12] Component B was produced from a strain of *Esherichia coli* containing a plasmid with the gene for B from *M. capsulatus* (Bath).[19] Purified hydroxylase was frozen at -80° C in 50 mM PIPES buffer at pH = 7.0 until further use at which point it was thawed and concentrated to approximately 11 mg protein /ml using a Centriprep. For **EXAFS10**, **EXAFS14**, **EXAFS15**, **EXAFS16**, and **EXAFS17**, component B was added in the stoichiometric molar ratio of 2:1 B:hydroxylase. For **EXAFS18**, **EXAFS19**, and **EXAFS20**, and for **EXAFS16** and **EXAFS17** after the addition of B, a 1000-fold excess of bromopropene (based on the concentration of protein) was added to insure that the substrate would remain bound to the hydroxylase during the subsequent concentration proceedure. The hydroxylase complexes were dialyzed into a 50% ethylene glycol solution of 50 mM MOPS buffer (pH = 7.0) for the non-bromopropene containing samples and **EXAFS11**, and into the above solution with a 10,000-fold excess of bromopropene for **EXAFS16**, **EXAFS17**, **EXAFS18**, **EXAFS19** and **EXAFS20**. After dialysis, the samples were further concentrated on a Centricon centrifugal microconcentrator, after which a 1000-fold excess of bromopropene was added to **EXAFS16-20**. For **EXAFS11**, no bromopropene was added until after the final concentration on the Centricon, at which point a 1000-fold excess was added.

The concentrated samples were degassed and brought into a wet box. The hydroxylase is isolated in its oxidized form; the reduced form was prepared by adding a 10-fold molar excess of sodium dithionite, 100 mM methyl viologen and 10mM proflavin to samples **EXAFS15**, **EXAFS17** and **EXAFS19** and letting the samples incubate for 40 minutes. The samples were loaded into lucite EXAFS cells equipped with caps and with 25 μm Kapton windows (23 mm x 2 mm x 3 mm; 140 μl), immediately frozen in liquid nitrogen upon removal from the box and stored in a liquid nitrogen refrigerator.

3.2.2. EXAFS Data Collection, Reduction and Analysis

A description of each sample is presented in Table 3.1. EXAFS and high-energy resolution edge scans were collected simultaneously by using a 1 mm vertical slit opening to maximize energy resolution and taking 0.15 eV steps over the edge region during an EXAFS scan. All of the samples were run on unfocused 8-pole wiggler beamline 7-3 (18 kG) at the Stanford Synchrotron Radiation Laboratory (SSRL) operating at 3 GeV and 40 - 90 mA. A Si(220) double-crystal monochromator was used, detuned 45% at the end of the Fe EXAFS scan (7995 eV, $k = 15$ Å^{-1}) to reduce harmonic contamination in the incident beam. The data were measured in fluorescence mode at 10 K using a continuous-flow LHe cryostat (Oxford Instruments, model CF1208). The fluorescence signal was monitored with a 13-element Ge solid-state detector array[20] (Canberra) windowed on the Fe Kα signal (6840 eV). Total count rates of between 25,000 and 35,000 per second per channel (measured at 7997 eV detuned 45%) were maintained throughout the experiments. At these count rates, the detector was below saturation limits. One of the channels showed persistently high count rates; it was therefore not included in further data analysis.

The energy of the individual scans was calibrated using an internal Fe foil standard,[21] assigning the first inflection point to 7111.2 eV. For every scan, 13 data files (1 from each channel in the detector) were collected; each was inspected individually. Individual channels of data were rejected if there were any discontinuities due to heat load problems for the detector electronics or if any of the channels exhibited poor statistics (erratic dark current values, persistently high count rates). Averages of the remaining data files for each scan were then made and inspected. Individual scans were rejected for signal-to-noise problems caused by low currents, or because of beam instability (short lifetimes, orbit shifts) or loss of beam, or due to irreproducibility of the scans. The remaining acceptable scans for each sample were then averaged and used for further analysis (summary of averages in Table 3.1).

The data were background subtracted by fitting a polynomial through the EXAFS region which was extrapolated through the pre-edge region and subtracted. A three- or four-segment spline was fit to the post-edge region and subtracted to isolate the EXAFS data and to normalize the edge jump to unity. The spline was chosen so that it removed the low frequency noise without reducing the true EXAFS amplitude; this was checked by monitoring the Fourier transform of the EXAFS data during the spline and normalization process. The normalized data were converted to k space, where k is the photoelectron wavevector defined by $[2m_e(E - E_0)/\hbar^2]^{1/2}$. In this expression, m_e is the electron mass, E

Table 3.1. Sample and Data Collection Summary[a]

Sample #	Description	[Fe] mM	scans avg./scans collected for EXAFS analysis
EXAFS10[b]	Oxidized hydroxylase w/ component B	2.0	269/403
EXAFS11[b]	Oxidized hydroxylase w/ bromopropene	3.2	226/234
EXAFS14[b]	Oxidized hydroxylase w/ component B	1.5	398/442
EXAFS16[b]	Oxidized hydroxylase w/ component B and bromopropene	1.2	255/286
EXAFS18[b]	Oxidized hydroxylase w/ bromopropene	1.4	230/260
EXAFS20[b]	Oxidized hydroxylase w/ bromopropene	< 1.9	124/143
EXAFS7	Oxidized hydroxylase non-complexed	3.4	84/91 Edge analysis only
EXAFS15	Reduced hydroxylase w/ component B	1.1	448/481
EXAFS17	Reduced hydroxylase w/ component B and bromopropene	1.6	426/481
EXAFS19	Reduced hydroxylase w/ bromopropene	1.7	276/286
EXAFS6[c]	Reduced hydroxylase non-complexed	4	91/91 Edge analysis only

[a]All samples were run in 1992 at SSRL on unfocused beamline 7-3 by using Si(220) monochromator crystals. A 13-element solid state Ge fluorescence detector was used in every case. [b]Sample was photoreduced to the semimet state by the X-ray beam. Only the scans after photoreduction was complete were averaged for further analysis. [c]The results of the EXAFS analysis for **EXAFS6** have been previously reported,[12] however edge data were collected during the 1992 run.

is the photon energy, $\hbar$ is Planck's constant divided by 2π, and E_0 is the threshold energy, 7130 eV (where k is defined to be zero).

All of the fits presented in this paper were based on k^3-weighted data. Non-linear least-squares curve-fitting techniques using empirical amplitude and phase parameters were used to analyze the data, as described in Chapter 1 and elsewhere.[22] The errors estimated in the EXAFS analysis are ± 0.03 Å in the distances and 25% in the coordination numbers.[22] The fits proceeded by allowing the initial coordination numbers and distances for an Fe-X pair of interest to vary. Empircal amplitude and phase parameters for the Fe-X scattering pairs of interest were obtained from the following models: Fe-N from [Fe(1,10-phenanthroline)$_3$](ClO_4)$_3$;[23] Fe-O and Fe-C from [Fe(acetylacetonate)$_3$];[24] Fe-Fe from [Fe_2(OH)(OAc)$_2$(HB(pz)$_3$)$_2$](ClO_4)$_2$.[25] Data for these model compounds were collected as previously described.[26] For all of the fits described in this paper, the EXAFS data from 3.5 to 12.5 Å^{-1} were Fourier transformed to R (Å) space to isolate the first and second shell contributions to the data. The individual contributions were isolated, backtransformed to k space, and fit from 4 to 12.0 Å^{-1}. In addition, both shells were backtransformed together and fit between 4.0 and 12.0 Å^{-1}, as were the unfiltered data. The windows used to isolate the peaks in the Fourier transforms for the backtransforms are presented in the tables of the fit results. A gaussian window width of 0.1 Å was used to reduce truncation artifacts in the Fourier transforms.

3.3. Results of XAS Experiments

The k^3-weighted EXAFS of the photoreduced semimet complexed samples are presented along with the EXAFS data of the non-complexed semimet hydroxylase in Figure 3.1. The Fourier transforms of the data (from 3.5 - 12.5 Å) are presented in Figure 3.2. The data for the non-complexed semimet hydroxylase (**EXAFS2**) were collected and analyzed as described in Chapter 2 and reference 12. The increased noise level of the EXAFS for the complexed-forms compared to the non-complexed forms reflects the lower iron concentration for the former (1-2 mM Fe as compared to ~ 4 mM Fe). The EXAFS of hydroxylase in the presence of component B of the MMO enzyme system (**EXAFS10** and **EXAFS14** w/ B; **EXAFS16** w/ B and bromopropene) are somewhat different from the non-complexed form between k = 7 and 9 Å^{-1}. For the non-complexed hydroxylase (**EXAFS2**, Figure 3.1a), the maxima at $k > 8$ Å^{-1} is greater in amplitude than the maxima at $k < 8$ Å^{-1}; in the B-complexed samples (**EXAFS10**, Figure 3.1b and **EXAFS14**, Figure 3.1c), the relative amplitudes of these maxima are reversed, and in the B plus bromopropene complex (**EXAFS16**, Figure 3.1g), the amplitudes are nearly equal. The

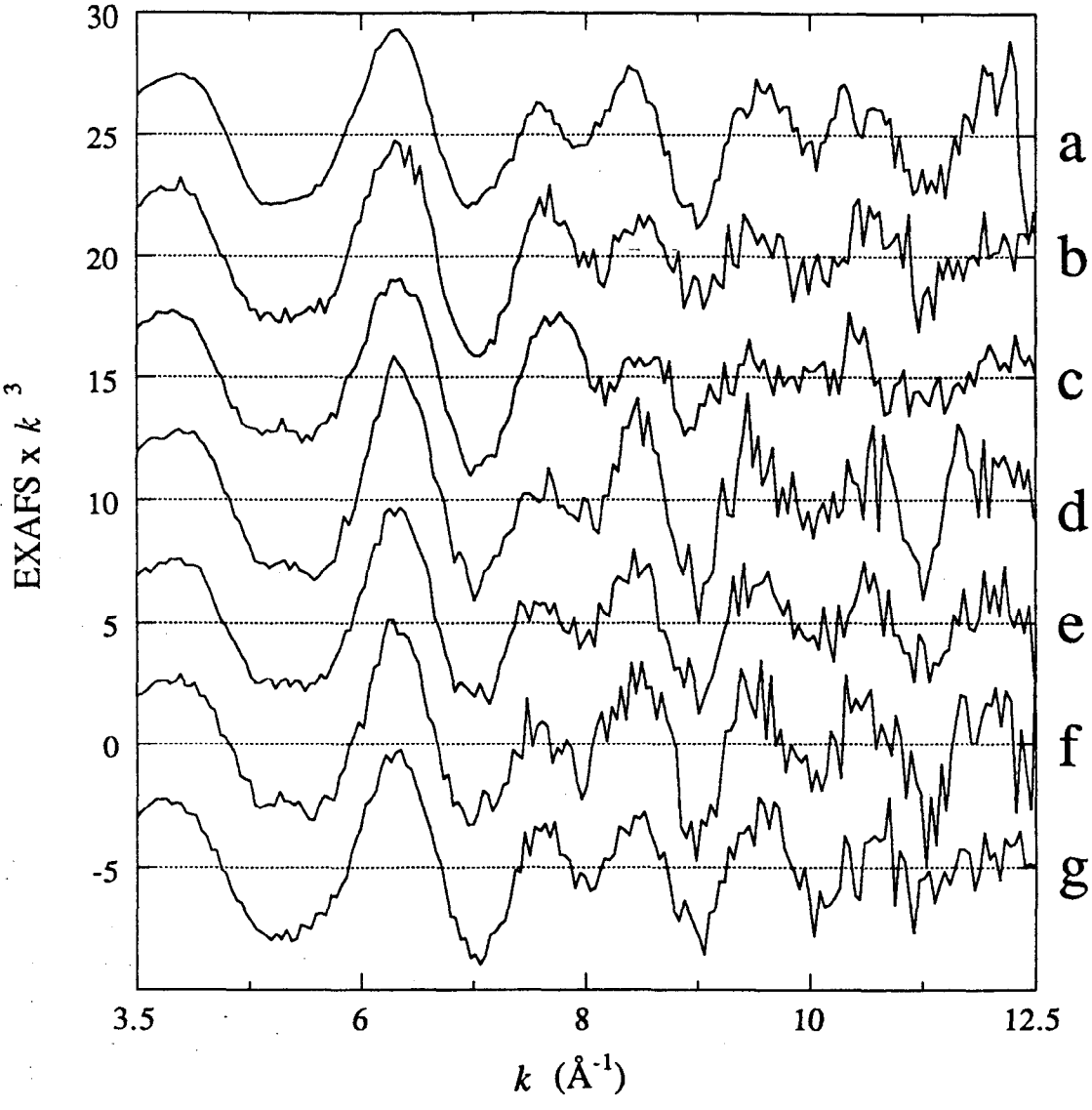

Figure 3.1. EXAFS of the semimet hydroyxlase samples. (a) Semimet hydroyxlase sample **EXAFS2**; with component B: (b) **EXAFS10**, (c) **EXAFS14**; with bromopropene: (d) **EXAFS11**, (e) **EXAFS18**, (f) **EXAFS20**; with B and bromopropene: (g) **EXAFS16**. The data shown here are the data used for Fourier transforms (k = 3.5-12.5 Å^{-1}). Note the difference in the appearance of the EXAFS between k = 7 and 10 Å^{-1}.

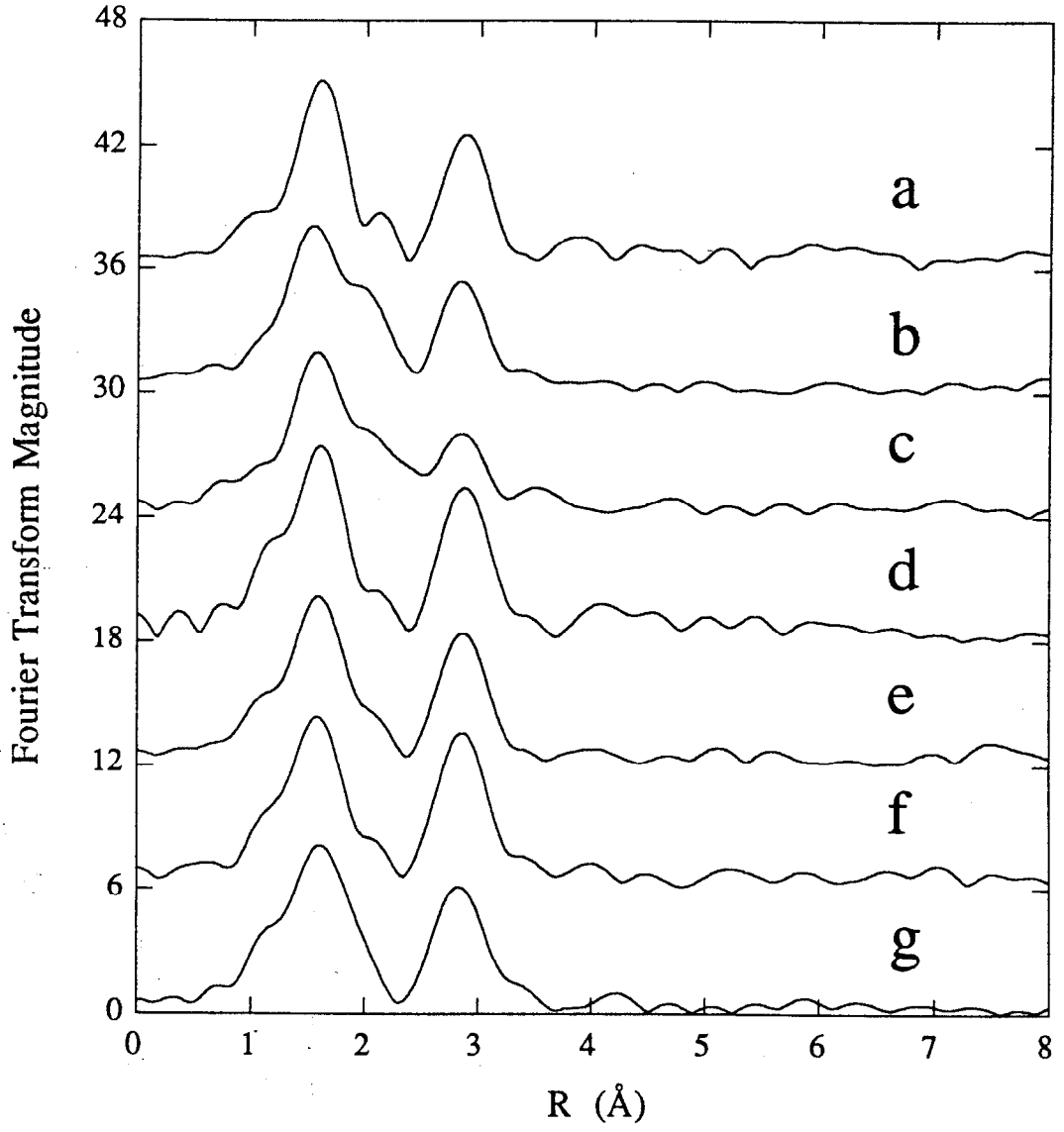

Figure 3.2. Fourier transforms of the semimet hydroxylase EXAFS presented in Figure 3.1. (a) Semimet hydroyxlase sample **EXAFS2**; with component B: (b) **EXAFS10**, (c) **EXAFS14**; with bromopropene: (d) **EXAFS11**, (e) **EXAFS18**, (f) **EXAFS20**; with B and bromopropene: (g) **EXAFS16**.

minimum at $k = 9$ Å^{-1} is deeper for **EXAFS10** and **EXAFS14** than for **EXAFS2** or **EXAFS16**. The EXAFS of the hydroxylase in the presence of bromopropene (**EXAFS11**, Figure 3.1d, **EXAFS18**, Figure 3.1e **EXAFS20**, Figure 3.1f) are very similar to the non-complexed form (Figure 3.1a).

Differences are seen in the Fourier transforms of the EXAFS data as well (Figure 3.2). The second shell peaks in the Fourier transform of the B-hydroxylase samples (**EXAFS10**, Figure 3.2b and **EXAFS14**, Figure 3.2c) are not as intense as the second shell peaks for the rest of the samples, nor as well resolved from the first shell peaks. The positions of the first and second shell peaks of the complexed forms of the hydroxylase are within 0.05 Å of the positions of the peaks of the non-complexed form, but the relative separation of the first and second shell peaks is slightly wider for **EXAFS10**, and slightly narrower for **EXAFS16**. The intensities of the peaks of the complexed forms (except for **EXAFS11** and **EXAFS20**) are lower than the non-complexed form, but the relative intensities of the second shell peaks to the first shell peaks for all of the samples (except **EXAFS14** and **EXAFS20**, and including **EXAFS11**) are within 10% of the value for the non-complexed form (0.72). For **EXAFS14**, the ratio of the second shell peak to the first shell peak differs from the value for the non-complexed form by 30%, and for **EXAFS20**, the ratio differs by 20%.

The EXAFS data for the reduced samples are presented in Figure 3.3, and the Fourier transforms of the data given in Figure 3.4. The data for the non-complexed reduced hydroxylase[12] are also presented for comparison. Here again, there are differences between the complexed vs. the non-complexed forms of the reduced hydroxylase. The EXAFS of the hydroxylase in the presence of component B (**EXAFS15** w/ B, Figure 3.3c and **EXAFS17** w/ B and bromopropene, Figure 3.3e) are shifted slightly to higher k, and the minimum at $k = \sim 8.5$ Å^{-1} in the non-complexed samples (**EXAFS3**, Figure 3.3a and **EXAFS6**, Figure 3.3b) is not as distinct in the B-hydroxylase samples. The bromopropene-hydroxylase sample (**EXAFS19**, Figure 3.3d) is more similar to the non-complexed samples (Figure 3.3a,b); however, the ~ 8.5 Å^{-1} minimum is shifted to lower k for **EXAFS19** relative to **EXAFS3** and **EXAFS6**. These differences in the EXAFS data are clearly seen in the Fourier transforms of the data (Figure 3.4), with the peak for the B-complexed forms of the hydroxylase (Figure 3.4c,e) appearing 0.08 - 0.09 Å to lower R than the peaks in the non-complexed (Figure 3.4a,b) and bromopropene-complexed (Figure 3.4d) forms. Although the Fourier transforms above 2 Å is different for all of the samples, there is no indication of a second shell Fe-Fe interaction like that seen in the semimet samples (Figure 3.4) for any of the reduced samples.

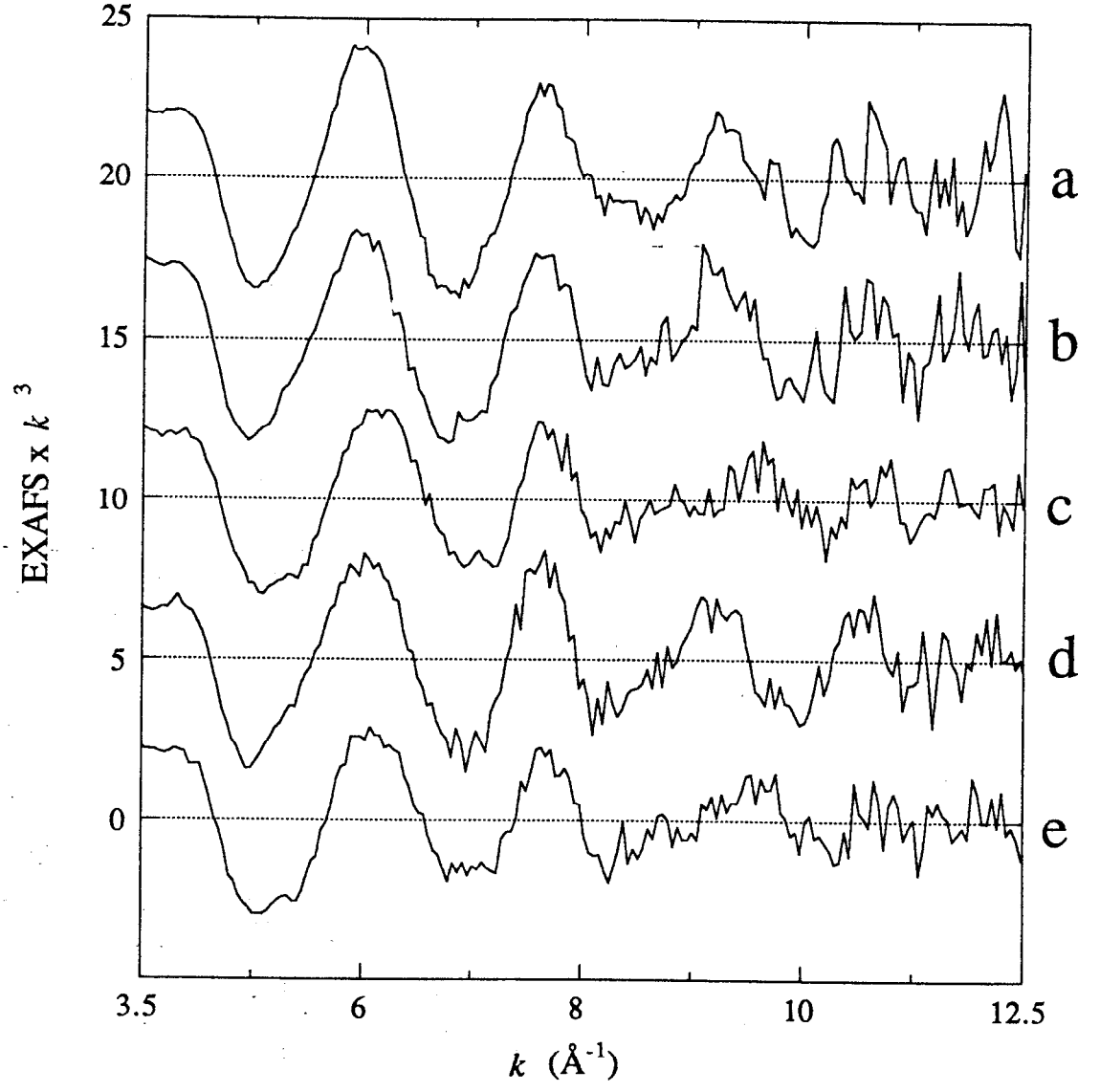

Figure 3.3. EXAFS data of the reduced hydroxylase samples. Reduced hydroxylase samples: (a) **EXAFS3**, (b) **EXAFS6**; with component B: (c) **EXAFS15**; with bromopropene: (d) **EXAFS19**; with B and bromopropene: (e) **EXAFS17**. The data shown are the data used for Fourier transforms (k = 3.5-12.5 Å^{-1}). Note the difference in the appearance of the EXAFS above k = 8 Å^{-1}.

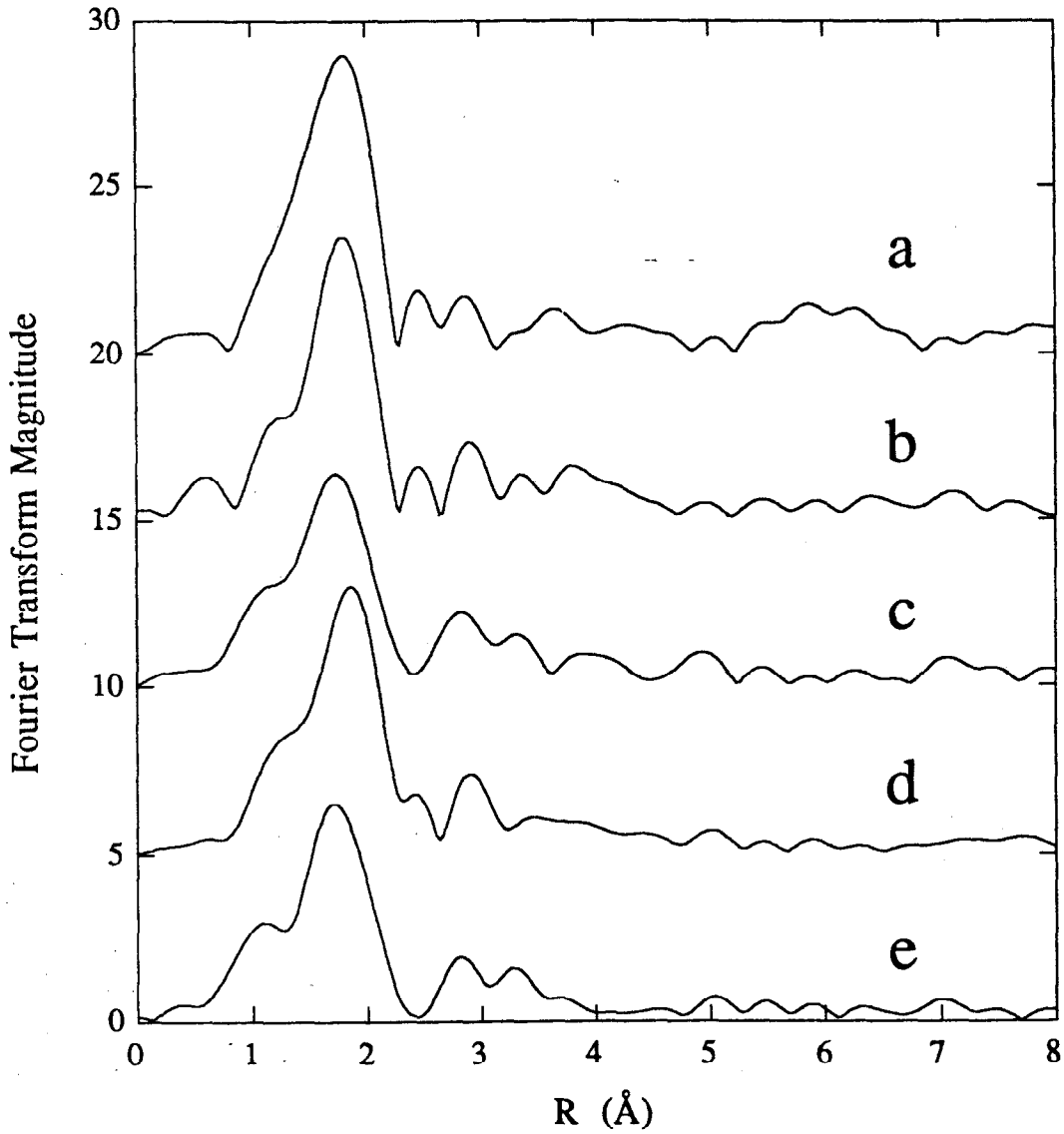

Figure 3.4. Fourier transforms of the reduced hydroxylase EXAFS data presented in Figure 3.3. Reduced hydroxylase samples: (a) **EXAFS3**, (b) **EXAFS6**; with component B: (c) **EXAFS15**; with bromopropene: (d) **EXAFS19**; with B and bromopropene: (e) **EXAFS17**.

3.3.1. Photoreduction of the Oxidized Hydroxylase Samples

As mentioned above, the oxidized samples of the complexed hydroxylase were photoreduced to the 1-electron reduced semimet state (FeIII/FeII) by the X-ray beam, a phenomenon which has been observed before.[12,26] Anticipating the photoreduction process, SSRL beamline 2-3 (unfocused bending magnet; Si(220) double crystal monochromator) was used to pre-photoreduce **EXAFS14**, **EXAFS16** and **EXAFS18** (temperature 95 - 100K, monochromator fully tuned at 7900 eV, slits 4 by 15 mm), as judged by monitoring the positon of the edge as a function of time (~ 2.0 eV shift to lower energy occurs from oxidized to semimet form). Scans were collected every 3-4 hours using a 1 mm high beam to maximize energy resolution with the monochromator detuned 50 % ccw at 7400 eV. During this process, it was noted that the rate of photoreduction decreased with decreasing ring current; after 21 hours in the beam between 58 -30 mA, the edge of **EXAFS14** had shifted only 0.8 eV. After injection to ~ 90 mA, an additional ~ 1 eV shift occured in 11 hours. After the pre-photoreduction process, the samples were moved to beamline 7-3 for data collection and in all cases, photoreduction of the samples continued for a few hours. Only the scans collected after the photoreduction process was judged to be complete were used for further data analysis.

3.3.2. Results of Fits

3.3.2.1. First Shell Fits. Results of the fits for the Fourier filtered first coordination shell are presented in Table 3.2. For all of the samples, a single N or O contribution did not adequately fit the data (fits A and B for all samples), however the data could be fit with two contributions at different bond lengths. This effect has been noted before in fits to structurally characterized model compounds by us and others,[27] in which single contribution fits resulted in both incorrect coordination numbers and average bond lengths. This has been attributed to interference effects between the N and O EXAFS at different but unresolvable distances.

Satisfactory fits were obtained with 2 N contributions, 2 O contributions, or a mixed N/O contribution (Table 3.2, fits C-F for all samples). The ability of two N **or** two O waves to fit the data as well as a mixed N/O contribution reflects the limitation of the EXAFS technique to discriminate between two atoms of similar backscattering strength as is the case with N and O. EPR studies are consistent with a mixed N/O coordination coordination for the Fe site;[28] the results with 2N or 2O contributions are therefore more indicative of a first shell consisting of atoms at two different distance distributions, rather

Table 3.2. Results of First Shell Fits[a] to the Hydroxylase Data.

Sample	Window Width (Å)	Fit	N		O		F
			CN[b]	R(Å)	CN	R(Å)	
EXAFS10	0.70 - 2.35	10A	2.1	2.07			1.2
semimet hydroxylase		10B			1.9	2.04	1.0
w/ component B		10C	4.1	2.15			0.28
			3.5	1.99			
		10D			2.9	2.12	0.31
					2.5	1.96	
		10E	3.5	2.17	2.9	1.98	0.29
		10F	2.9	1.97	3.2	2.11	0.27
EXAFS11	0.75 - 2.30	11A	2.5	2.02			1.0
semimet hydroxylase		11B			2.2	2.00	0.82
w/ bromopropene		11C	3.0	2.15			0.38
			3.8	1.99			
		11D			2.1	2.13	0.29
					2.9	1.97	
		11E	2.4	2.17	3.2	1.98	0.30
		11F	3.2	1.97	2.5	2.10	0.35

Table 3.2. continued

Sample	Window Width (Å)	Fit	N		O		F
			CN[b]	R(Å)	CN	R(Å)	
EXAFS14	0.75 - 2.40	14A	2.0	2.06			1.1
semimet hydroxylase		14B			1.9	2.04	0.94
w/ component B		14C	3.6	2.16			0.35
			3.4	1.99			
		14D			2.5	2.13	0.43
					2.4	1.97	
		14E	3.0	2.17	2.7	1.98	0.39
		14F	2.8	1.98	2.8	2.11	0.39
EXAFS16	0.70 - 2.20	16A	2.3	2.05			0.95
semimet hydroxylase		16B			2.1	2.03	0.76
w/ component B and		16C	3.2	2.15			0.35
bromopropene			3.3	1.99			
		16D			2.2	2.13	0.27
					2.4	1.97	
		16E	2.5	2.17	2.8	1.99	0.30
		16F	2.6	1.98	2.6	2.10	0.31

Table 3.2. continued

Sample	Window Width (Å)	Fit	N		O		F
			CN[b]	R(Å)	CN	R(Å)	
EXAFS18	0.70 - 2.30	18A	2.1	2.04			0.95
semimet hydroxylase		18B			1.9	2.01	0.78
w/ bromopropene		18C	3.0	2.15			0.29
			3.4	1.99			
		18D			2.1	2.13	0.23
					2.5	1.97	
		18E	2.5	2.18	2.8	1.98	0.25
		18F	2.9	1.98	2.4	2.11	0.26
EXAFS20	0.70 - 2.25	20A	2.1	2.03			0.96
semimet hydroxylase		20B			1.9	2.00	0.80
w/ bromopropene		20C	3.0	2.15			0.32
			3.5	1.99			
		20D			2.1	2.13	0.23
					2.7	1.97	
		20E	2.4	2.18	2.9	1.98	0.26
		20F	3.0	1.98	2.4	2.10	0.28

Table 3.2. continued

Sample	Window Width (Å)	Fit	N		O		F
			CN[b]	R(Å)	CN	R(Å)	
EXAFS15	0.50 - 2.30	15A	2.0	2.11			0.80
reduced hydroxylase		15B			1.8	2.08	0.64
w/ component B		15C	2.9	2.18			0.36
			2.5	2.03			
		15D			2.1	2.15	0.29
					1.8	2.00	
		15E	2.4	2.20	2.2	2.02	0.30
		15F	1.9	2.01	2.4	2.13	0.34
EXAFS17	0.50 - 2.30	17A	2.0	2.11			0.78
reduced hydroxylase		17B			1.8	2.09	0.64
w/ component B and		17C	2.8	2.19			0.38
bromopropene			2.6	2.04			
		17D			2.0	2.16	0.32
					1.8	2.02	
		17E	2.2	2.22	2.2	2.04	0.33
		17F	1.9	2.02	2.3	2.14	0.36

Table 3.2. continued

Sample	Window Width (Å)	Fit	N		O		F
			CN[b]	R(Å)	CN	R(Å)	
EXAFS19	0.70 - 2.20	19A	2.9	2.15			0.67
reduced hydroxylase		19B			2.5	2.12	0.49
w/ bromopropene		19C	3.7	2.18			0.33
			1.9	2.04			
		19D			2.9	2.14	0.29
					1.0	1.99	
		19E	3.0	2.20	1.8	2.04	0.31
		19F	1.1	2.00	3.1	2.13	0.29

[a]Fitting range $k = 4 - 12$ Å^{-1}. Errors are estimated to be about $\pm$ 0.03 Å for distances and 25% for coordination numbers.[22] [b]CN = coordination number.

than suggesting an all N or all O first shell. Accordingly, the chemically relevant mixed N/O fits will be focused on for the present studies.

For a mixed N/O fit to the data, two possible minima were found in every case depending on the relative starting distances of the N vs. O contributions, one corresponding to $R_N > R_O$ and one to $R_N < R_O$ (where R_N and R_O are the starting Fe-N and Fe-O bond lengths, respectively). The N and O parameters were highly correlated for the limited *k* range of the data and we therefore place a greater emphasis on the coordination-weighted average bond lengths than on the individual Fe-N and Fe-O contributions. Since Fe-N bond distances are generally longer than Fe-O bond distances in compounds of this type, the fit results with $R_N > R_O$ were used as the starting point for wide-shell fits to the data. The validity of this approach has previously been confirmed by similar fits to mixed N/O dinuclear iron models[12] (see Chapters 2 and 4).

The average first shell coordination for all of the complexed forms of the semimet hydroxylase are very similiar to each other. For semimet hydroxylase in the presence of component B, an average coordination of 6.4 N/O at 2.08 Å from the iron center (Table 3.2, fit 10E) was found for **EXAFS10**, and of 5.7 N/O at 2.08 Å (Table 3.2, fit 14E) for **EXAFS14**. The bromopropene-complexed form of the hydroxylase had an average coordination of 5.6 N/O at 2.06 Å for **EXAFS11** (Table 3.2, fit 11E), and 5.3 N/O at 2.07 Å for **EXAFS18** and **EXAFS20** (Table 3.2, fits 18E and 20E respectively). In the presence of both component B and bromopropene (**EXAFS16**), the average first shell coordination was found to be 5.3 N/O at 2.07 Å (Table 3.2, fit 16E). No evidence of a short Fe-O contribution which would be consistent with the presence of an oxo-bridged iron center was found. For the reduced forms of the hydroxylase, the average coordination number dropped and the average bond length increased relative to the semimet forms of the hydroxylase. For the reduced hydroxylase with component B (**EXAFS15**) a first shell coordination of 4.6 N/O at 2.11 Å (Table 3.2, fit 15E) was found, consistent with the shift of the first peak in the Fourier transform to shorter R relative to the non-complexed form (average first shell coordination ~ 5 N/O at 2.15 Å, reference 12). For reduced hydroxylase with bromopropene, the average coordination of the first shell was 4.8 N/O at 2.14 Å (**EXAFS19**, Table 3.2, fit 19E), and with both B and bromopropene (**EXAFS17**), the first shell was found to consist of 4.4 N/O at 2.13 Å (Table 3.2, fit 17E).

Although the average first shell coordinations are similar for the semimet samples and the reduced samples, there is a systematic difference in the individual contributions to the fits discussed above. For the B-complexed samples (**EXAFS10** and **EXAFS14**), the coordination numbers of each contribution is about 3, but for the bromopropene-complexed

samples (**EXAFS11**, **EXAFS18** and **EXAFS20**), the coordination number of the long distance contribution is lower than the coordination number of the short distance contribution (compare the E fits in Table 3.2). This is similar to the results of the first shell fits for the non-complexed hydroxylase sample (see Chapter 2, Table 2.2, fit 2C). For the reduced samples, the coordination numbers are equal for the two contributions for the B-complexed sample (**EXAFS15**), but the coordination number for the long distance contribution is greater than the short distance contribution for the bromopropene-complexed sample (**EXAFS19**). The contributions of each wave in the B + bromopropene sample are similar to the bromopropene samples in the semimet state, and to the B samples in the reduced state. The differences in the relative contributions may be responsible for the metrical differences seen in the EXAFS of the various samples at $k \sim 8$ Å^{-1} discussed above and illustrated later.

3.3.2.2. Second Shell Fits The results of second shell fits to the data are presented in Table 3.3. Two minima were found for Fe-only fits to the data, one corresponding to ~ 3.0 Å and one to ~ 3.4 Å, with the better fit corresponding to the 3.4 Å fit. We have previously described the bias of the second shell fits for the Fe-Fe distance corresponding to the distance in the model compound from which parameters were obtained.[12] However, based on the lack of an oxo-bridge in the iron center, it is best to use a non-oxo-bridged model compound for obtaining the empirical parameters.[12,29] For that reason, the hydroxo-bridged model $[Fe_2(OH)(OAc)_2(HB(pz)_3)_2](ClO_4)_2$ (3.4 Å Fe-Fe distance)[25] was used to extract parameters for modeling the second shell Fe-Fe interaction. For the semimet hydroxylase in the presence of component B (**EXAFS10** and **EXAFS14**), the best fit Fe-only minimum corresponded to 1.0 - 0.8 Fe at 3.39 Å (Table 3.3, fits 10G and 14G respectively). The Fe-Fe coordination for the hydroxylase with bromopropene was found to be 1.5 Fe at 3.40 Å for **EXAFS11** (Table 3.3, fit 11G), 1.2 Fe at 3.41 Å for **EXAFS18** (Table 3.3, fit 18G) and 1.4 Fe at 3.41 Å for **EXAFS20** (Table 3.3, fit 20G). For the hydroxylase with both B and bromopropene (**EXAFS16**), the best Fe-only fit corresponded to 1.2 Fe at 3.40 Å (Table 3.3, fit 16G). The 3.0 Å minima (Table 3.3, fits H for all samples) are believed to be due to coincidence of the Fe phase with the phase of the contribution from the low Z atoms which are almost certainly present at ~ 3.0 Å from the iron in bridged, dinuclear iron centers.[30]

The limitations involved with the use of second shell Fe-C parameters obtained from $Fe(acac)_3$ have been described elsewhere (Chapter 2 and reference 12). Although the Fe-C parameters are known not to be entirely reliable, we have used them to try to obtain additional information about contributions to the second shell data.[12] For C-only fits to the data, two minima were again found, at ~ 3.0 Å and ~ 3.4 Å, however the best fit

Table 3.3. Results of Second Shell Fits[a] to the Hydroxylase Data.

Sample	Window Width (Å)	Fit	Fe		C		F
			CN[b]	R(Å)	CN	R (Å)	
EXAFS10	2.30 - 3.15	10G	1.0	3.39			0.37
semimet hydroxylase		10H	0.6	3.01			0.65
w/ component B		10I			4.9	3.03	0.36
		10J			3.7	3.38	0.74
		10K	0.6	3.36	3.4	3.05	0.24
		10L	1.3	3.42	3.4	3.39	0.31
		10M	0.5	3.01	2.8	3.38	0.54
		10N	0.3	2.93	5.1	3.04	0.27
EXAFS11	2.20 - 3.50	11G	1.5	3.41			0.62
semimet hydroxylase		11H	0.9	3.04			0.91
w/ bromopropene		11I			7.0	3.05	0.52
		11J			5.9	3.39	1.0
		11K	0.8	3.36	5.8	3.07	0.36
		11L	1.8	3.45	6.5	3.32	0.48
		11M	0.8	3.04	4.4	3.39	0.71
		11N	0.3	2.96	7.1	3.06	0.46

Table 3.3. continued

Sample	Window Width (Å)	Fit	Fe		C		F
			CN[b]	R(Å)	CN	R (Å)	
EXAFS14	2.30 - 3.15	14G	0.8	3.39			0.26
semimet hydroxylase		14H	0.4	2.99			0.53
w/ component B		14I			3.4	3.02	0.38
		14J			2.5	3.38	0.59
		14K	1.1	3.39	1.7	3.22	0.23
		14L	0.4	2.98	2.2	3.40	0.45
		14M	0.3	2.91	3.8	3.04	0.25
EXAFS16	2.15 - 3.50	16G	1.2	3.40			0.48
semimet hydroxylase		16H	0.8	3.02			0.71
w/ component B and		16I			5.9	3.03	0.43
bromopropene		16J			5.0	3.37	0.84
		16K	0.6	3.37	4.0	3.05	0.32
		16L	1.7	3.44	6.3	3.30	0.29
		16M	0.7	3.02	3.7	3.38	0.52
		16N	0.3	2.97	5.4	3.04	0.37

Table 3.3. continued

Sample	Window Width (Å)	Fit	Fe		C		F
			CN[b]	R(Å)	CN	R (Å)	
EXAFS18	2.20 - 3.45	18G	1.2	3.41			0.51
semimet hydroxylase		18H	0.8	3.04			0.74
w/ bromopropene		18I			6.1	3.05	0.39
		18J			4.7	3.39	0.88
		18K	0.6	3.37	4.8	3.07	0.29
		18L	1.7	3.45	6.0	3.32	0.37
		18M	0.7	3.04	3.4	3.39	0.59
		18N	0.3	2.97	6.0	3.06	0.33
EXAFS20	2.15 - 3.45	20G	1.4	3.41			0.75
semimet hydroxylase		20H	1.0	3.04			0.88
w/ bromopropene		20I			7.3	3.05	0.54
		20J			5.8	3.38	1.10
		20K	0.6	3.36	6.4	3.07	0.47
		20L	2.0	3.46	9.0	3.32	0.53
		20M	0.9	3.04	4.2	3.38	0.69
		20N	0.3	2.99	6.6	3.06	0.49

[a]Fitting range $k = 4 - 12$ Å^{-1}. Errors are estimated to be about $\pm$ 0.03 Å for distances and 25% for coordination numbers.[22] [b]CN = coordination number.

corresponded to the 3.0 Å minimum for the C-only fits (Table 3.3, fits I for all samples). For fits including both Fe and C, the individual contributions were highly correlated, affecting both coordination numbers and distances. The best fit to the data corresponded to a long (3.4 Å) Fe-Fe distance, and a short (3.0 Å) Fe-C distance for **EXAFS10**, **EXAFS11**, **EXAFS18**, and **EXAFS20** (Table 3.3, fits 10K, 11K, 18K, 20K). For these fits, both the Fe and the C coordination numbers were lower than the values obtained for the long Fe-only fit and the short C-only fit (fits G and I, respectively), and the Fe-Fe distance decreased while the Fe-C distance increased. For **EXAFS16**, the long Fe/short C fit was the second best fit (Table 3.3 fit 16K) and showed the same correlation effect. It should be noted that for **EXAFS14**, fit 14K was the result for both a long Fe/long C and a long Fe/short C starting point.

These results demonstrate that there are two contributions to the second shell data, from atoms at an average distance of 3.0 Å and 3.4 Å from the iron center. A strong preference for a 3.4 Å Fe-Fe distance and a 3.0 Å Fe-C distance was given by the fit results (Table 3.3, fits G and I respectively). The assignment of the longer distance to Fe and the shorter distance to C is consistent with the lack of an oxo-bridged iron center and with the distribution of low Z atoms in structurally characterized models.[25,29] To aid in the interpretation of these results, it is useful to compare the Fourier transforms of the fits (4 - 12 $Å^{-1}$) with the 4 - 12 $Å^{-1}$ Fourier transform of the second shell contribution. The fits to the filtered second shell data and the Fourier transforms of the fits to the data for **EXAFS10** are presented in Figure 3.5. The 3.39 Å Fe fit (Table 3.3, fit 10G; Figure 3.5a) matches the Fourier transform of the second shell wave (at 2.68 Å) better than the 3.01 Å Fe fit (Table 3.3, fit 10H; Figure 3.5b) both in terms of peak height and position. The Fourier transform of the 3.39 Å Fe fit is shifted 0.11 Å to longer R (at 2.79 Å), and is 81% of the height of the data peak, whereas the 3.01 Å Fe fit is 0.27 Å to shorter R (at 2.41 Å) and only 61% of the peak height. The Fourier transform of the 3.03 Å C-only fit to the data (Table 3.3, fit 10I; Figure 3.5c) matches the Fourier transform of the data very well, with only a 0.02 Å shift in the peak position of the fit to lower R (at 2.66 Å), whereas the 3.38 Å C-only fit to the data (Table 3.3, fit 10J; Figure 3.5d) occurs 0.33 Å to higher R (at 3.01 Å). The height of the peak of the short C fit is 84% that of the data and the long C fit is 52% of the data peak height. Clearly, the 3.39 Å Fe fit or the 3.03 Å C fit better explain the second shell data than the 3.01 Å Fe fit or the 3.38Å C fit, supporting the assignment of the longer distance contribution as iron and the shorter distance contribution as carbon. For the Fe + C fits to the data, the fits consisting of long Fe and short C (Fit 10K, Figure 3.5e), long Fe and long C (Fit 10L, Figure 3.5f) and short Fe and short C (Fit

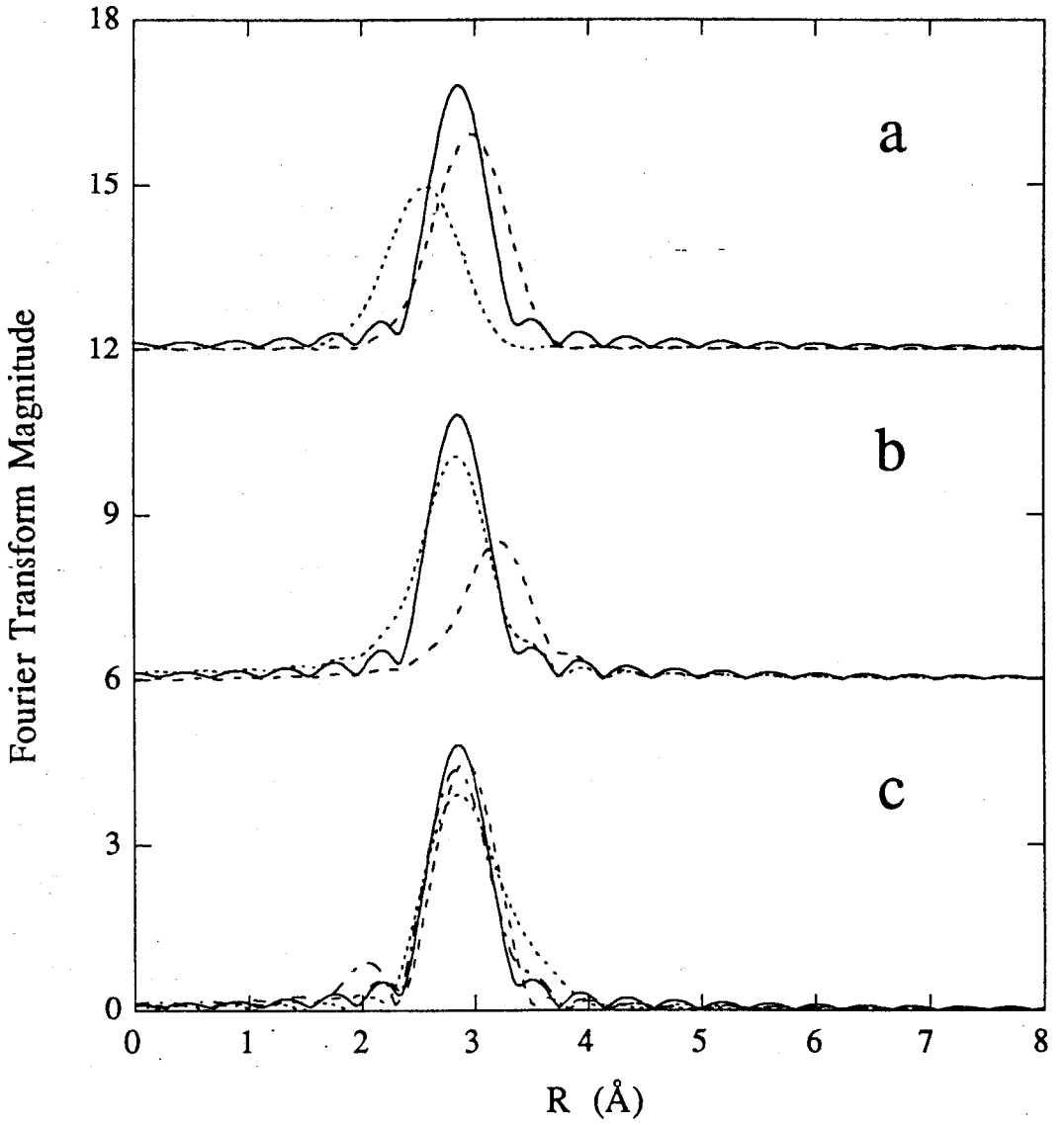

Figure 3.5. Fourier transforms of the second shell fits to the data for **EXAFS10** (k = 4-12 Å^{-1}). The solid line is the Fourier transform of the second shell EXAFS in every case. (a) Fe-only fits to the data; 3.39 Å Fe fit (Table 3.3, fit 10G) (dash) and 3.01 Å Fe fit (Table 3.3, fit H) (dot). (b) C-only fits to the data; 3.38 Å C fit (Table 3.3, fit 10J) (dash) and 3.03 Å C fit (Table 3.3, fit 10I) (dot). (c) Fe + C fits to the data; long Fe and short C (Table 3.3, fit 10K) (dash), long Fe and long C (Table 3.3, fit 10L) (dot), and short Fe and short C (Table 3.3, fit 10M) (dash dot).

10M, Figure 3.5g) are all quite good, however the improvement to the fits simply reflects the correlation of the Fe and the C parameters in the latter two fits to the data.

For the reduced data sets, fits to the filtered data over the region between 2.5 and 3.5 Å were attempted with Fe or C and could be adequately fit with either less than 0.5 Fe at ~ 3.4 Å or about 2 C at ~ 3.0 Å. These results are chemically unreasonable for the diiron center based on a comparison of these contributions with the known second shell contributions in structurally characterized diferrous models. In the second shell of the multiply-bridged diferrous model compounds $[Fe_2OH(O_2CH_3)_2(Me_3TACN)_2](ClO_4)\text{-}H_2O$[31] and $[Fe_2(O_2CH)_4(BIPhMe)_2]$,[32] there are 11 C atoms between 2.89 and 3.16 Å, and 1 O atom at 3.3 Å (the Me_3TACN compound also has Fe at 3.32 Å; the Fe distance in the BIPhMe model is 3.57 Å). The low height of the peak in the second shell region of the Fourier transform, and the low coordination numbers for the fits especially in the 3.0 - 3.2 Å range, suggest that there is some high frequency contribution to the data that can be mathmatically modeled with the Fe and C parameters, but does not necessarily reflect the true second shell environment of the ferrous iron center.[33]

3.3.2.3. Wide Shell Fits. The same trends seen in the first and second shell fits to the semimet data were seen in the fits to the backtransform of both of the peaks in the Fourier transform (Table 3.4). Only the results for $R_N > R_O$ are reported, although all of the fits with $R_N < R_O$ were performed. The fit function for the N/O fit to the data was about 1 for all of the samples (Table 3.4, fits O), and improved by a factor of 1.8 to 2 with the addition of a either a 3.4 Å Fe contribution (Table 3.4, fits P) or by a factor of 1.3 to 2.6 with a 3.0 Å C contribution (Table 3.4, fits S). With the addition of both a 3.4 Å Fe and a 3.0 Å C contribution (Table 3.4, fits T), the fits improved only slightly over the 3.4 Å Fe-only or the 3.0 Å C-only fits, and the same correlation effects (reduction in the Fe and C coordination number and Fe distance, increase in C distance) were seen for all samples with the exception of **EXAFS14**, for which no minimum corresponding to a 3.4 Å Fe and 3.0 Å C initial starting point was found.

The data and fits to the data are presented in Figure 3.6 for **EXAFS10**. The description here is entirely analagous for the rest of the samples as well. The N/O fit describes both the low frequency contribution to the data and the overall amplitude of the data (Table 3.4, fit 10O, Figure 3.6a) but does not explain the higher frequency components of the EXAFS. The effect of adding the high frequency Fe to the N and O fit (Table 3.4, fit 10P) is seen in Figure 3.6b, with the beat pattern above $k = 7$ Å^{-1} in the data now being mimicked by the fit to the data. The inclusion of the short C contribution to fit 10P (Table 3.4, fit 10T, Figure 3.6c) primarily improves the match in the frequency above $k = 10$ Å^{-1}.

Table 3.4. Results of Wide Shell Fits[a] to the Hydroxylase Data.

Sample	Window Width (Å)	Fit	N		O		Fe		C		F
			CN[b]	R(Å)	CN	R(Å)	CN	R(Å)	CN	R(Å)	
EXAFS10	0.70 - 3.15	10O	3.5	2.16	2.8	1.97					0.96
semimet hydroxylase		10P	3.4	2.16	2.7	1.97	1.1	3.39			0.47
w/ component B		10Q	3.3	2.16	2.6	1.97	0.7	3.00			0.69
		10R	3.4	2.16	2.7	1.97			3.6	3.38	0.82
		10S	3.5	2.17	2.9	1.98			4.9	3.03	0.51
		10T	3.4	2.17	2.8	1.98	0.7	3.37	2.6	3.05	0.42
EXAFS11	0.75 - 3.50	11O	2.5	2.17	3.1	1.98					1.3
semimet hydroxylase		11P	2.5	2.17	3.1	1.97	1.5	3.41			0.68
w/ bromopropene		11Q	2.4	2.16	3.0	1.97	1.0	3.03			0.93
		11R	2.4	2.17	3.0	1.97			5.8	3.39	1.1
		11S	2.5	2.19	3.3	1.98			7.3	3.05	0.59
		11T	2.3	2.18	3.2	1.98	0.7	3.37	5.6	3.07	0.49
EXAFS14	0.75 - 3.15	14O	2.9	2.17	2.7	1.98					0.80
semimet hydroxylase		14P	2.9	2.17	2.6	1.98	0.8	3.39			0.45
w/ component B		14Q	2.6	2.16	2.5	1.98	0.5	2.97			0.61
		14R	2.9	2.17	2.6	1.98			2.5	3.38	0.73
		14S	3.1	2.18	2.8	1.98			3.2	3.02	0.60
		14T	3.0	2.16	2.6	1.98	1.5	3.38	4.1	3.18	0.36

Table 3.4. continued

Sample	Window Width (Å)	Fit	N		O		Fe		C		F
			CN[b]	R(Å)	CN	R(Å)	CN	R(Å)	CN	R(Å)	
EXAFS16	0.70 - 3.50	16O	2.5	2.17	2.6	1.99					1.1
semimet hydroxylase		16P	2.4	2.16	2.6	1.99	1.2	3.40			0.59
w/ component B and		16Q	2.4	2.15	2.4	1.98	0.9	3.02			0.74
bromopropene		16R	2.4	2.17	2.6	1.99			5.0	3.37	0.92
		16S	2.6	2.18	2.9	1.99			6.2	3.03	0.51
		16T	2.4	2.18	2.8	1.99	0.5	3.37	4.4	3.04	0.46
EXAFS18	0.70 - 3.45	18O	2.5	2.17	2.7	1.98					1.1
semimet hydroxylase		18P	2.5	2.17	2.6	1.98	1.2	3.41			0.57
w/ bromopropene		18Q	2.4	2.16	2.6	1.98	0.9	3.04			0.75
		18R	2.4	2.17	2.7	1.98			4.7	3.39	0.93
		18S	2.5	2.19	2.9	1.99			6.2	3.04	0.46
		18T	2.4	2.18	2.8	1.99	0.5	3.37	5.0	3.06	0.39
EXAFS20	0.70 - 3.45	20O	2.5	2.17	2.8	1.97					1.3
semimet hydroxylase		20P	2.5	2.17	2.8	1.97	1.4	3.41			0.79
w/ bromopropene		20Q	2.5	2.16	2.7	1.97	1.1	3.04			0.87
		20R	2.4	2.17	2.7	1.97			5.8	3.38	1.1
		20S	2.5	2.19	3.0	1.98			7.6	3.05	0.57
		20T	2.4	2.19	2.9	1.98	0.4	3.36	6.7	3.06	0.53

[a]Fitting range $k = 4 - 12$ Å^{-1}. Errors are estimated to be about $\pm$ 0.03 Å for distances and 25% for coordination numbers.[22] [b]CN = coordination number.

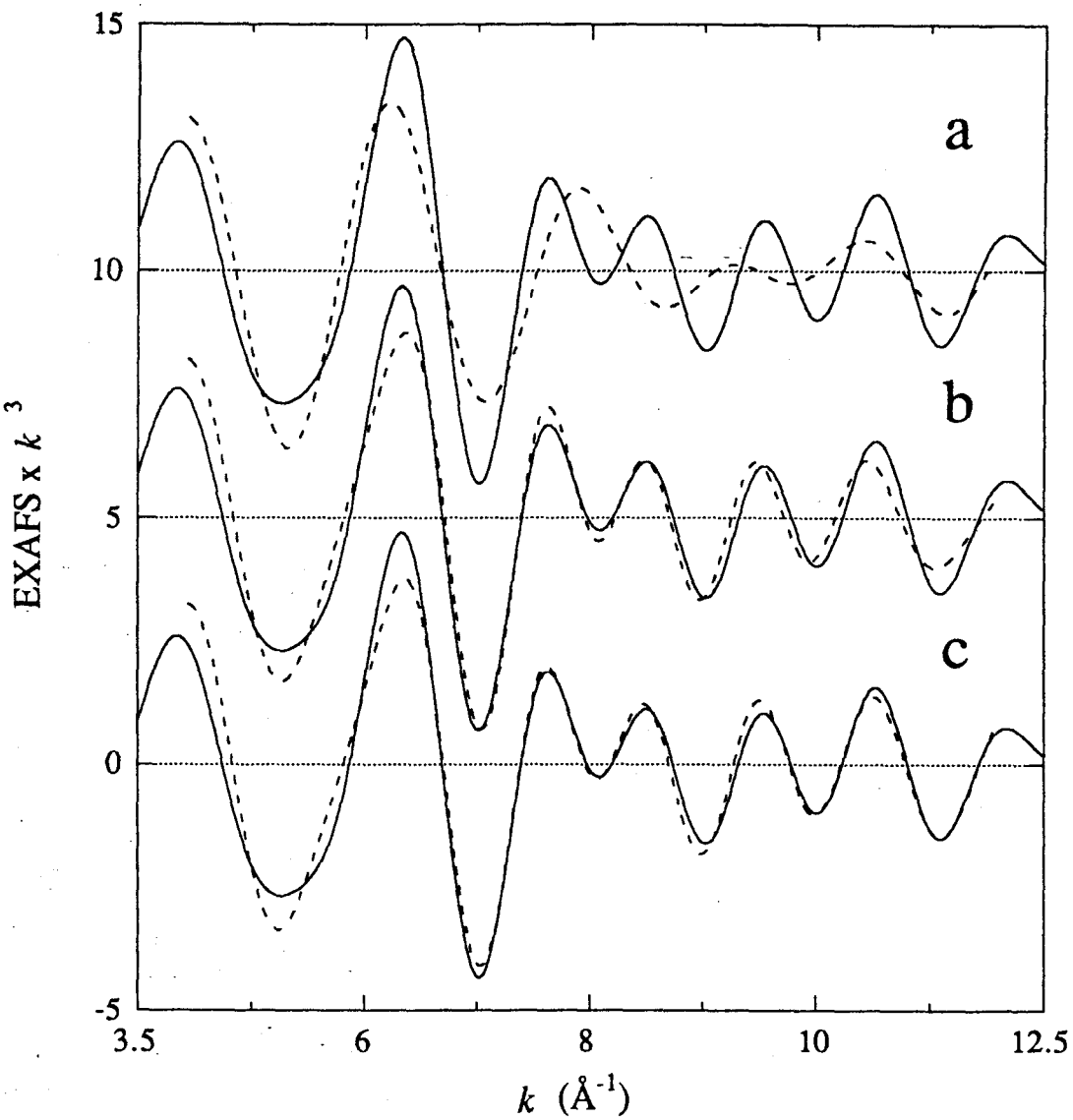

Figure 3.6. Fits to the Fourier filtered first and second shell EXAFS for **EXAFS10** (k = 4-12 Å^{-1}). The solid line is the data and the dashed line is the fit. (a) Fit to the data with N and O (Table 3.4, fit 10O), (b) fit to the data with N, O, and Fe (Table 3.4, fit 10P), (c) Fit to the data with N, O, Fe, and C (Table 3.4, fit 10T). Note the improvement in the fit with the addition of Fe to the N and O contributions.

3.3.2.4. The Origin of the Metrical Differences in the EXAFS. There are subtle differences in the beat pattern of the EXAFS data seen above $k = 7$ Å^{-1} (Figure 3.1) for the hydroxylase complexes vs. the non-complexed hydroxylase as described above. These differences suggest that there may be a structural change that occurs in the complexed forms of the hydroxylase, however the fit results do not support a significant change in the ligation of the iron atoms as a result of the presence of component B or substrate based on a comparison of the average first shell coordination. Although the differences in the EXAFS cannot be completely accounted for by the fit results, qualitatively it can be shown that the differences arise from differences in the first shell EXAFS. The backtransforms of the first shell data for representative complexed forms of the hydroxylase are compared to the first shell EXAFS of the non-complexed hydroxylase in Figure 3.7, and of the second shell data in Figure 3.8. Significant changes in the first shell EXAFS occur in both amplitude and phase above $k = 7$ Å^{-1} for all of the samples, although the non-complexed form and the bromopropene-complexed forms are very similar. The second shell data, while not identical for all of the samples, are certainly more similar to each other than the first shell data. The differences in the beat pattern of the EXAFS can therefore be attributed to the differences in the first shell data above $k = 7$ Å^{-1} interacting with a relatively constant second shell contribution. The differences in the first shell EXAFS are probably reflected by the differences in the relative coordination numbers of the long and short distance contributions to the first shell fits of the B-complexed vs. bromopropene-complexed samples described above. The effect of the first shell data on the appearance of the EXAFS is illustrated in Figure 3.9, which shows the filtered EXAFS of the B-complexed hydroxylase (**EXAFS10**), along with the EXAFS from the addition of the first shell data from **EXAFS10** to the second shell data of the non-complexed sample and the filtered EXAFS of the non-complexed hydroxylase. Addition of the second shell EXAFS of the non-complexed form to the first shell EXAFS of the B-complexed form (Figure 3.9b) results in EXAFS more like that of the true B-complexed samples (Figure 3.9a) than the non-complexed sample (Figure 3.9c).

3.3.2.5. Fits to the Non-Filtered Data. Fits to the non-filtered data between 4 and 12 Å^{-1} were done for all of the semimet and reduced samples (Table 3.5). All of the trends described above were seen for the fits to the wide filtered data, although the fit functions were higher due to the increased noise level of the data. The data and the fit to the data (Table 3.5, fit U) for all of the semimet samples are shown in Figure 3.10. The Fourier transforms (4 - 12 Å^{-1}) of the fits in Table 3.5 for **EXAFS10** are compared to the 4 - 12 Å^{-1} Fourier transform of the data in Figure 3.11. The N/O contribution to the data matches the first shell peak in the Fourier transform very well for all of the fits. For

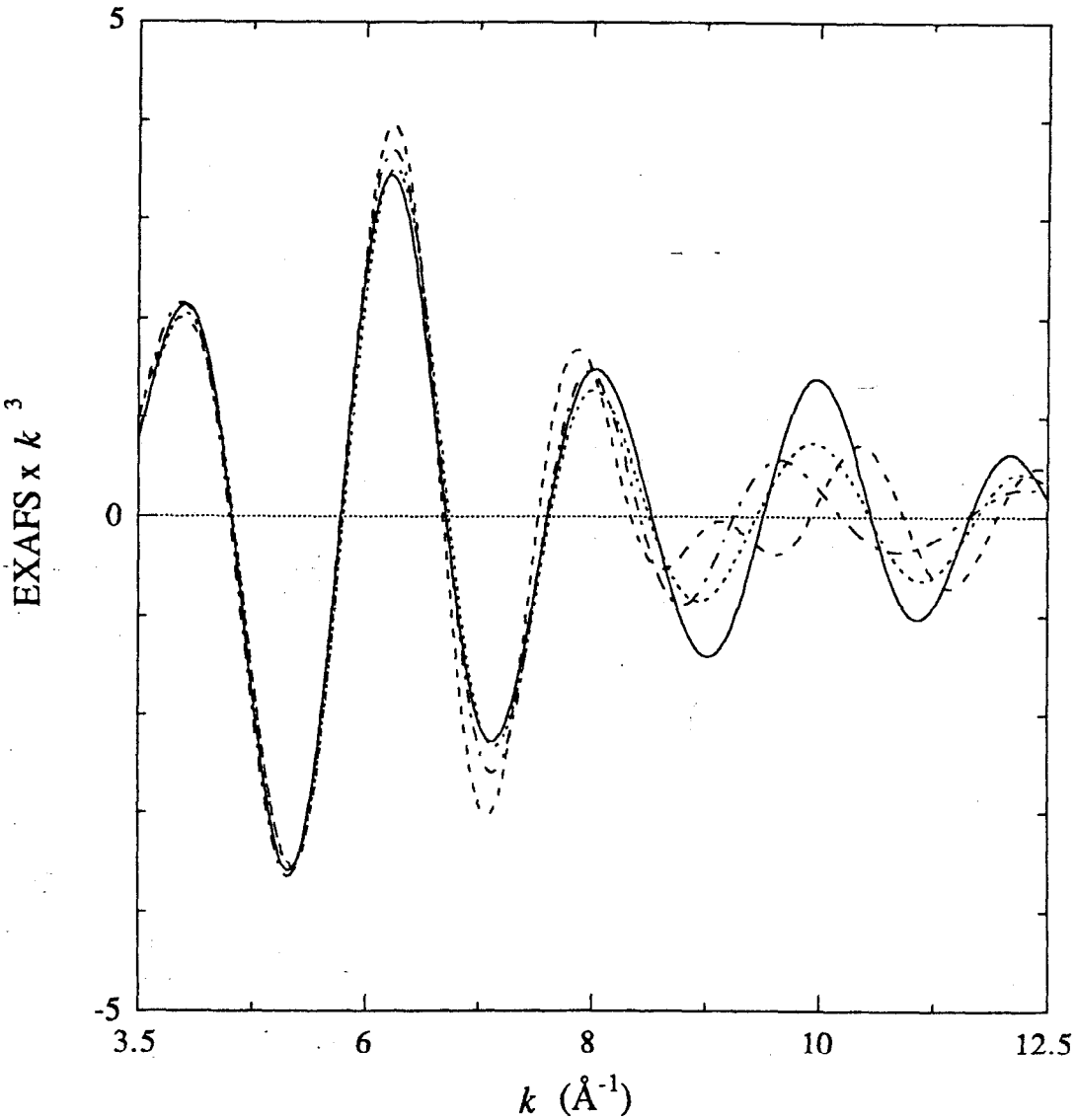

Figure 3.7. Comparison of the Fourier backtransforms of the first shell data (see Figure 3.2) for the semimet hydroxylase samples. Semimet hydroxylase sample, **EXAFS2** (solid); with component B, **EXAFS10** (dash); with bromopropene, **EXAFS18** (dot); and with B and bromopropene, **EXAFS16** (dash dot). The Fourier filter window widths used for these backtransforms are given in Table 3.2. Note the difference in the EXAFS above $k = 8$ Å^{-1}, especially for **EXAFS10**.

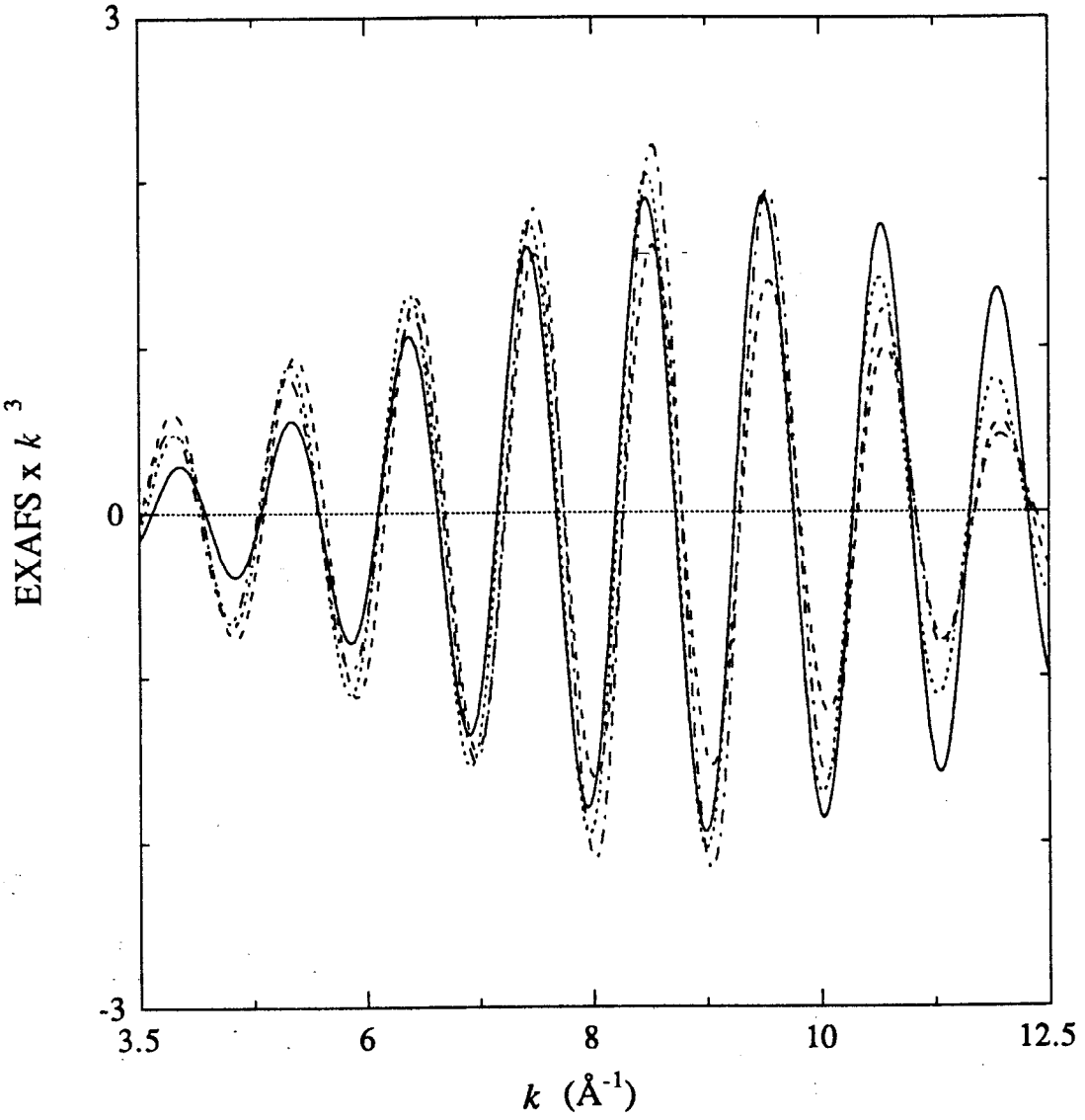

Figure 3.8. Fourier backtransforms of the second shell data (see Figure 3.2) for the semimet hydroxylase samples. Semimet hydroxylase sample, **EXAFS2** (solid); with component B, **EXAFS10** (dash); with bromopropene, **EXAFS18** (dot); and with B and bromopropene, **EXAFS16** (dash dot). The Fourier filter window widths used for these backtransforms are given in Table 3.3.

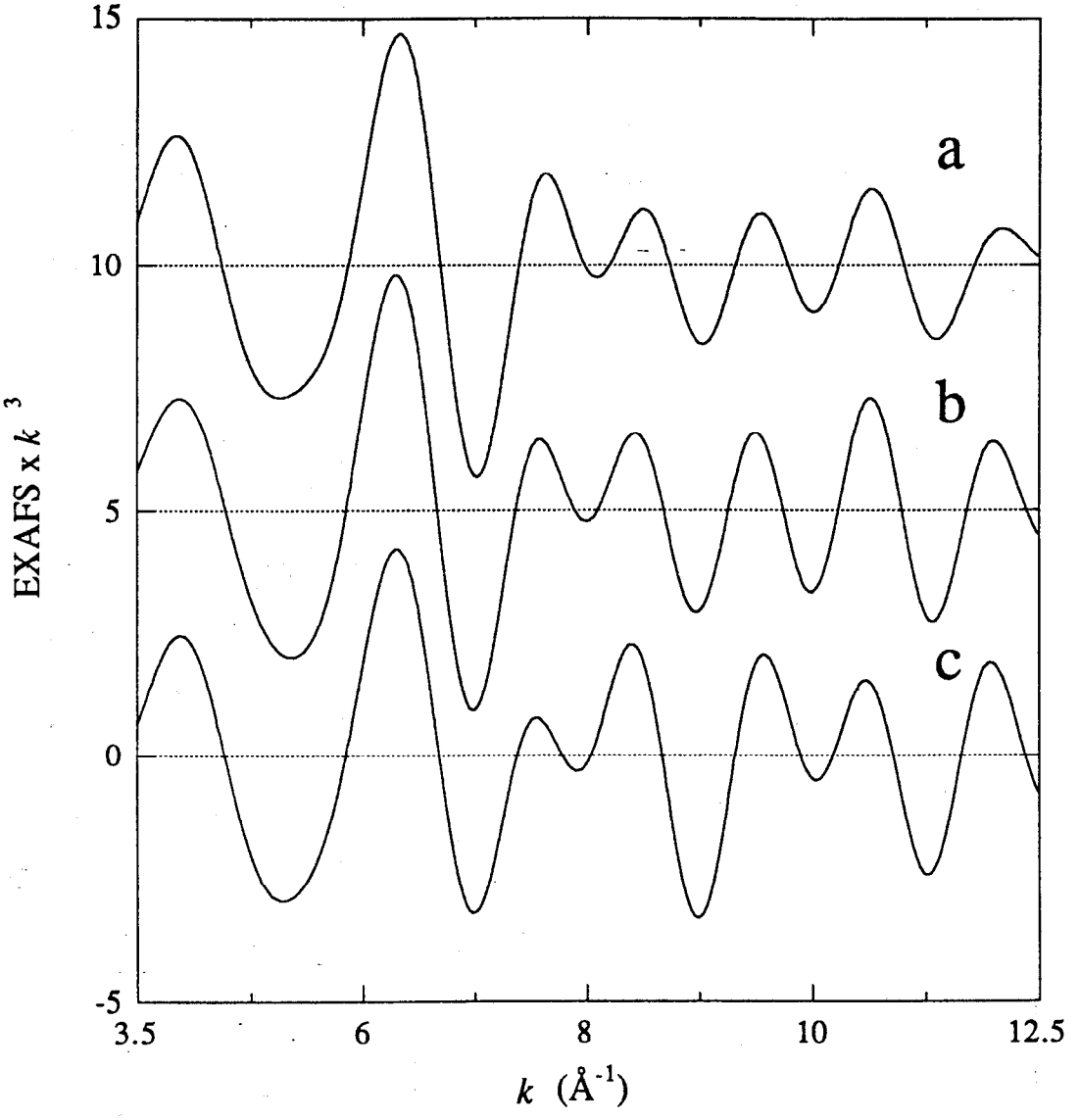

Figure 3.9. A comparison of the interaction between the first and second shell semimet hydroxylase EXAFS data. (a) Fourier filtered EXAFS of **EXAFS10** (with component B); (b) the 1:1 addition of the Fourier filtered first shell data of **EXAFS10** with the Fourier filtered second shell data of **EXAFS2**; (c) Fourier filtered EXAFS of **EXAFS2** (non-complexed form).

Table 3.5. Results of Fits[a] to the Non-Filtered Hydroxylase EXAFS Data.

Sample	Fit	N		O		Fe		C		F
		CN[b]	R(Å)	CN	R(Å)	CN	R(Å)	CN	R(Å)	
EXAFS10	10U	3.5	2.16	2.7	1.97					1.1
semimet hydroxylase	10V	3.5	2.16	2.7	1.97	1.1	3.39			0.72
w/ component B	10W	3.3	2.15	2.6	1.97	0.7	3.00			0.89
	10X	3.4	2.16	2.7	1.97			4.0	3.37	0.98
	10Y	3.5	2.17	2.9	1.98			4.9	3.02	0.78
	10Z	3.4	2.16	2.8	1.97	0.8	3.37	2.2	3.06	0.70
EXAFS11	11U	2.4	2.17	3.1	1.97					1.6
semimet hydroxylase	11V	2.4	2.16	3.0	1.97	1.5	3.41			1.0
w/ bromopropene	11W	2.4	2.15	3.0	1.97	1.0	3.03			1.2
	11X	2.4	2.16	3.0	1.97			6.1	3.39	1.3
	11Y	2.4	2.19	3.3	1.98			7.3	3.04	1.0
	11Z	2.2	2.18	3.1	1.98	0.9	3.37	5.0	3.04	0.95
EXAFS14	14U	2.9	2.17	2.6	1.98					0.95
semimet hydroxylase	14V	2.9	2.17	2.6	1.98	0.9	3.39			0.67
w/ component B	14W	2.6	2.16	2.5	1.98	0.5	2.97			0.80
	14X	2.9	2.17	2.6	1.98			3.0	3.38	0.87
	14Y	3.0	2.18	2.7	1.98			3.1	3.01	0.81
	14Z	3.0	2.17	2.6	1.98	1.6	3.38	4.5	3.19	0.60

Table 3.5. continued

Sample	Fit	N		O		Fe		C		F
		CN[b]	R(Å)	CN	R(Å)	CN	R(Å)	CN	R(Å)	
EXAFS16	16U	2.5	2.16	2.5	1.98					1.2
semimet hydroxylase	16V	2.4	2.16	2.5	1.98	1.2	3.40			0.79
w/ component B and	16W	2.5	2.15	2.4	1.98	0.9	3.02			0.90
bromopropene	16X	2.4	2.16	2.5	1.99			4.8	3.38	1.1
	16Y	2.5	2.18	2.8	1.99			6.1	3.03	0.73
	16Z	2.4	2.18	2.7	1.99	0.5	3.38	4.3	3.04	0.70
EXAFS18	18U	2.5	2.17	2.7	1.98					1.2
semimet hydroxylase	18V	2.5	2.17	2.7	1.98	1.2	3.41			0.75
w/ bromopropene	18W	2.5	2.16	2.6	1.97	0.9	3.03			0.87
	18X	2.4	2.17	2.6	1.98			4.4	3.39	1.0
	18Y	2.5	2.18	2.9	1.99			6.2	3.04	0.64
	18Z	2.4	2.18	2.8	1.98	0.4	3.38	5.0	3.05	0.62
EXAFS20	20U	2.6	2.17	2.8	1.97					1.5
semimet hydroxylase	20V	2.6	2.17	2.8	1.97	1.4	3.41			1.1
w/ bromopropene	20W	2.6	2.16	2.8	1.97	1.0	3.04			1.2
	20X	2.5	2.17	2.8	1.97			5.7	3.38	0.95
	20Y	2.7	2.19	3.0	1.98			7.4	3.05	1.3
	20Z	2.5	2.18	2.9	1.98	0.5	3.36	6.5	3.06	0.92

Table 3.5. continued

Sample	Fit	N		O		Fe		C		F
		CN[b]	R(Å)	CN	R(Å)	CN	R(Å)	CN	R(Å)	
EXAFS15	15G	2.3	2.11	2.1	2.03					0.68
reduced hydroxylase	15H	2.3	2.20	2.1	2.03	0.5	3.35			0.56
w/ component B	15I	2.5	2.19	2.1	2.02			2.2	2.99	0.58
EXAFS17	17G	2.1	2.22	2.2	2.04					0.65
reduced hydroxylase	17H	2.1	2.22	2.2	2.04	0.3	3.34			0.58
w/ component B and bromopropene	17I	2.3	2.21	2.2	2.03			1.6	2.99	0.60
EXAFS19	19G	3.1	2.19	1.7	2.04					0.69
reduced hydroxylase	19H	3.1	2.20	1.7	2.04	0.4	3.39			0.61
w/ bromopropene	19I	3.2	2.20	1.8	2.04			1.3	3.03	0.65

[a]Fitting range $k = 4 - 12$ Å^{-1}. Errors are estimated to be about $\pm$ 0.03 Å for distances and 25% for coordination numbers.[22] [b]CN = coordination number.

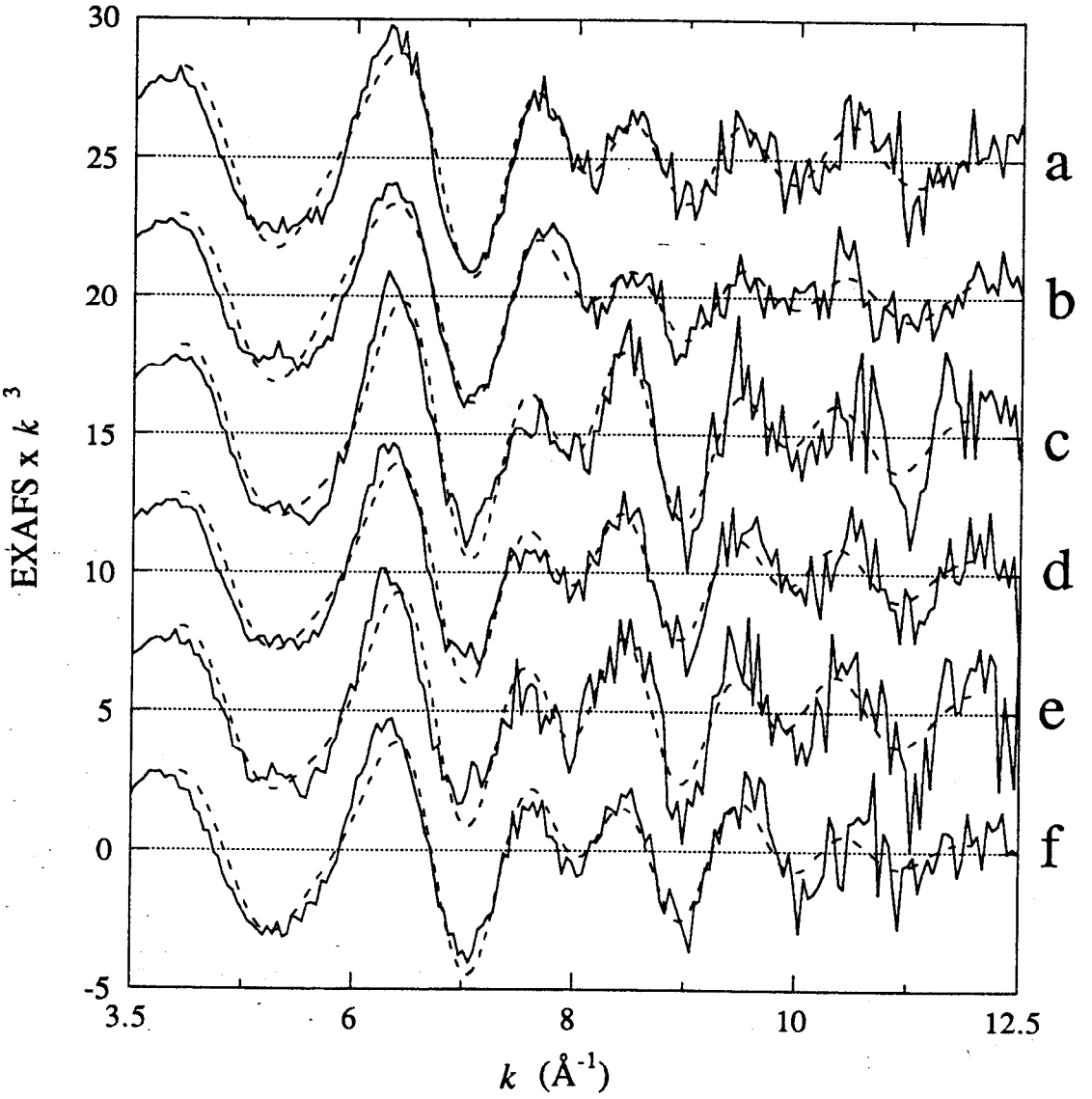

Figure 3.10. Fits to the non-filtered data for the semimet hydroxylase samples (fitting range k = 4-12 Å^{-1}). The solid line is the data and the dashed line is the fit to the data. The fit shown is the N,O and Fe fit (Table 3.5, fit U for all). (a) **EXAFS10**, (b) **EXAFS14**, (c) **EXAFS11**, (d) **EXAFS18**, (e) **EXAFS20**, (f) **EXAFS16**.

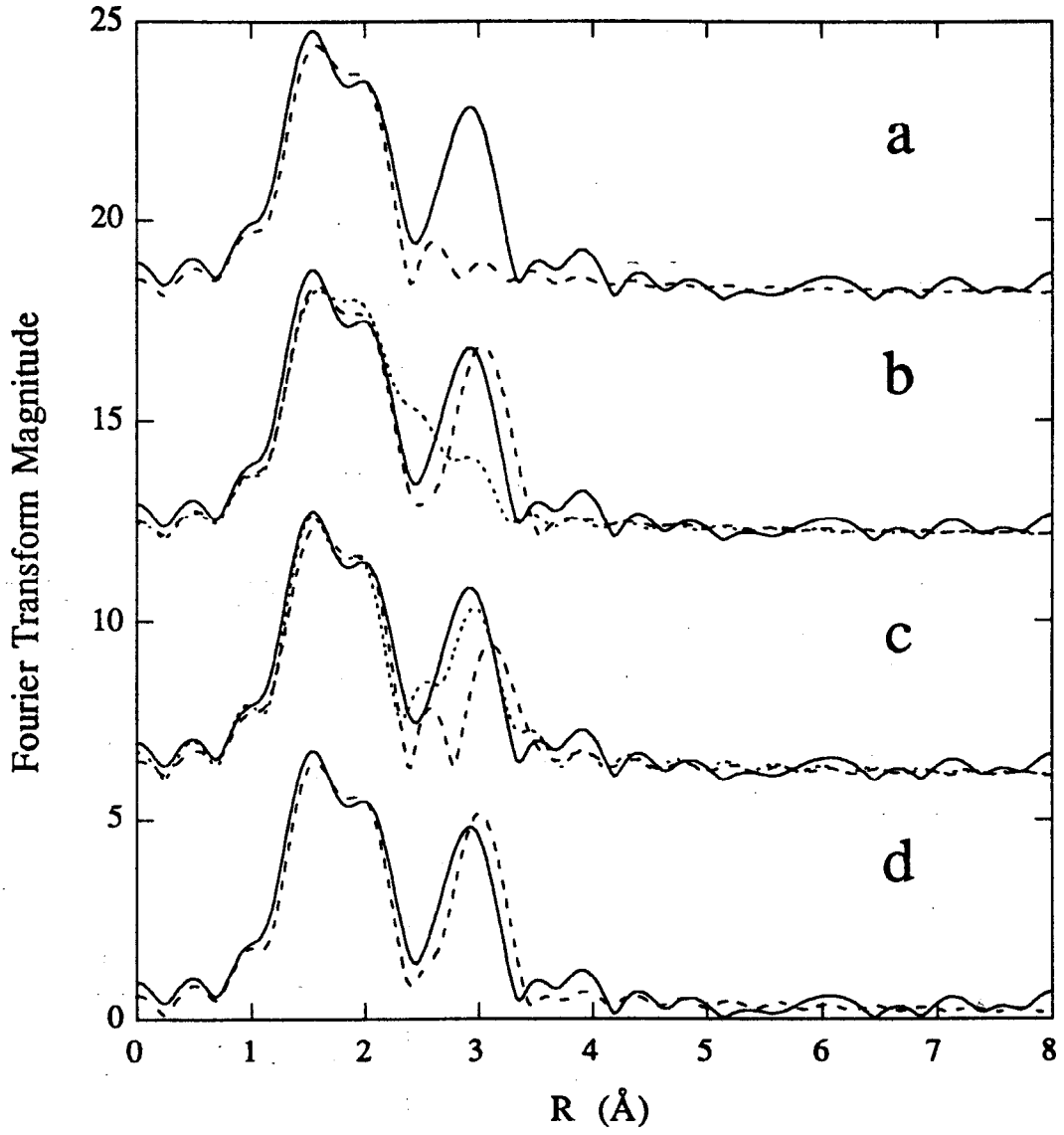

Figure 3.11. Fourier transforms of the fits to the non-filtered data for **EXAFS10** (Fourier transform range k = 4-12 Å^{-1}). The solid line is the data. (a) Fit to the data with N and O (dash) (Table 3.5, fit 10U), (b) fit to the data with N, O and long Fe (dash) (Table 3.5, fit 10V) and N,O and short Fe (dot) (Table 3.5, fit 10W), (c) fit to the data with N, O and long C (dash) (Table 3.5, fit 10X) and N, O and short C (dot) (Table 3.5, fit 10Y), (d) fit to the data with N, O, Fe and C (dash) (Table 3.5, fit 10Z). Note that the fit to the data with N, O and a long Fe contribution is better than the N, O and short Fe fit, while the fit including the short Fe-C contribution is better than the fit including the long Fe-C contribution.

Fit 10V (Table 3.5, Figure 3.11b), the second shell peak is slightly mismatched in position, with the fit to the data occuring at a slightly higher R value, but the amplitude of the peaks is well-matched, similar to what was described for the second shell fits above. The Fourier transform of the N/O/short Fe fit to the data (Table 3.5, fit 10W) is a poor match for the data (Figure 3.11b). For Fit 10Z, the amplitude of the fit in the second shell region is slightly high, but the addition of the short C contribution to the N/O/long Fe fit improves the match in the position of the peak of the fit to the data with the second shell peak of the data (Figure 3.11d). Clearly, this shows that the Fe-Fe parameters employed cannot by themselves explain the second shell data completely, and that something in addition to iron needs to be added to the fits.

The same procedure was performed for the reduced data, and the fit results are also presented in Table 3.5. Although the N/O fits to the data were adequate to explain the data, the broad feature suggested on the low k side of the 10 $Å^{-1}$ maximum was not accounted for (Figure 3.12a,c,d). However, with either the addition of a small 3.0 Å C contribution or a 3.4 Å Fe contribution, a better fit to the data at higher k was found (illustrated for **EXAFS15**, Figure 3.12b). As described above in the fits to the second shell data, that while improving the fit to the data mathematically, the actual numerical results of the high frequency contribution should not be interpreted as reflecting a true second shell environment. The Fourier transforms of the data and the fits to the data shown in Figure 3.12 are presented in Figure 3.13. The inclusion of Fe or C to the fit models the small peak above 2.5 Å.

3.3.3. X-ray Absorption Near Edge Spectra

The edge spectra of the semimet hydroxylase samples are presented in Figure 3.14. The spectra consist of a small, low intensity feature at ~ 7114 eV (Feature A), the main transition at ~ 7129 eV (Feature B) and a broad maximum at ~ 7134 eV (Feature C). The intensity of feature B increases in the presence of component B (**EXAFS10** and **EXAFS16**) and a shoulder appears on the rising edge at ~ 7124 eV (Feature A'). The energy position of Feature A does not change for the various samples, but its intensity increases for the samples with component B (see Figure 3.14 inset). The shapes of the pre-edge features for the other two complexes of the hydroxylase are not significantly different from the non-complexed form.

Upon reduction to the diferrous state (Figure 3.15), the the main transition moves to lower energy (~ 7125 eV) and the shape changes dramatically, increasing in intensity and becoming narrow. This change is typical of the reduction of Fe(III) to Fe(II) in models

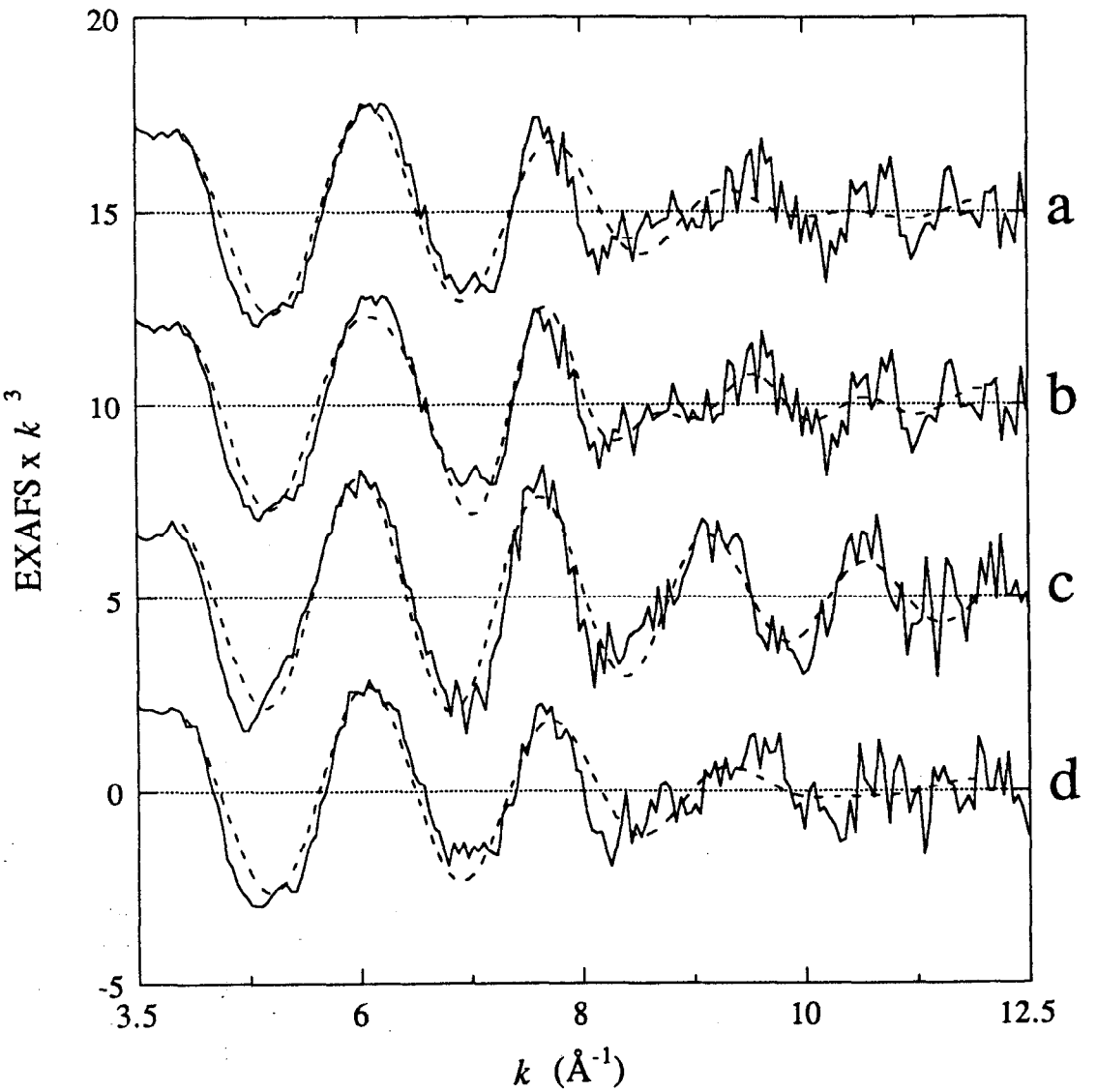

Figure 3.12. Fits to the non-filtered data for the reduced hydroxylase samples (fitting range k = 4-12 Å^{-1}). The solid line is the data and the dashed line is the fit to the data. (a) Fit to the data for **EXAFS15** with N and O (Table 3.5, fit G), (b) fit to the data for **EXAFS15** with N, O and Fe (Table 3.5, fit H). N and O only fits to (c) **EXAFS19** (Table 3.5, fit 19G) and (d) **EXAFS17** (Table 3.5, fit 17G). Note that the inclusion of Fe to the fit for **EXAFS15** accounts for the shoulder in the EXAFS between k = 8 and 9 Å^{-1}.

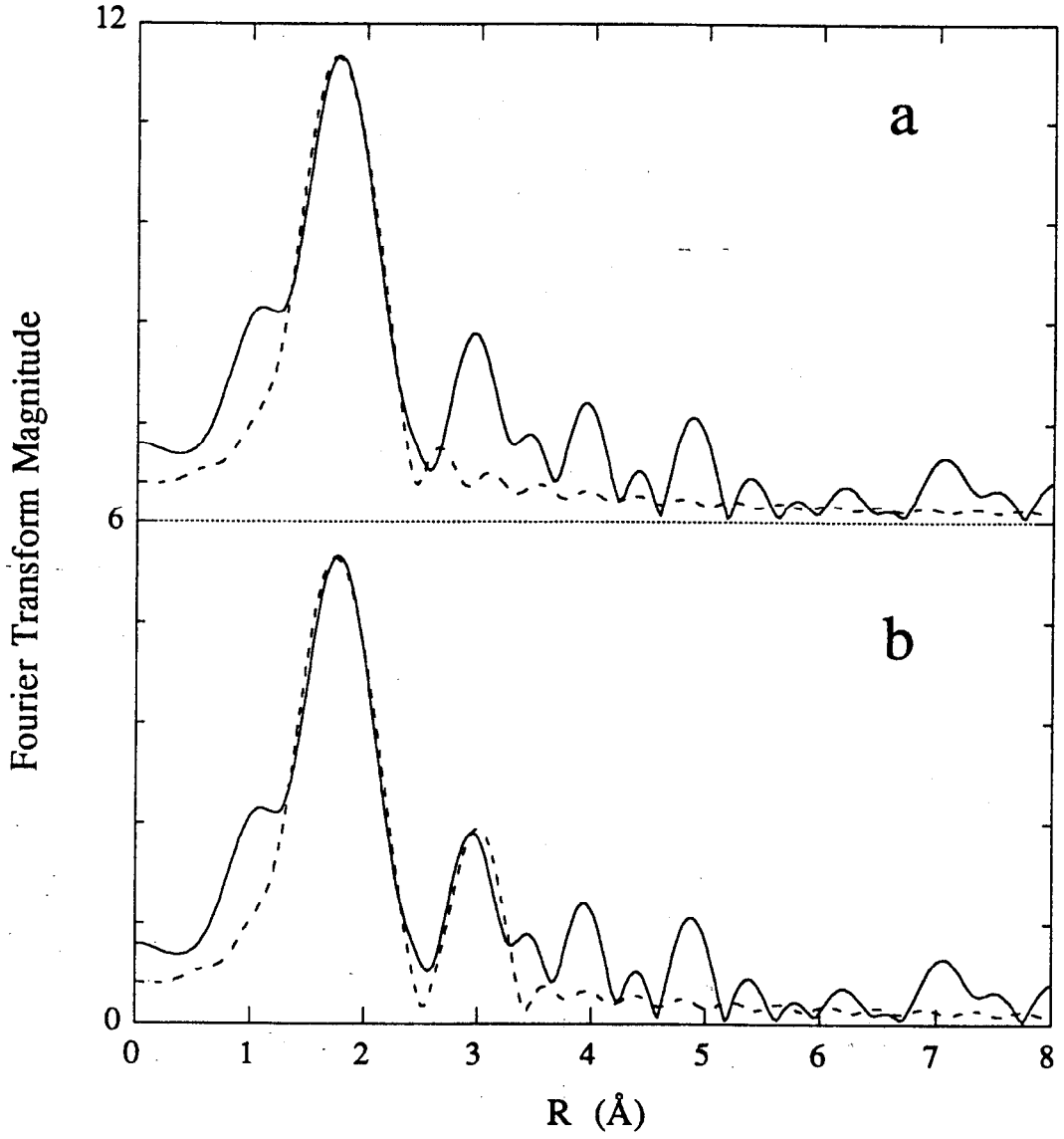

Figure 3.13. Fourier transforms of the fits to the non-filtered data for **EXAFS15** (Fourier transform range k = 4-12 Å^{-1}). The solid line is the Fourier transform of the data and the dashed line is the fit for (a) N and O fit (Table 3.5, fit G) and (b) N, O and Fe fit (Table 3.5, fit H). Note that the inclusion of Fe to the fit explains the 3.0 Å peak in the Fourier transform.

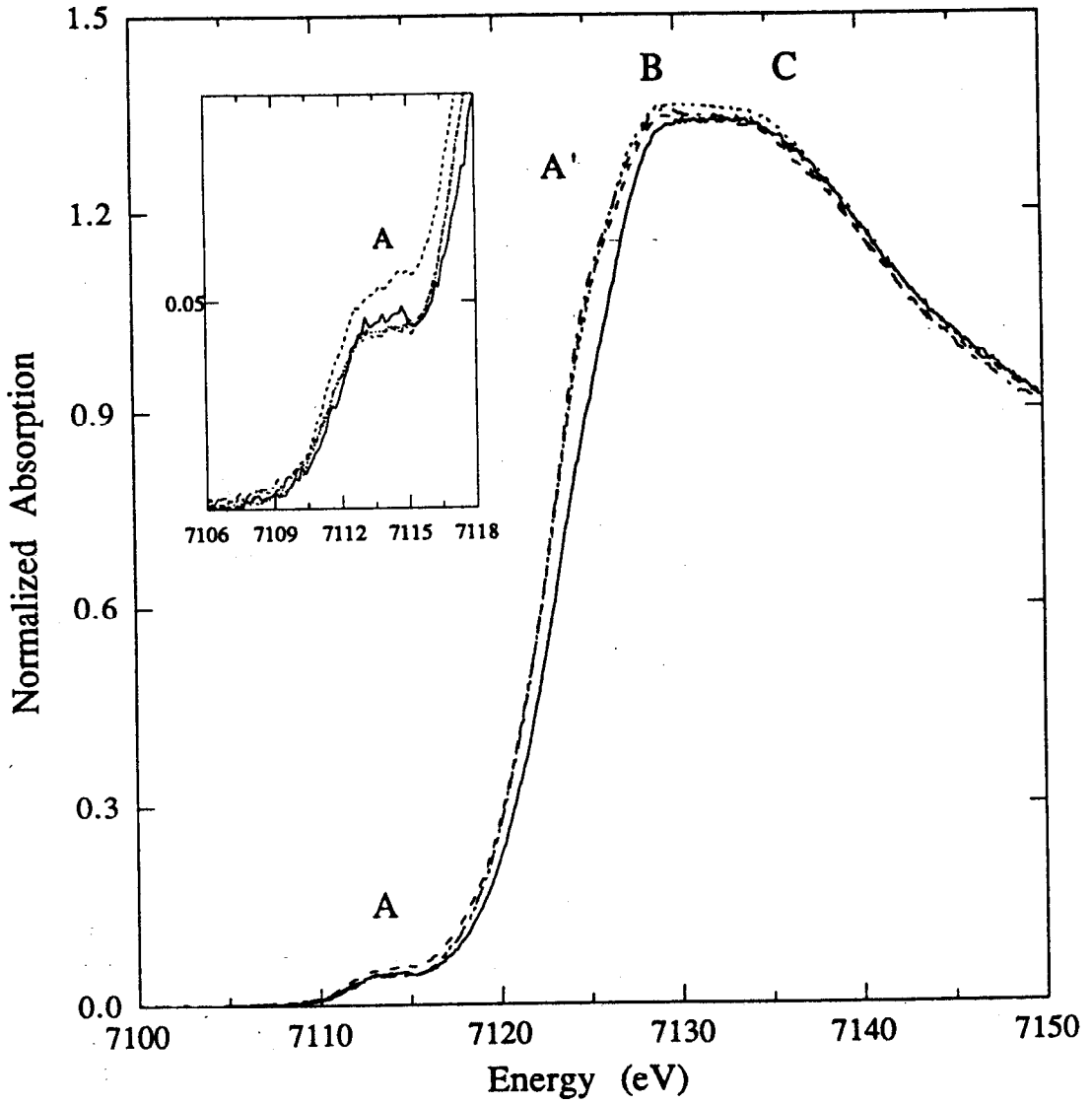

Figure 3.14. Edge spectra of semimet hydroxylase samples. Non-complexed sample, **EXAFS7** (solid); sample with component B, **EXAFS10** (dash); sample with bromopropene, **EXAFS18** (dot); sample with B and bromopropene **EXAFS16** (dash dot). Note the appearance of a shoulder on the rising edge in the spectra of the hydroxylase samples in the presence of B and bromopropene. The pre-edge feature of **EXAFS10** is more intense than the pre-edge features of the other samples.

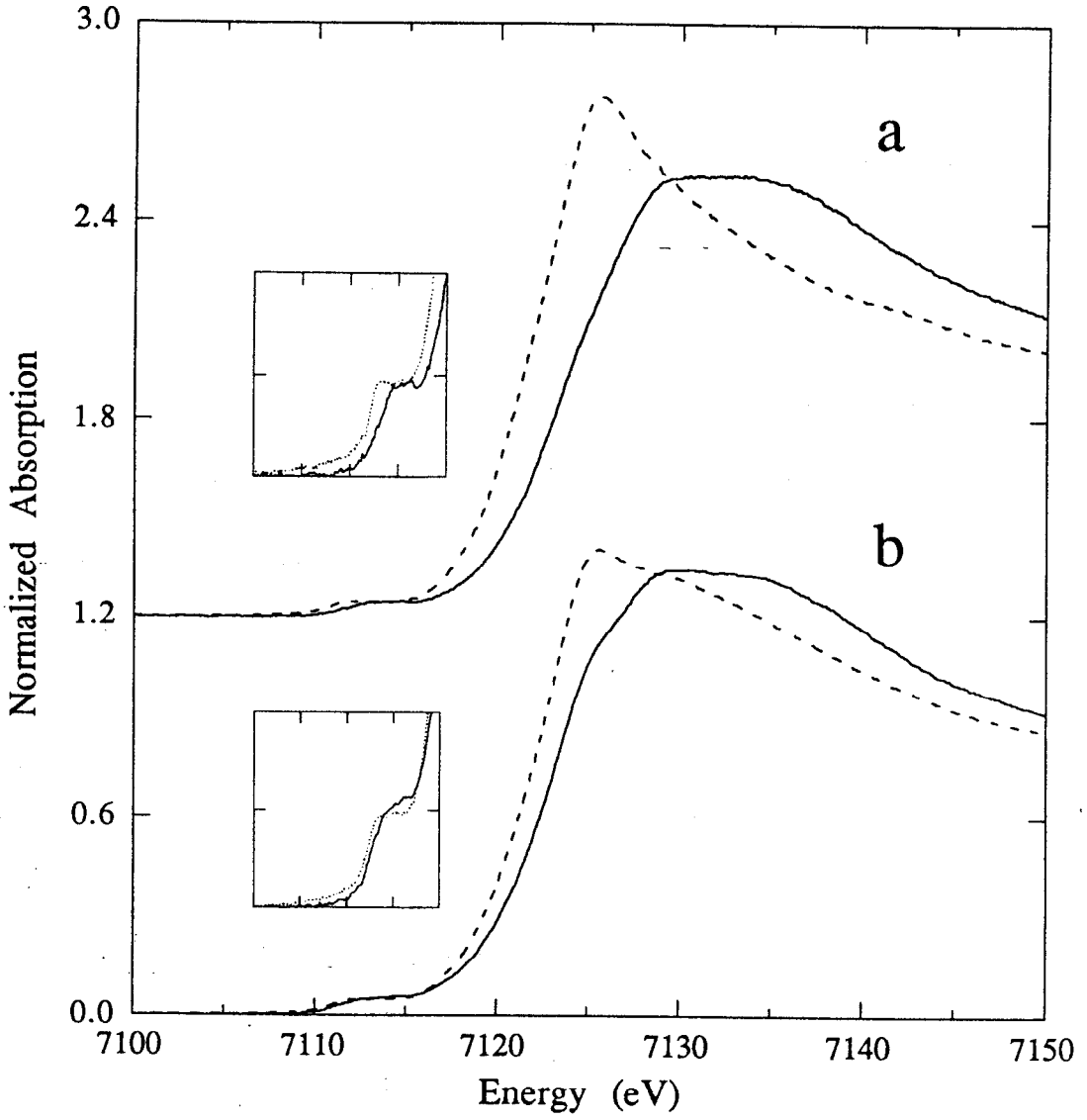

Figure 3.15. Edge spectra of semimet (solid) and reduced (dash) hydroxylase samples. The data shown are for (a) the non-complexed forms of the hydroxylase (**EXAFS7** and **EXAFS6**) and (b) the hydroxylase samples with component B (**EXAFS10** and **EXAFS15**). The change in the appearance of the edge spectra of the hydroxylase samples in the presence of component B is not as great as the change that occurs in the non-complexed samples.

with mixed O and N ligation (see Chapter 5). The shape of the pre-edge feature (Feature A) changes (Figure 3.15 inset) and the positon of the pre-edge feature moves to lower energy by about 1 eV to 7113 eV.

The edges of the reduced hydroxylase complexes are compared in Figure 3.16. The position of Feature A does not change, but the intensity decreases relative to the non-complexed sample edge. Among the hydroxylase complexes, the intensity of the feature is slightly greater for the hydroxylase sample in the presence of bromopropene than for the other samples. The shape of Feature A is different for the complexes with component B (**EXAFS15** and **EXAFS17**) from the bromopropene-complexed and non-complexed hydroxylase (**EXAFS19** and **EXAFS6**). The pre-edge feature rises to a maximum more steeply for **EXAFS6** and **EXAFS19** than for **EXAFS15** and **EXAFS17**. The intensity of the main transition decreases and becomes more narrow relative to the edge of the non-complexed samples, and a shoulder to the high energy side of Feature B (Feature C) at ~ 7131 eV appears for the hydroxylase in the presence of component B.

3.4. Discussion

3.4.1. The Empirical Fitting Proceedure

The underlying assumption of the empirical fitting approach applied herein is that only single scattering interactions contribute to the EXAFS, and multiple scattering contributions to outer shell data are neglected. The empirical fitting proceedure used for these fits has proven to be very reliable for the first coordination sphere and is especially sensitive to the distance distribution around the Fe atom, although it may not always accurately reflect the relative numbers of one atom type to another, as has been seen for these samples. Second shell empirical fitting methods are hampered by the difficulty in adequately modeling all of the second-shell low-Z atoms distributed at various distances and in various numbers around metal atoms in dinuclear metalloproteins. The Fe-C parameters obtained from Fe(acetylacetonate)$_3$, commonly used to model the second shell low-Z atom contribution to the data, describe a wave which mimicks the second shell Fe-Fe contribution (Chapter 2, Figure 2.8), resulting in the satisfactory "C-only" fits to the data at the same distances as the Fe-only fits. This also contributes to the high degree of correlation between the Fe and C contributions to the fits when both Fe and C were used to fit the second shell data. The ability of second shell carbon to mimic a first row transition metal contribution has been noted before in fits to dinuclear copper proteins.[34] The net result is that it is difficult to isolate the second shell metal-metal interaction from the second

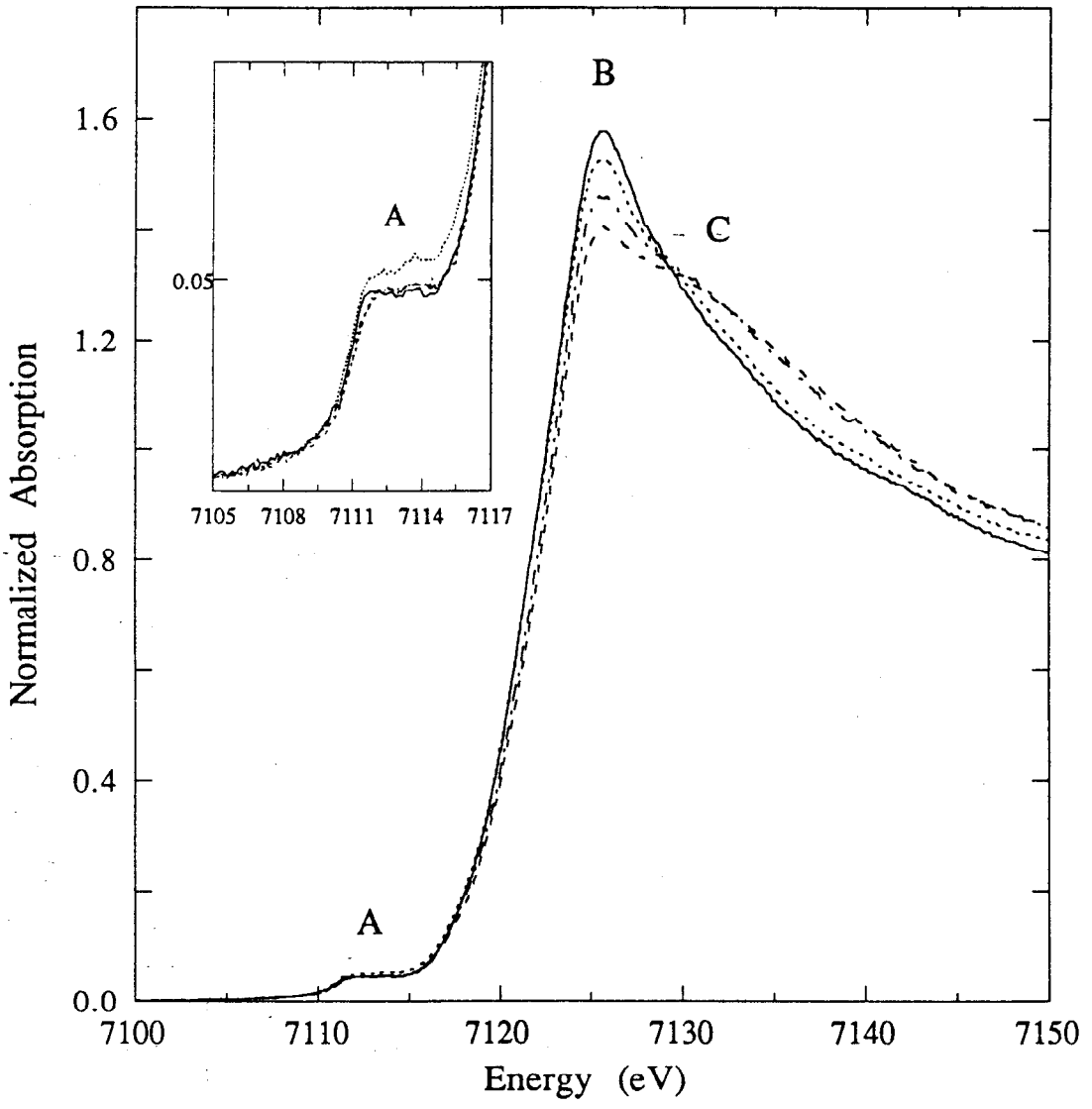

Figure 3.16. Edge spectra of reduced hydroxylase samples. Reduced hydroxyalse sample, **EXAFS6** (solid); sample with component B, **EXAFS15** (dash); sample with bromopropene, **EXAFS19** (dot); sample with component B and brompropene, **EXAFS17** (dash dot). Note that the intensity of the main feature decreases in the presence of component B and bromopropene.

shell metal-low-Z atom interaction using a single-scattering empirical approach, an effect clearly seen in the fits to the second shell EXAFS data. The inclusion of this shell clearly shows that at least a second contribution is needed to model the second shell properly.

Multiple scattering interactions from the presence of rigid ligand groups such as imidazoles can often contribute significantly to the outer shell data. Semi-empirical methods of dealing with the presence of imidazole groups, in which a set of amplitude and phase parameters which describe the contribution of the imidazole group as a unit, have had limited success.[35] Recent efforts have focused on including the individual multiple-scattering pathways based on theoretical calculations within the imidazole group in fits to the data.[36] The possibility that multiple scattering from other ligands bound to the iron atom are contributing to the second shell data cannot be ruled out, as it has recently been shown that multiple scattering contributes significantly to the outer shell data in $Fe(acac)_3$.[37] This suggests that in addition to imidazole groups, multiple scattering interactions from bidentate coordination of a carboxylate group to a single Fe atom may also contribute to the second shell data. The crystal structure of ribonucleotide reductase B2[38] shows an aspartate group coordinated to an Fe atom in just such a manner and it is certainly possible, based on the similarity between the average first shell data for RR and MMO hydroxylase as determined by EXAFS,[12] that similar coordination of carboxylate groups occur in the hydroxylase active site. The application of a multiple scattering analysis to the second shell data is currently under developement.[37]

3.4.2. The Effect of Substrate and Component B on the Structure of the Diiron Center

Perturbations in the EPR spectrum of the semimet hydroxylase in the presence of substrate was the first indication that the hydroxylase component interacted directly with substrate.[4c,17] In the presence of small molecules, the EPR spectrum was generally sharpened and intensified, however the presence of component B caused a dramatic difference in the EPR spectrum of the semimet hydroxylase.[16a] The hydroxylase no longer exhibited the $g_{av} = 1.85$ signal (*M. trichosporium* (OB3b)), and a different saturation behaviour was observed, resulting in an EPR signal with $g_{av} = 1.75$. These results suggest that the interaction of component B with the hydroxylase in its semimet form is more significant than the interaction of substrate. In the fully reduced form, the presence of component B does not affect the EPR as drastically as in the semimet form and only sharpens and intensifies the $g = 16$ signal, suggesting that the interaction of B with the reduced hydroxylase is not as significant as its interaction with the semimet hydroxylase.

These trends are qualitatively seen in the EXAFS of the semimet (Figure 3.1) and reduced samples (Figure 3.3). The EXAFS of the complex formed between semimet hydroxylase and bromopropene (Figure 3.1d-f) is very similar to the non-complexed EXAFS (Figure 3.1a), whereas the EXAFS of the semimet hydroxylase with component B (Figure 3.1b,c) is different from the non-complexed form. The B plus bromopropene sample (Figure 3.1g) resembles a combination of the B-hydroxylase and the bromopropene-hydroxylase samples. The EXAFS of the reduced hydroxylase in the presence of component B (Figure 3.3c) is somewhat different from the non-complexed form (Figure 3.3a,b).

The presence of component B and substrate also alters the redox potentials of the hydroxylase iron site.[18] The redox potentials of the Fe(III)Fe(III)/Fe(II)Fe(III) and Fe(II)Fe(III)/Fe(II)Fe(II) pairs were slightly lowered in the presence of propylene, suggesting a decrease in the electron affinity of the iron site and a slight inhibition of the reduction process. In the presence of stoichiometric amounts of component B and reductase, no reduction of the hydroxylase occured, suggesting that both component B and reductase are required to inhibit reduction of the hydroxylase. Earlier kinetic studies suggested that component B alone was responsible for the inhibition of the reduction of hydroxylase in the absence of substrate.[6,11] The XAS sample of the reduced form of the hydroxylase with component B was subjected to the reduction mediators *after* the protein complex had been formed. The edge spectrum (Figure 3.16) is consistent with the reduced form of a diiron center, therefore reduction of the hydroxylase *can* proceed in the presence of component B and the absence of substrate. This confirms that both the reductase and component B are required in the absence of substrate to effectively inhibit reduction of the hydroxylase diirion site.

3.4.2.1 Changes in the Coordination Sphere of the Iron Center. The fit results do not show any significant difference in the iron coordination sphere due to the formation of hydroxylase complexes. The average first shell coordination of the complexed forms of the semimet hydroxylase (5.3 - 6.4 N/O at 2.06 - 2.08 Å, Table 3.6) do not vary significantly from the average first shell coordination of the non-complexed semimet hydroxylase (5.6 N/O at 2.08 Å, Table 3.6). Considering the Fe-only fits to the second shell data, the Fe-Fe distance for all of the semimet complexes is also very similar, varying from 3.39 Å to 3.41 Å. Based on a comparison of the coordination weighted average first shell date, the results suggest that no significant change in the coordination of the iron occurs due to the formation of hydroxylase complexes with component B or substrate. However, there is a change in the relative coordination numbers of the long and short distance contributions to the first shell data for the B-hydroyxlase samples. Given the inability of EXAFS to strictly determine the relative numbers of similar strength

Table 3.6. Comparison of the Results of Fits to the Hydroxylase Data.

Sample	Description	Avg. First Shell Coordination[a]	Second Shell Fe-Fe Coordination[b]
EXAFS5[c]	oxidized	5.8 N/O at 2.04 Å	1.1 Fe at 3.42 Å
EXAFS2[c]	semimet	5.6 N/O at 2.08 Å	1.1 Fe at 3.41 Å
EXAFS10	semimet w/ componet B	6.4 N/O at 2.08 Å	1.0 Fe at 3.39 Å
EXAFS11	semimet w/ bromopropene	5.6 N/O at 2.06 Å	1.5 Fe at 3.41 Å
EXAFS14	semimet w/ component B	5.7 N/O at 2.08 Å	0.8 Fe at 3.39 Å
EXAFS16	semimet w/ component B and bromopropene	5.3 N/O at 2.07 Å	1.2 Fe at 3.40 Å
EXAFS18	semimet w/ bromopropene	5.3 N/O at 2.07 Å	1.2 Fe at 3.41 Å
EXAFS20	semimet w/ bromopropene	5.3 N/O at 2.07 Å	1.4 Fe at 3.41 Å

Table 3.6. continued

Sample	Description	Avg. First Shell Coordination[a]	Second Shell Fe-Fe Coordination[b]
EXAFS3[c]	reduced	5.6 N/O at 2.15 Å	
EXAFS6[c]	reduced	4.6 N/O at 2.16 Å	
EXAFS15	reduced w/ component B	4.6 N/O at 2.11 Å	
EXAFS17	reduced w/ bromopropene	4.4 N/O at 2.13 Å	
EXAFS19	reduced w/ component B and bromopropene	4.8 N/O at 2.14 Å	

[a]The average distance given is the coordination-weighted average distance for the fit with initial $R_N > R_O$ (Table 3.2, fit E for all samples). [b]The Fe coordination reported is for the long Fe-only fit to the data (Table 3.3, fit G) as this is the most reasonable result. [c]See Chapter 3 and reference 12 for the original analysis of the data for these samples.

backscattering atoms, we hesitate to interpret the change in the contributions of the individual waves as representing a real change in the relative N and O ligation to the iron center, however the results indicate that some minor change does occur in the first coordination sphere. Whether the origin of the difference arises from a change in the ligation of the iron atoms, or a distortion of the coordination environment, or a change in the covalency of the metal site can not be determined based on the EXAFS analysis.

Although it is known that substrate interacts with the hydroxylase component, the location of the binding site has not been determined. A brominated substrate was used for the hydroxylase/substrate complex to provide information about the proximity of the substrate binding site to the iron center. Bromine is a stronger backscatterer than Fe, so an Fe-Br interaction should be detected if the substrate were to bind close enough to an iron atom in an ordered configuration (with little rotational or vibrational motion). If 1-bromopropene were to bind to an Fe atom, the Fe-Br distance would be on the order of 2.5-3.75 Å if the terminal C to which Br is attached binds to the iron atom, depending on the angles of the Fe-C to C-Br bonds. If the second carbon, at the internal end of the double bond, binds to iron the Fe-Br distance would be on the order of 3.0-5.3 Å, again depending on the relative bonding angles. EXAFS should be sensitive to a Br interaction within 4.0 Å. Since Br is such a strong backscatterer, it might be possible to detect an Fe-Br interaction at a longer distance and therefore be able to determine the distance to the substrate binding site.

To evaluate this, we have collected EXAFS data on a brominated derivative of $Fe(acac)_3$, [tris-(3-bromo-2,4-pentanedionate)$_3$ iron (III)][39] (or $Fe(3\text{-Br-acac})_3$) in which the Fe-Br distance is expected to be on the order of 5.2 Å.[40] The contributions of the three bromine atoms at this distance are clearly seen in the Fourier transform of $Fe(3\text{-Br-acac})_3$ compared to $Fe(acac)_3$ (Figure 3.17), suggesting that an Fe-Br interaction at a distance as long as 5 Å could be detectable by XAS. Inspection of the Fourier transforms of the semimet and reduced bromopropene complexes (**EXAFS11, EXAFS16, EXAFS18, EXAFS20**, Figure 3.2; **EXAFS17, EXAFS19**, Figure 3.4) shows no suggestion of a strong interaction above 3.5 Å, suggesting that substrate binds at a distance greater than 5 Å. If the bromine were located between 3 and 3.5 Å from the iron atoms, it would be expected that the fit results to the second shell data would be different for the hydroxylase samples with bromopropene from the non-bromopropene complexed samples, however this was not the case. We have not yet identified an appropriate model for an Fe-Br interaction at 3-3.5 Å, so we have been unable to fit the second shell data to test for the presence of bromine. Pending the application of appropriate Fe-Br parameters to the fitting proceedure, and given that the data can be well explained by only second shell Fe and C

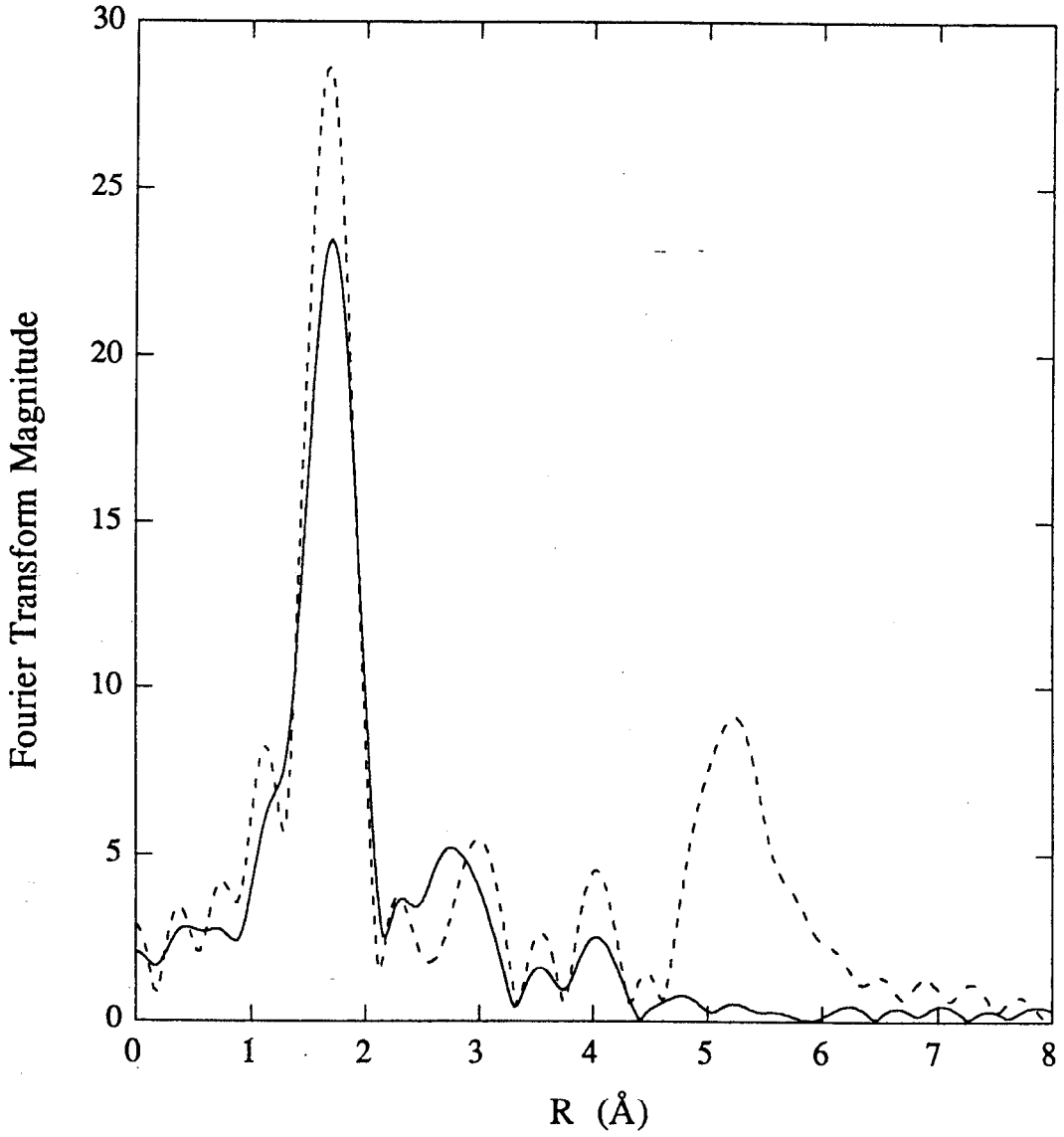

Figure 3.17. Fourier transforms of the EXAFS data for $Fe(acac)_3$ (solid) and $Fe(3\text{-}Br\text{-}acac)_3$ (dash). The peak at ~ 5 Å in the Fourier transform of $Fe(3\text{-}Br\text{-}acac)_3$ is due to the Fe-Br interaction.

contributions, these results suggest that substrate does not bind directly to the iron atoms; instead, it binds at a location such that the Br atom is more more than 4 Å away from the iron site. This conclusion is consistent with the results of an ENDOR study of the hydroxylase in the presence of methanol,[16b] in which no evidence was seen for coupling of the methyl protons to the iron site. Coupling with exchangeable imidazole protons 5-6 Å away from the iron site was seen, so the methanol binding site must be more than 6 Å away from the iron atoms. In addition, the limited deuterium exchange that occured during the course of this study suggested limited access to the diiron site for water; therefore access is probably limited for larger molecules such as bromopropene as well.

3.4.2.2. Interpretation of the Hydroxylase Edge Spectra. The weak pre-edge feature seen well below the 4p transition in transition metal spectra has been assigned to a formally dipole forbidden 1s→3d transition made allowed by 4p mixing into the 3d states as a result of symmetry distortions and vibronic coupling.[41,42] The intensity of this feature is inversely proportional to the symmetry of the metal site and increases as the metal site is distorted from octahedral to tetrahedral symmetry. The intensity of the feature can be therefore be used to infer the coordnation number and/or site symmetry of the metal atom.[43] The presence of the 1s→3d feature in the edge spectra of the hydroxylase samples (Figure 3.14 and 3.15, feature A) indicates that the Fe site is distorted from octahedral symmetry. The intensity of this transition is consistent with the proposed 5-6 atom coordination of the iron site in the MMO hydroxylase. The increase in the intensity of the 1s→3d transition for **EXAFS10** relative to **EXAFS7** suggests that the Fe site is more distorted in the presence of component B.

The appearance of the shoulder of the rising edge of the semimet hydroxylase spectra (Feature A') is similar to changes seen in the edge spectra of Cu and Fe systems as a result of the increase in the covalency of the metal site.[41,44] This feature has been assigned as a ligand-to-metal charge transfer (LMCT) shake-down feature[45] associated with 1s→4p transition in the Cu systems. If Feature A' reflects covalency in the iron site, then the improved resolution of this feature in the hydroxylase complexes suggests that the covalency of the iron site increases as a result of the interaction with component B and/or bromopropene. The decrease in the electron affinity of the iron site in the presence of propylene as measured by the change in the redox potentials is consistent with an increase in the covalency of the Fe(III) iron center.[18]

For the reduced hydroxylase samples, the 1s→3d feature appears to be split by about 2 eV in the complex formed with bromopropene (**EXAFS19**) and in the non-complexed form (**EXAFS6**). Splitting seen in ferrous compounds has been attributed to transitions to the ^4F (lower energy transition) and ^4P (higher energy transition) multiplet

levels of the d^7 final state.[44] The relative intensities of the two features in the reduced hydroxylase spectra are not in accord with predictions (^4F:^4P 7:3).[44] Due to the noise level and the reduction in intensity of the leading edge of the feature for the B-complexed forms, it cannot be established if the pre-edge feature is split for these samples.

During XAS sample preparation, the hydroxylase complexes were made before the samples were reduced. This suggests that the changes in the edge of the reduced samples derive from an interference in the reduction process as a result of the complex formed between the hydroxylase and component B or bromopropene. The intensity difference of the main transition for the semimet and reduced complexes with B (Feature B, Figure 3.15b) is not as great as the intensity difference of the main transition for the non-complexed semimet and reduced samples (Feature B, Figure 3.15a). If the difference in the edge of the non-complexed forms represents a conversion from semimet to diferrous, then perhaps a lesser degree of change represents an incomplete conversion to the fully reduced form. Therefore, perhaps the intensity of the 1s→4p transition is directly related to the ability of the hydroxyalse component to undergo chemical reduction.

In the edge spectra of the reduced hydroxylase samples (Figure 3.16), the intensity of the 1s→4p transition decreases from the non-complexed form (**EXAFS6**) to the complex with bromopropene (**EXAFS19**) followed by the complex with both B and bromopropene (**EXAFS17**) and the complex with only B (**EXAFS15**). Based on the arguement presented above, this suggests that in the presence of B reduction is inhibited, but the inhibition is lifted if substrate is added to B, and further decreased if substrate is added and B is removed. This trend is consistent with the results of kinetic studies[10,11] in which the reduction of the hydroxylase was inhibited or halted by the presence of component B in the absence of substrate, but occured in the presence of substrate. In addition, the reduction of the redox potentials of the hydroxylase in the presence of substrate (E_1^o = 30 mV; E_2^o = -156 mV) as compared to the redox potentials of the hydroxylase alone (E_1^o = 48 mV; E_2^o = -135 mV)[18] suggest a slight decrease in the electron affinity of the iron site in the presence of substrate. These studies suggest that reduction of the hydroxylase in the presence of substrate is very slightly inhibited, and in the presence of component B without substrate, reduction of the hydroxylase is strongly inhibited. The interpretation of the decrease in the intensity of the 1s→4p transition in the edge spectra of the reduced hydroxylase samples is consistent with these results. It would be interesting to see if longer exposure to the reduction mediators would result in more complete reduction of the complexed forms of the hydroxylase (samples were incubated for approximately 40 minutes).

3.5. Conclusions

The results of the EXAFS analysis for the range of data available do not show any significant change in the average coordination environment of the iron center as a result of complex formation. The interaction of component B and bromopropene therefore occurs at a location other than the iron site. Based on the comparison of the Fourier transforms of the bromopropene-hydroxylase samples and $Fe(3\text{-Br-acac})_3$, and the results of an ENDOR study of the hydroxylase component,[16b] the site of the substrate interaction is more than 4 Å away from the iron site. The presence of component B has an effect on the first shell of the hydroyxlase active site, reflected in the change in the distance distribution of the individual contributions to the first shell data (Table 3.2). The nature of this change cannot be determined for the data range available, but possible explanations include distortion of the iron environment, changes in the ligation of the iron atoms, or a change in the covalency of the iron site due to distant interactions between the hydroxylase and component B.

Direct evidence for the inhibition of the chemical reduction of the hydroxylase in the presence of component B and bromopropene is seen in the edge spectra. The appearance of a shoulder on the rising edge of the spectra of the semimet edges suggests that the covalancy of the diiron center changes due to the presence of component B and substrate. These studies suggest that the changes which occur in the hydroxylase diiron center in the presence of the component B or substrate involve subtle perturbations in the coordination environment of the iron atoms accompanied by changes in the electronic structure of the iron center.

3.6. Acknowledgements

The data were collected at the Stanford Synchrotron Radiation Laboratory and the National Synchrotron Light Source, Brookhaven National Laboratory, which are supported by the Department of Energy, Office of Basic Energy Sciences, Division of Chemical Sciences and Division of Materials Sciences. SSRL is also supported by the National Institutes of Health, Biomedical Resource Technology Program, Division of Research Resources (RR-01209) and the Department of Energy, Office of Health and Environmental Research. Grant support was provided by the National Science Foundation (CHE 91-21576 to KOH).

3.7. References and Notes

1. Anthony, C. *The Biochemistry of the Methylotrophs*; Academic Press: London, 1982.

2. (a) Colby, J.; Dalton, H. *Biochem. J.* **1978**, *171*, 461-468. (b) Colby, J.; Dalton, H. *Biochem. J.* **1976**, *157*, 495-497.

3. (a) Stirling, D. I.; Dalton, H. *J. Biochem.* **1979**, *96*, 205-212.

4. (a) Woodland, M. P.; Dalton, H. *Anal. Biochem.* **1984**, *139*, 459-462. (b) Woodland, M. P.; Patil, D. S.; Cammack, R.; Dalton, H. *Biochim. Biophys. Acta* **1986**, *873*, 237-242. (c) Woodland, M. P.; Dalton, H. *J. Biol. Chem.* **1984**, *259*, 53-59.

5. Colby, J.; Dalton, H. *Biochem. J.* **1979**, *177*, 903-908. (b) Lund, J.; Dalton, H. *Eur. J. Biochem.* **1985**, *147*, 291-296.

6. Green, J.; Dalton, H. *J. Biol. Chem.* **1985**, *260*, 15795-15801.

7. (a) Colby, J.; Stirling, D. I.; Dalton, H. *Biochem. J.* **1977**, *165*, 395-402. (b) Green, J.; Dalton, H. *J. Biol. Chem.* **1989**, *264*, 17698-17703.

8. Fox, B. G.; Lipscomb, J. D. *Biochem. Biophy. Res. Comm.* **1988**, *154*, 165-170.

9. (a) Burrows, K. J.; Cornish, A.; Scott, D.; Higgins, I. J. *J. Gen. Microbiol.* **1984**, *130*, 3327-3333. (b) Fox, B. G.; Borneman, J. G.; Wackett, L. P.; Lipscomb, J. D. *Biochemistry*, **1990**, *29*, 6419-6427.

10. (a) Fox, B. G.; Froland, W. A.; Dege, J. E.; Lipscomb, J. D. *J. Biol. Chem.* **1989**, *264*, 10023-10033. (b) Andersson, K. K.; Froland, W. A.; Lee, S-K.; Lipscomb, J. D. *New J. Chem.* **1991**, *15*, 411-415.

11. (a) Lund, J.; Woodland, M. P.; Dalton, H. *Eur. J. Biochem.* **1985**, *147*, 297-305. (b) Green, H.; Dalton, H. *Biochem. J.* **1989**, *259*, 167-172.

12. DeWitt, J. G.; Bentsen, J. G.; Rosenzweig, A. C.; Hedman, B.; Green, J.; Pilkington, S.; Papaefthymiou, G. C.; Dalton, H.; Hodgson, K. O.; Lippard, S. J. *J. Am. Chem. Soc.* **1991**, *113*, 9219-9235.

13. Fox, B. G.; Surerus, K. K.; Münck, E.; Lipscomb, J. D. *J. Biol. Chem.* **1988**, *263*, 10553-10556.

14. (a) Lippard, S. J. *Angew. Chem., Int. Ed. Engl.* **1988**, *27*, 344-361. (b) Sanders-Loehr, J. *Iron Carriers and Iron Proteins*; VCH Publishers Inc.: New York, 1989, pp 373-466. (c) Que, L., Jr.; True, A. E. *Prog. Inorg. Chem.* **1990**, *38*, 97-200.

15. Hendrich, M. P.; Münck, E.; Fox, B. G.; Lipscomb, J. D. *J. Am. Chem. Soc.* **1990**, *112*, 5861-5865.

16. (a) Fox. B. G.; Liu, Y.; Dege, J. E.; Lipscomb, J. D. *J. Biol. Chem.* **1991**, *266*, 540-550. (b) Hendrich, M. P.; Fox, B. G.; Andersson, K. K.; Debrunner, P. G.; Lipscomb, J. D. *J. Biol. Chem.* **1992**, *267*, 261-269.

17. (a) Dalton, H. *Adv. Appl. Microbiol.* **1980**, *26*, 71-87. (b) Dalton, H. *Microbial Growth on C1 Compounds*; Heyden Press: London, 1980, pp 1-10.

18. Liu, K. E.; Lippard, S. J. *J. Biol. Chem.*, **1991**, *266*, 12836-12839.

19. Wu, W.; Rosenzweig, A. C.; Lippard, S. J. unpublished results.

20. Cramer, S. P.; Tench, O.; Yocum, M.; George, G. N. *Nucl. Instrum. Methods Phys. Res.* **1988**, *A266*, 586-591.

21. Scott, R. A.; Hahn, J. E.; Doniach, S. ; Freeman, H. C.; Hodgson, K. O. *J. Am. Chem. Soc.* **1982**, *104*, 5364-5369.

22. (a) Cramer, S. P.; Hodgson, K. O.; Stiefel, E. I.; Newton, W. E. *J. Am. Chem. Soc.* **1978**, *100*, 2748-2761. (b) Cramer, S. P.; Hodgson, K. O. *Prog. Inorg. Chem.* **1979**, *15*, 1-39. (c) Scott, R. A. *Methods Enzymol.* **1985**, *117*, 414-459.

23. Johansson, L. *Chem. Scr.* **1976**, *9*, 30-35. The crystal structure of the perchlorate salt has not been determined, but the $[Fe(phenanthroline)_3]^{2-}$ complex structure can be assumed to be identical with that of the corresponding iodide salt (Johansson, L.; Molund, M.; Oskarsson, Å. *Inorg. Chim. Acta* **1978**, *31*, 117-123).

24. Iball, J.; Morgan, C. H. *Acta Cryst.* **1976**, *23*, 239-244. (b) Roof, R. B. Jr. *Acta Cryst.* **1956**, *9*, 781-786.

25. Armstrong, W. H.; Lippard, S. J. *J. Am. Chem. Soc.* **1984**, *106*, 4632-4633.

26. Ericson, A.; Hedman, B.; Hodgson, K. O.; Green, J.; Dalton, H.; Bentsen, J. G.; Beer, R. H.; Lippard, S. J. *J. Am. Chem. Soc.* **1988**, *110*, 2330-2332.

27. Scarrow, R. C.; Maroney, M. J.; Palmer, S. M.; Que, L. Jr.; Roe. A. L.; Salowe, S. P.; Stubbe, J. *J. Am. Chem. Soc.* **1987**, *109*, 7857-7864.

28. The EPR signal at $g_{av} < 2.0$ and the value of the coupling constant ($J = -32$ cm^{-1}, ref. 12) are consistent with an oxo-group bridged diiron center; ENDOR and ESEER studies suggest the presence of 2 N-donating groups coordinated to the iron center (ref. 16b).

29. Zhang, K.; Stern, E. A.; Ellis, F.; Sanders-Loehr, J.; Shiemke, A. K. *Biochemistry*, **1988**, *27*, 7470-7479.

30. (a) Hedman, B.; Co, M. S.; Armstrong, W. H.; Hodgson, K. O.; Lippard, S. J. *Inorg. Chem.*, **1986**, *25*, 3708-3711.

31. Me_3TACN = 1,4,7-trimethyl-1,4,7-triazacyclononane. Hartman, J. R.; Rardin, R. L.; Chaudhuri, P.; Pohl, K.; Wieghardt, K.; Nuber, K.; Weiss, J.; Papaefthymiou, G. C.; Frankel, R. B.; Lippard, S. J. *J. Am. Chem. Soc.* **1987**, *109*, 7387-7396

32. BIPHME = bis(1-methylimidazol-2-yl)phenylmethoxymethane. Tolman, W. B.; Bino, A.; Lippard, S. J. *J. Am. Chem. Soc.* **1989**, *111*, 8522-8523.

33. EXAFS data has been collected on the above models, however fits to the data were not correct.

34. Scott, R. A.; Eidsness, M. K. *Comments Inorg. Chem.* **1988**, *7*, 235-267.

35. Co, M. S.; Scott, R. A.; Hodgson, K. O. *J. Am. Chem. Soc.* **1981**, *103*, 986-988

36. Hasnain, S. S., Ed. *Synchrotron Radiation and Biophysics*; Ellis Horwood Ltd.; Chichester, 1990; Chapters 3 and 4.

37. Westre, T. E.; Di Cicco, A.; Filipponi, A.; Natoli, C. R.; Solomon, E. I.; Hedman, B.; Hodgson, K. O. to be submitted.

38. Nordlund, P.; Sjöberg, B.-M.; Eklund, H. *Nature* **1990**, *345*, 593-598.

39. Kluiber, R. W. *J. Am. Chem. Soc.* **1960**, *82*, 4839-4842.

40. The crystal structure of the Fe complex has not been solved; the distance is based on the average Cr-Br distance for a crystallographically characterized Cr dimer of the same ligand. Estes, E. D.; Scaringe, R. P.; Hatfield, W. E.; Hodgson, D. J. *Inorg. Chem.* **1977**, *16*, 1605-1610. The sample of $Fe(3\text{-}Br\text{-}acac)_3$ was diluted with BN powder, finely ground with a mortar and pestle, and pressed into a 1 mm Al spacer windowed with Mylar tape. The sample was run in transmission mode at SSRL on beamline 7-3 by using a Si(220) monochromator detuned 50% at 7997 eV. The incident and transmitted beam intensity were monitored by using N_2-filled ionization chambers of standard design. The data were collected at 10 K, maintained by a continuous-flow LHe cryostat (Oxford Instruments model CF1208).

41. Shulman, R. G.; Yafet, Y.; Eisenberger, P.; Blumberg, W. E. *Proc. Natl. Acad. Sci. USA* **1976**, *73*, 1384-1388.

42. This transition could also be casued by a quadropole transition, in which case the selection rule is ± 2 and the $1s \rightarrow 3d$ transition is allowed. The authors of reference 41 have estimated that the quadropole transitions would be three orders of magnitude weaker than the intensity of the Fe preedge feature, and concluded that the feature is due to an Fe $1s \rightarrow 3d$ transition made allowed by vibronic coupling of the 4p and 3d states.

43. Roe, A. L.; Schneider, D. J.; Mayer, R. J.; Pyrz, J. W.; Que, L. Jr. *J. Am. Chem. Soc.* **1984**, *106*, 1676-1681.

44. Kau, L.-S.; Spira-Solomon, D. J.; Penner-Hahn, J. E.; Hodgson, K. O.; Solomon, E. I. *J. Am. Chem. Soc.* **1987**, *109*, 6433-6442.

45. The LMCT shake-down transiton involves the transfer of an electron from the valence level of the ligand to the metal 3d manifold made possible by final state relaxation. This transiton occurs at an energy below that of the metal 1s→4p transition by an amount equal to the energy difference between the ligand valence and metal 3d orbitals. The position of the LMCT shake-down feature would be expected to move to lower energy as the covalency of the ligands increased because the valence energy level of a more covalent ligand would be higher than that of a less covalent ligand resulting in a larger energy difference between the ligand and metal orbitals.

Chapter 4

An Investigation of the Model Dependency of EXAFS Data Analysis for Dinuclear Non-Heme Iron Systems

4.1. Introduction

EXAFS has been used for many years to elucidate the local structure around metal atoms in biological systems and has been applied to a wide variety of metalloproteins.[1] We have been using EXAFS to study the structure of the non-heme dinuclear iron center in the hydroxylase component of methane monooxygenase from *Methylococcus capsulatus* (Bath) and *Methylosinus trichosporium* (OB3b).[2] These early studies on the hydroxylase component and relevant dinuclear iron model compounds[3] have revealed the sensitivity of the EXAFS technique to the presence or absence of a μ-oxo bridge in the first coordination sphere of a dinuclear iron center, and the accuracy which can be achieved in determining the average first shell coordination of the iron atoms. Additionally, these investigations have revealed various difficulties arising from the applications of experimentally derived amplitude and phase parameters in fits to second shell data.[2a] However, the use of amplitude and phase functions derived from EXAFS analysis of appropriate model compounds has been shown to give more accurate results in fits to metal foil EXAFS data than the use of theoretical amplitude and phase functions.[4] We have therefore used empirically derived amplitude and phase functions for the investigations discussed in this work.

We have previously discussed fits to the second shell data using second shell Fe-C parameters from $Fe(acac)_3$ (see Chapters 2 and 3 and reference 2a) and have remarked on the ability of the second shell low-Z parameters to mimic a second shell metal-metal interaction, an effect which has been seen by others in fits to binuclear copper and mixed metal systems.[5] We also have noted the high degree of correlation between the Fe-Fe and Fe-C parameters, which makes the interpretation of the results of second shell fits less definitive. A more interesting effect was noted in fits to the second shell oxidized and semimet hydroxylase data with only an iron contribution, which suggested that the fits to the second shell data may exhibit a model bias.[2a]

In the earlier studies, Fe-Fe parameters were obtained from two tribridged models, one which has an oxo bridge and one which has a hydroxo bridge ($[Fe_2O(OAc)_2(HB(pz)_3)_2]$ and $[Fe_2OH(OAc)_2(HB(pz)_3)_2](ClO_4)$).[2] Use of the parameters from either one of these models resulted in the same two minima in least-squares fits to the second shell hydroxylase data at distances separated by about 0.4 Å.[2a] It was found that the minimum which corresponded to the best fit to the data depended on which set of parameters were used. Most significantly, it was found that the shorter Fe-Fe distance was a better fit to the hydroxylse data when the oxo-bridged model (Fe-Fe 3.14 Å) parameters were used, and the longer Fe-Fe distances was a better fit when the hydroxo-bridged model

(Fe-Fe 3.44 Å) parameters were used. Therefore, the best fit to the hydroxylase data corresponded to the fit result with a distance most like the Fe-Fe distance of the model compound used to extract the amplitude and phase parameters employed in the fits, suggesting that the fit results were model-dependent.

To more fully explore the apparent bias of the second shell Fe fits to the hydroxylase data, Fe K-edge EXAFS was collected on 6 dinuclear iron models. The data from these 6 models plus the 3 models previously investigated[2] were used to investigate model dependence of second shell fit results for dinuclear non-heme iron centers. Di- and tribridged models with a variety of bridging groups and Fe-Fe distances were used in this study to determine if the model dependence was a function of the numbers of bridges, the types of bridges, or the Fe-Fe distance. Fits to the data which included a low-Z atom contribution were done for some of the models to test the capabilities of the Fe-Fe and Fe-C parameters to discriminate between Fe and C contributions occuring at the same distance. In addition, the model compounds investigated represented a range of different ligation to the Fe atoms, from 6 O atoms to 3 O and 3 N atoms. Fits to the first shell data of these models as well as to the first shell data for two iron monomers (with 6 O and 6 N atoms in the first shell, respectively) were done to investigate the ability of EXAFS to distinguish between different numbers of N and O atoms in the first coordination sphere.

4.2. Experimental

The model compounds investigated for this study are summarized in Table 4.1.[6] The compounds were synthesized according to the references listed in the Table with the following exceptions. All of the tribridged samples were provided by Prof. Stephen Lippard of the Massachusetts Institute of Technology. The SALMP dibridged compounds in all three oxidation states were provided by Prof. Richard Holm of Harvard University.

Data for $[Fe_2(OH)(OAc)_2(HB(pz)_3)_2](ClO_4)_2$,[6d] $[Fe_2O(OAc)_2(HB(pz)_3)_2]$,[6e] $[FeO(O_2CH)_4(BIPhMe)_2](CH_3OH)$,[6c] $[Fe(acac)_3]$[6h,i] and the oxidized and semimet forms of the hydroxylase component of MMO from *Methylococcus capsulatus* (Bath) (**EXAFS5** and **EXAFS2** respectively) were collected as previously described.[2] Samples for XAS experiments were diluted with BN powder, finely ground with a mortar and pestle, and pressed into a 1mm thick Al sample spacer windowed with Mylar tape (total sample weight, ~ 55 mg). The samples were run in transmission mode at the Stanford Synchrotron Radiation Laboratory (SSRL) on unfocused 8-pole wiggler beamlines 4-3 or 7-3 (18 kG) or on unfocused bending magnet beamline X19A at the National Synchrotron Light Source (NSLS) at Brookhaven National Laboratory using either a Si(220) or a

Table 4.1. Summary of Information for Dinuclear and Mononuclear Model Compounds.

Sample	$[FeOH(H_2O)Chel]_2(H_2O)_4$	$[FeOH(H_2O)Dipic]_2$	$[Fe_2(salmp)_2]\cdot 2DMF$
Reference	6a	6a	6b
Sample Name	**FECHEL**[a]	**FEDIPIC**[a]	**FESALMP0**[a]
Experimental	Beamline 7-3, Si(111)[b]	Beamline 4-3, Si(220), 1 pt.[b]	Beamline 7-3, Si(220), 6 pts.[b]
Oxidation State	diferric, Fe(III)/Fe(III)	diferric, Fe(III)/Fe(III)	diferric, Fe(III)/Fe(III)
Bridging Geometry	dibridged, $(OH)_2$	dibridged, $(OH)_2$	dibridged, $(OPh)_2$[c]
First Shell Ligation	5 O, 1 N	5 O, 1 N	4 O, 2 N
Fe-O_{br} (Å)	1.938, 1.989 (1.964)	1.938, 1.993 (1.966)	2.023, 2.064 (2.044)
Fe-O^d (Å)	2.044	2.021	
Fe-O^e (Å)	2.064, 2.021 (2.043)	2.078, 2.053 (2.066)	1.894, 1.921 (1.908)
Fe-N (Å)	2.057	2.070	2.156, 2.138 (2.147)
Fe-$N_{trans\ oxo}$ (Å)			
Fe-Fe (Å)	3.078	3.089	3.063
Fe-O_{br}-Fe angle (°)	103.2	102.9	97.06

Table 4.1. continued

Sample	$[Fe_2OH(OAc)_2(HB(pz)_3)_2)](ClO_4)$	$[Fe_2O(OAc)_2(HB(pz)_3)_2)]$	$[Fe_2O(OAc)_2\{[OP(OEt)_2]_3Co(C_5H_5)\}_2]$
Reference	6c	6d	6e
Sample Name	**FEHBPZOH**[f]	**FEHBPZO**[f]	**FE2CO2**[f]
Experimental	Beamline 2-2, Si(111)[g]	Beamline 2-2, Si(111)[g]	Beamline X19A, Si(220)[b]
Oxidation State	diferric, Fe(III)/Fe(III)	diferric, Fe(III)/Fe(III)	diferric, Fe(III)/Fe(III)
Bridging Geometry	tribridged, $(OH)(OAc)_2$	tribridged, $O(OAc)_2$	tribridged, $O(OAc)_2$
First Shell Ligation	3 O, 3 N	3 O, 3 N	6 O
Fe-O_{br} (Å)	1.956	1.785	1.795
Fe-O^d (Å)	1.999	2.044	2.028
Fe-O^e (Å)			2.06, 2.13[h]
Fe-N (Å)	2.094	2.151	
Fe-$N_{trans\ oxo}$ (Å)	2.109	2.187	
Fe-Fe (Å)	3.439	3.145	3.174
Fe-O_{br}-Fe angle (°)	123.1	123.5	124.4

Table 4.1. continued

Sample	$[Fe_2O(O_2CH)_4(BIPhMe](CH_3OH)$	$(Et_4N)[Fe_2(salmp)_2]\cdot 2DMF$	$(Et_4N)_2[Fe_2(salmp)_2]\cdot 4MeCN$
Reference	6f	6b	6b
Sample Name	**FE3BIPHME**[f]	**FESALMP1**[i]	**FESALMP2**[a]
Experimental	Beamline 7-3, Si(220)[g]	Beamline 7-3, Si(220), 6 pts.[b]	Beamline 7-3, Si(220), 3 pts.[b]
Oxidation State	diferric, Fe(III)/Fe(III)	semimet, Fe(II)/Fe(III)	diferrous, Fe(II)/Fe(II)
Bridging Geometry	tribridged, $O(O_2CH)_2$	dibridged, $(OPh)_2$[c]	dibridged, $(OPh)_2$[c]
First Shell Ligation	4 O, 2 N	4 O, 2 N	4 O, 2 N
Fe-O_{br} (Å)	1.789	2.102, 2.079; 2.068, 2.115	2.157, 2.162 (2.160)
Fe-O^d (Å)	2.08		
Fe-O^e (Å)	2.03	1.961, 1.991; 1.970, 1.994	2.064, 2.049 (2.057)
Fe-N (Å)	2.12	2.177, 2.180; 2.177, 2.158	2.176, 2.175 (2.176)
Fe-$N_{trans\ oxo}$ (Å)	2.16		
Fe-Fe (Å)	3.201	3.081; 3.116	3.202
Fe-O_{br}-Fe angle (°)	127.0	94.9; 96.3	95.8

Table 4.1. continued

Sample	$[Fe(HB(pz)_3)_2](ClO_4)$	[Fe(acetylacetonate)$_3$]
Reference	6g	6h,i
Sample Name	**FE3HBPZ**	**FEACAC**
Experimental	Beamline 7-3, Si(111)[b]	Beamline 2-2, Si(111)[h]
Oxidation State	ferric, Fe(III)	ferric, Fe(III)
Bridging Geometry	mononuclear	mononuclear
First Shell Ligation	6 N	6 O
Fe-N (Å)	1.95	
Fe-O (Å)		1.99

[a]The iron site is centrosymmetric, so only one set of distances is reported. Average values are listed in parentheses. [b]This work. [c]The bridge derives from the ligand coordinating the iron atoms. Two additional extended bridges involving the N atoms are also present. [d]For **FECHEL** and **FEDIPIC**, the Fe-O distance corresponds to terminal H_2O groups. For **FEHBPZOH**, **FEHBPZO** and **FE2CO2**, the Fe-O distance is for the bridging acetate groups. For **FE3BIPH**, the Fe-O distance is for the bridging formate groups. [e]For **FECHEL** and **FEDIPIC**, the Fe-O distance is for ligand-derived O. For **FE3BIPH**, the Fe-O distance corresponds to the terminal formate groups. [f]The distances reported are the average distances. [g]Data collection for these samples have been previously reported (refs. 2 and 3). [h]This distance is the average distance of oxygen atoms trans to the oxo bridge. The other distance is the average distance of oxygen atoms *cis* to the oxo bridge. [i]The **FESALMP1** compound has two centrosymmetric iron sites. The distances corresponding to each are separated by a semicolon in the table.

Si(111) monochromator (see Table 4.1). Ring operating conditions were 3.0 GeV and 40-90 mA at SSRL, and 2.5 GeV and 90-200 mA at NSLS. Higher harmonics in the incident beam were rejected by detuning the monochromator 50% at 7820 eV on beamline X19A, and at 7997 eV on beamlines 4-3 and 7-3. The incident and transmitted beam intensity were monitored by using N_2-filled ionization chambers of standard design. The temperature of the samples was 10 K maintained by a continuous flow LHe cryostat (Oxford Instruments model CF1208).

Energy calibration for each scan was perfomed by using an internal foil calibration method[7], setting the energy of the first inflection point of an iron foil as 7111.2 eV. More than one scan was measured to insure reproducibility of the data. In general, 4 scans were averaged together for each sample and a single-point replacement method was used to remove monochromator glitches in the averaged data where necessary (see Table 4.1). The data were background subtracted by fitting a polynomial to the EXAFS region which was extrapolated through the preedge region and subtracted. A three or four segment spline was fit to the postedge region and subtracted to isolate the EXAFS data and to normalize the edge jump to unity. The spline was chosen so that it removed the low frequency noise without reducing the true EXAFS amplitude; this was checked by monitoring the Fourier transform of the EXAFS data during the normalization process. The normalized data were converted to k space, where k is the photoelectron wavevector defined by $[2m_e(E - E_o)/\hbar^2]^{1/2}$. In this expression, m_e is the electron rest mass, E is the photon energy (eV), E_o is the threshold energy (7130 eV for iron, where $k = 0$) and $\hbar$ is Planck's constant divided by 2π.

The EXAFS data between 3.5 and 12.5 $Å^{-1}$ for all of the models with the exception of **FE2CO2** and **FESALMP2** were Fourier transformed to R (Å) space to isolate the first and second shell contributions to the data. For **FE2CO2**, the data between 3.8 and 12.3 $Å^{-1}$ were Fourier transformed to R (Å) space due to the presence of the Co edge above 12.3 $Å^{-1}$ and duplicated data points in the region between 3.5 and 3.8 $Å^{-1}$ caused by a problem in the data aquisition program. For **FESALMP2**, the data between 3.5 and 12.3 $Å^{-1}$ were Fourier transformed to R (Å) space because of a spike in the data above 12.3 $Å^{-1}$ which was too broad to be removed by the standard editing methods without the risk of altering the data.

The individual first and second shell contributions to the data were backtransformed to k space and fit from 4.0 to 12.0 $Å^{-1}$. The windows used to isolate the peaks in the Fourier transforms for the backtransforms are presented in the tables of the fit results. A gaussian window of width 0.1 Å was applied to minimize truncation artifacts introduced by the Fourier transform technique. Non-linear least-squares curve-fitting techniques using

empirical amplitude and phase parameters were used to analyze the data, as described in Chapter 1 and elsewhere.[8] All curve fitting was based on k^3-weighted data and applied to individual filtered shells. Only the structure-dependent parameters, i.e. the distance and the number of atoms in the shell were allowed to vary in the refinements. A "goodness-of-fit" parameter, F, was calculated as $F = \{[k^6(\text{data} - \text{fit})^2]/(\text{no. of points})\}^{1/2}$ for each fit. The fits proceeded by allowing the initial coordination numbers and distances for an Fe-X pair of interest to vary. Empircal amplitude and phase parameters for the first coordination shell Fe-X scattering pairs of interest were obtained from the following models: Fe-N from [Fe(1,10-phenanthroline)$_3$](ClO$_4$)$_3$;[9] Fe-O from [Fe(acetylacetonate)$_3$].[6h,i] Data for these samples were collected as previously described.[2]

For second shell fits to the data, Fe-Fe parameters were extracted from 6 of the model compounds discussed in this paper, chosen to represent a variety of Fe-Fe distances and bridging geometries. The Fe-Fe parameters were extracted by fitting the second shell data using the correct Fe-Fe distance from the crystal structure of the model compound, a coordination number of 1, and initial amplitude and phase parameters from one of the standards previously used for second shell Fe-Fe fits (**FEHBPZO** or **FEHBPZOH**, see Chapters 2 and 3). The amplitude and phase parameters were allowed to vary in an iterative manner with the distance and coordination number fixed. In the first cycle, all of the amplitude and phase parameters were allowed to vary. The optimized parameters were then used as the starting point for the next iteration by successively allowing just the amplitude or the phase parameters to vary in the fits to the data. Once the sets of amplitude and phase parameters no longer changed during the fits (after 4 cycles), all of the parameters were allowed to vary for the final iteration. The parameters thus obtained were confirmed by repeating the method using initial amplitude and phase parameters from the other Fe-Fe standard, and verifying that the Fe-Fe parameters for the new model compound refined to the same values independently of the initial starting values. These parameters were then applied in fits to the second shell data of all of the dimers and to the second shell data of the oxidized and semimet forms of the hydroxylase of MMO from *Methylococcus capsulatus* (Bath).

4.3. Results of Fits to the Model Data

The model compounds used in this investigation were predominantly ferric, and all were octahedrally coordinated by a mixture of N and O atoms, ranging from 6 N (**FE3HBPZ**, monomeric ferric compound) to 6 O (**FEACAC**, monomeric ferric compound and **FE2CO2**, ferric dimer) with various combinations of N and O ligation

represented in the series (Table 4.1). Both di- and tri-bridged compounds were investigated, with the bridging groups consisting of combinations of hydroxo, alkoxo, oxo and carboxylato ligands (Table 4.1). The Fe-Fe distances represented by the compounds discussed below range between 3.06 and 3.44 Å, and the Fe-O_{br}-Fe angles range from 94.9° to 124.4°. Most of the classes of multiply-bridged diferric non-heme iron models currently available[10] are represented by the compounds listed in Table 4.1. The exception is the dibridged (μ-oxo)(μ-carboxylato) models.[11] The data should provide a sufficient framework to investigate the trends and limitations of the empirical non-linear least-squares fitting approach used in XAS studies of dinuclear non-heme iron centers. The EXAFS data of the model compounds discussed in this paper are presented in Figures 4.1-4.3, and the Fourier transforms of the EXAFS data in Figures 4.4-4.6.

4.3.1. A Description of the Trends Seen in First Shell Fits.

The results of the fits to the first shell data are presented in Table 4.2. The results presented in the Table will not be exhaustively discussed; rather, a few models will be discussed to illustrate the general trends noted. Fits to the data were attempted with single N and single O contributions, with two N or two O contributions, and with a combined N and O contribution. For the monomeric models **FEACAC** and **FE3HBPZ**, which have respectively an octahedral first shell of O or N atoms, the fits with more than a single contribution resulted in either unreasonably high or negative coordination numbers. The fits with just a single N or O contribution (Table 4.2, fits 4.2-1, 4.2-2, 4.2-3, 4.2-4) were satisfactory in each case, but a better fit was obtained with only N atoms for **FE3HBPZ** (Table 4.2, fit 4.2-1). For **FEACAC**, a better fit was obtained for the O-only fit (Table 4.2, fit 4.2-4), which is not surprising when one considers that the parameters used for this fit were obtained from **FEACAC**.

For the dimeric models, which have a mixed N and O first shell environment at a range of distances, the fits consisting of just a single N or O contribution resulted in low coordination numbers. The best fits to the data corresponded to two separate contributions (either two N, two O, or N and O) at different distances for the non-oxo-bridged models. For example, for **FEHBPZOH**, the addition of an O contribution to the N contribution results in the total coordination number increasing from 4 (Table 4.2, fit 4.2-23) to ~ 6 (Table 4.2, fits 4.2-27 and 4.2-28) with a drop in the fit function, F, from 0.95 to 0.22. The improvement seen in the fit to the first shell data of **FEHBPZOH** with the addition of a second contribution is presented in Figure 4.7. For the oxo-bridged models, a third contribution corresponding to the Fe-O_{oxo} distance was required in addition to the other

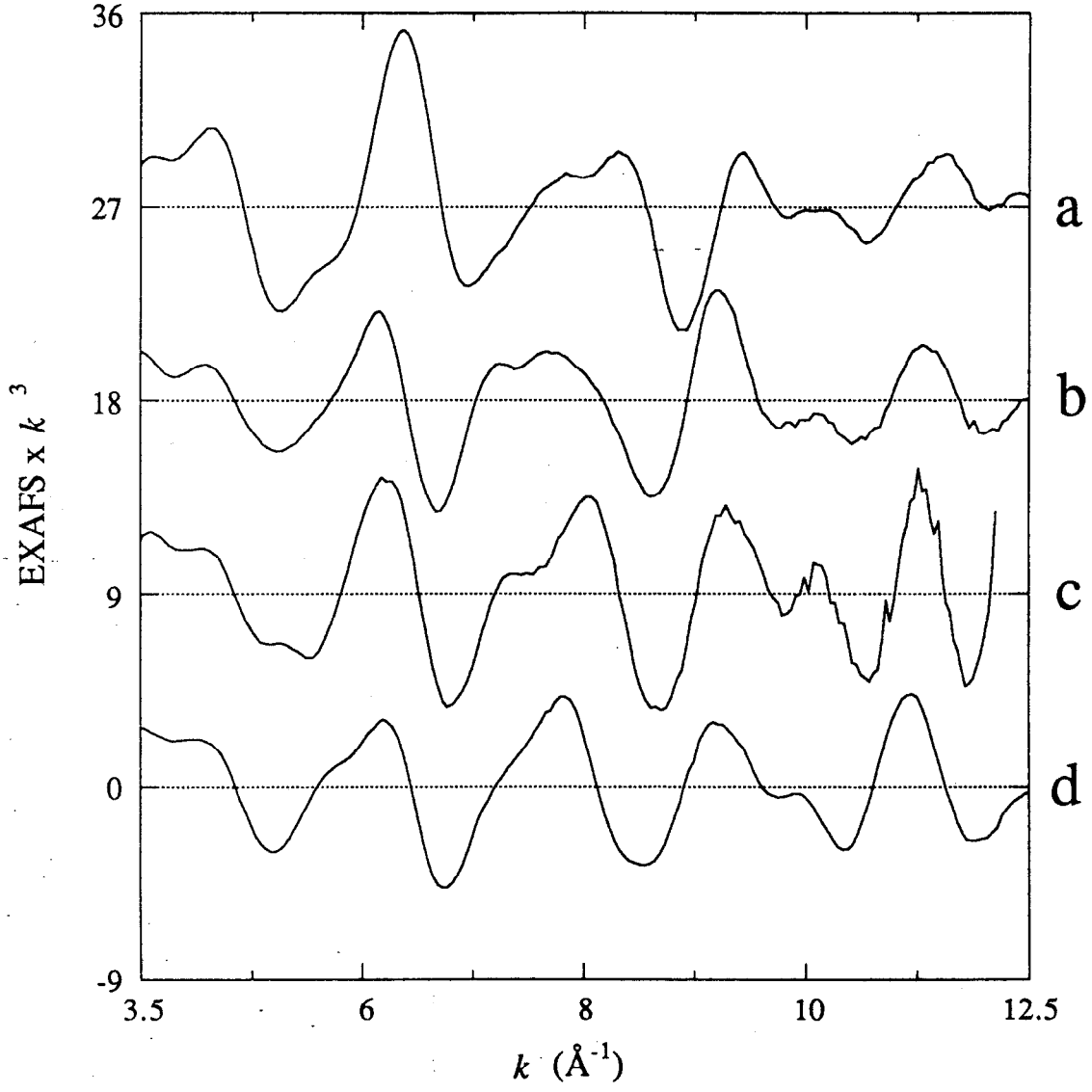

Figure 4.1. EXAFS of tribridged model compounds. (a) **FEHBPZOH**, (b) **FEHBPZO**, (c) **FE2CO2**, (d) **FE3BIPHME**.

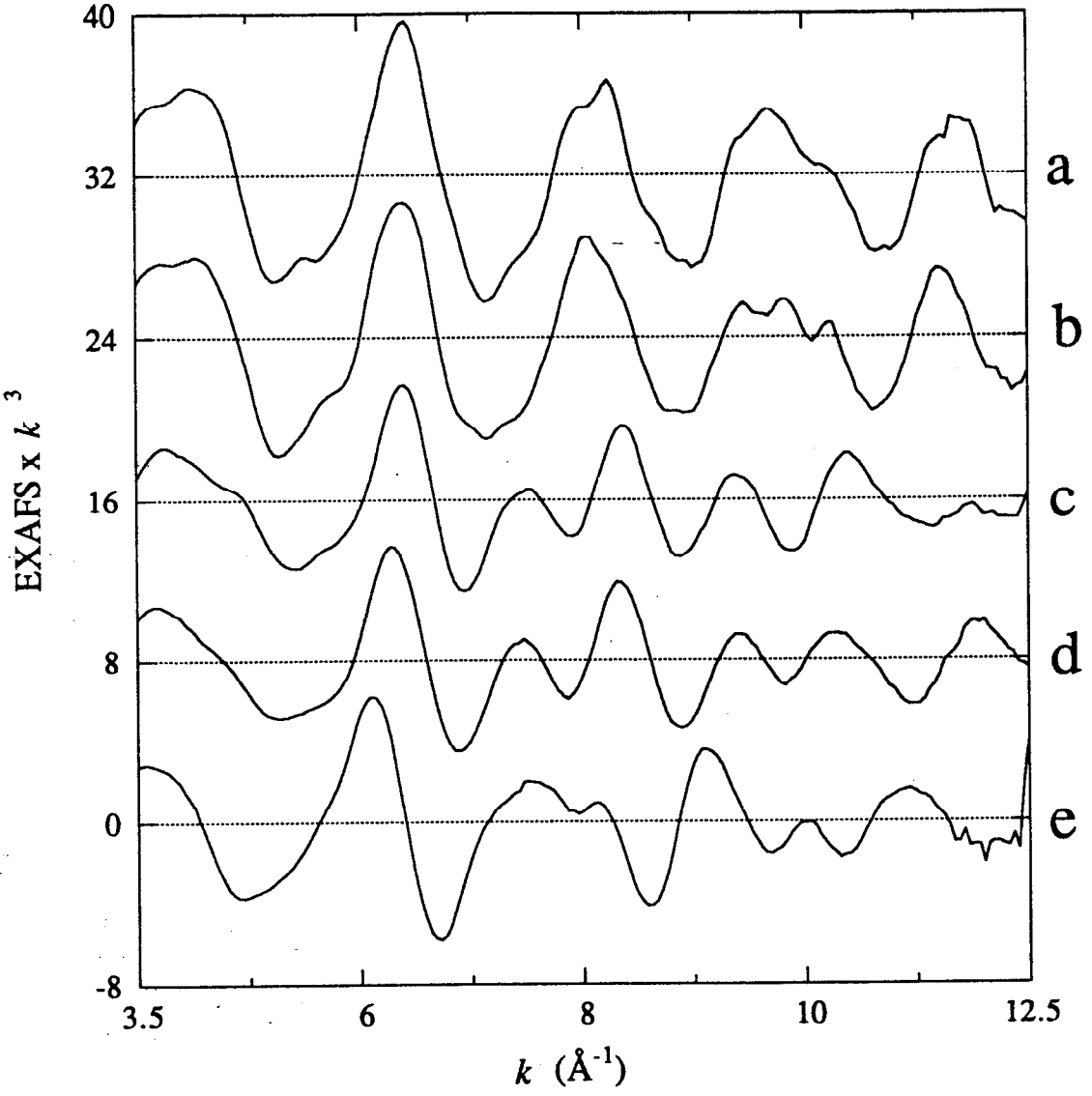

Figure 4.2. EXAFS of dibridged model compounds. (a) **FECHEL** , (b) **FEDIPIC**, (c) **FESALMP0**, (d) **FESALMP1**, (e) **FESALMP2**.

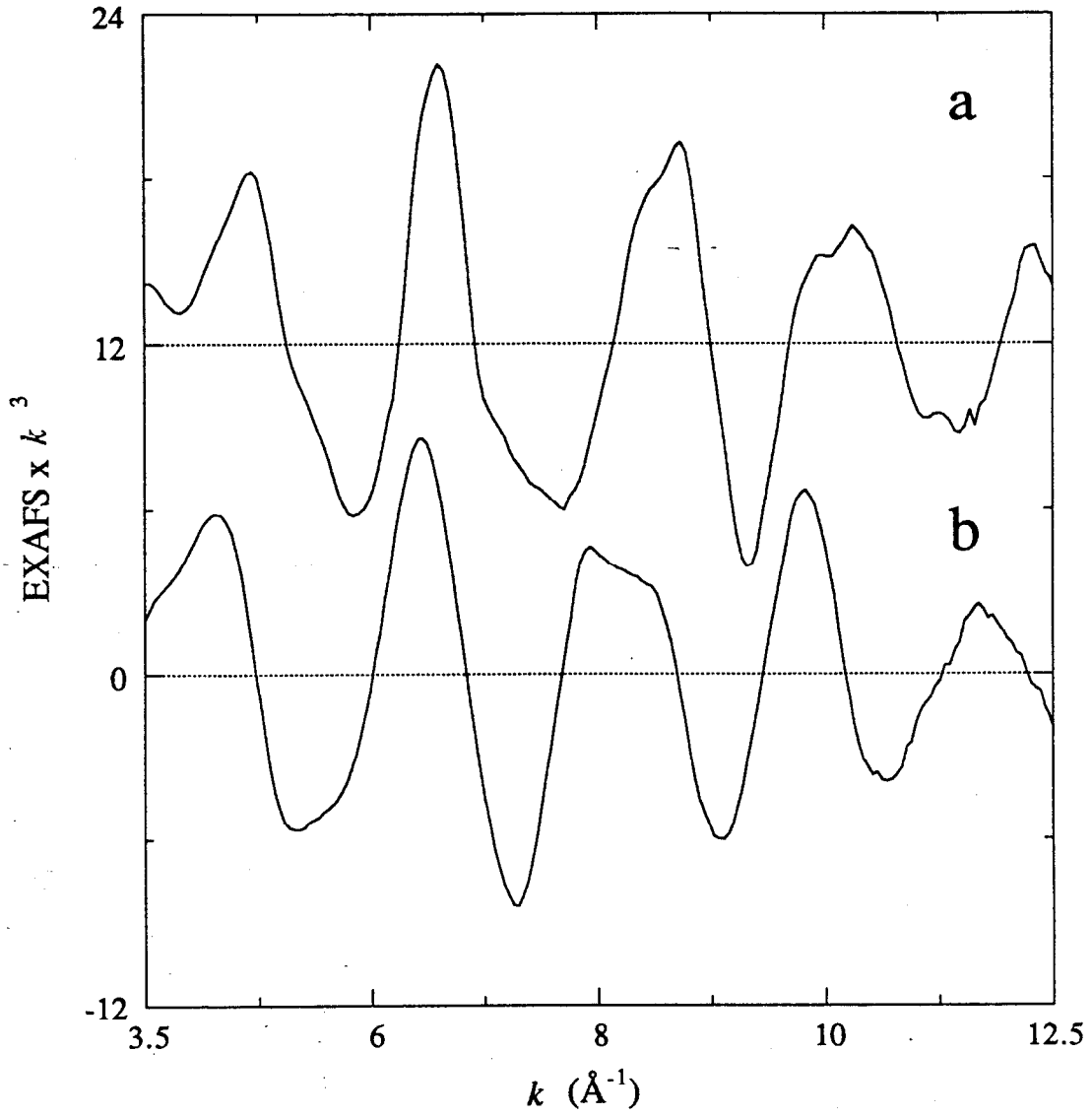

Figure 4.3. EXAFS of monomeric model compounds. (a) **FE3HBPZ**, (b) **FEACAC**.

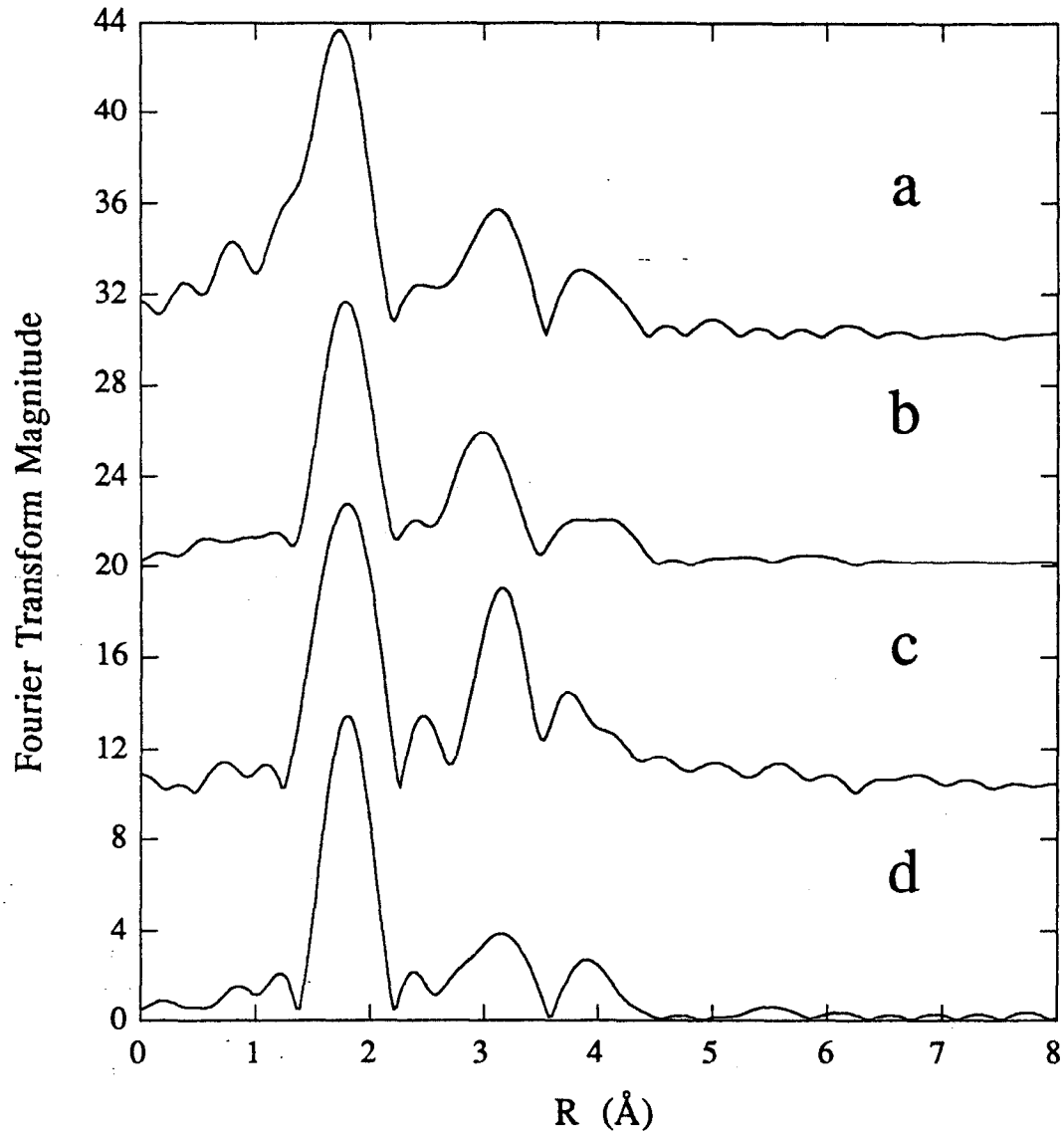

Figure 4.4. Fourier transforms of the EXAFS of tribridged model compounds (Figure 4.1). (a) **FEHBPZOH**, (b) **FEHBPZO**, (c) **FE2CO2**, (d) **FE3BIPHME**.

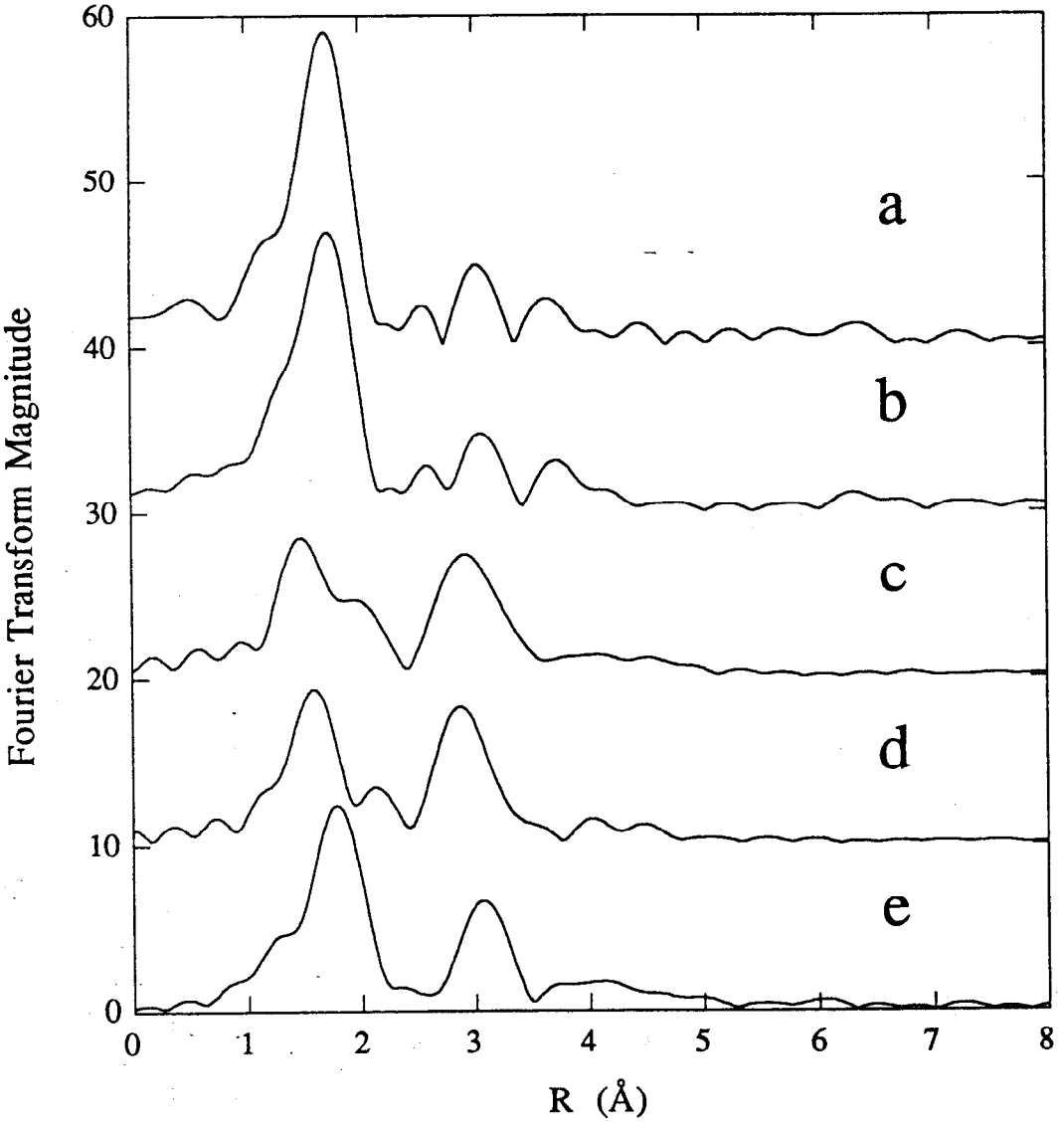

Figure 4.5. Fourier transforms of the EXAFS of dibridged model compounds (Figure 4.2). (a) **FECHEL**, (b) **FEDIPIC**, (c) **FESALMP0**, (d) **FESALMP1**, (e) **FESALMP2**.

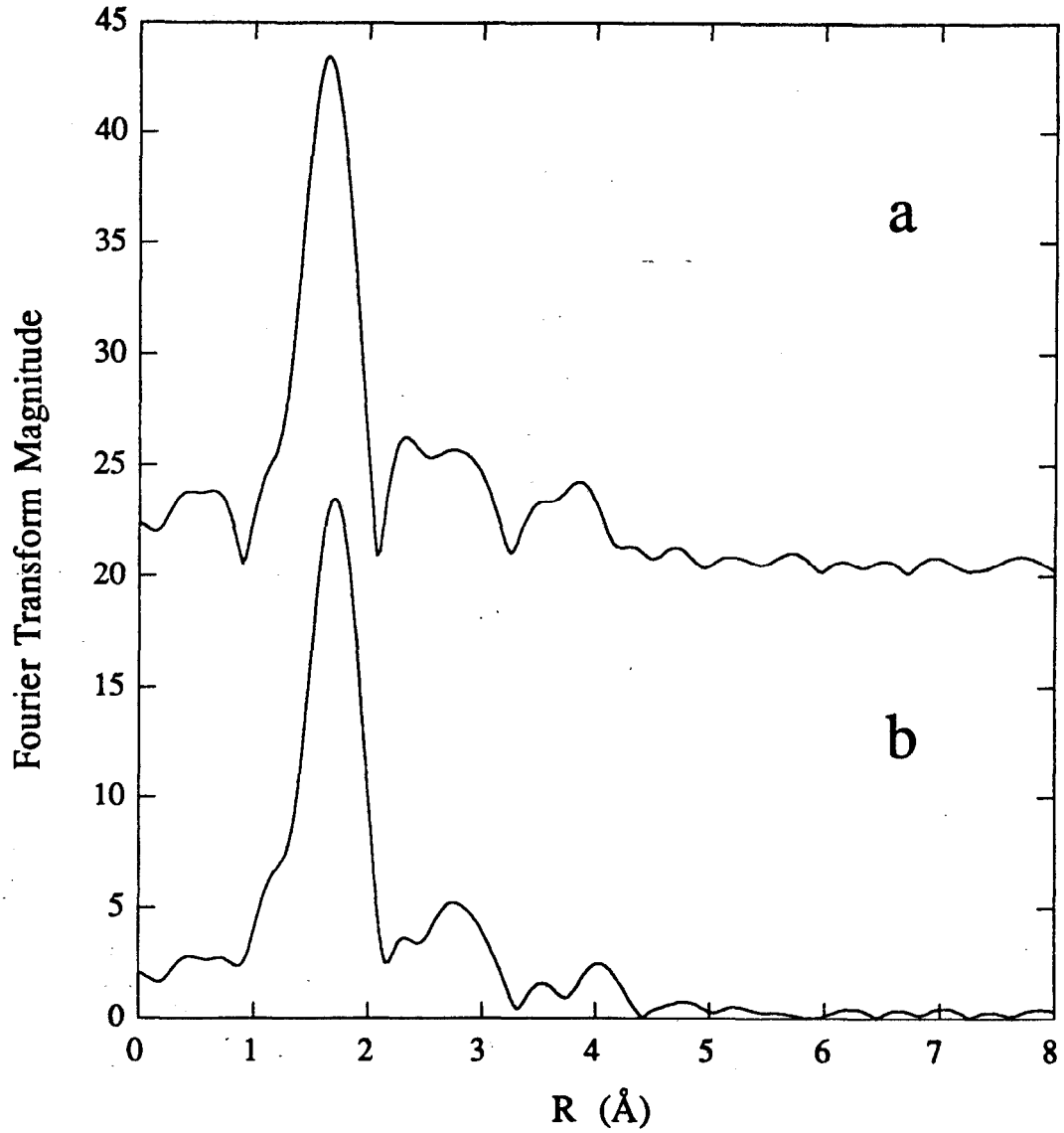

Figure 4.6. Fourier transforms of the EXAFS of monomeric model compounds (Figure 4.3). (a) **FE3HBPZ**, (b) **FEACAC**.

Table 4.2. Results of First Shell Fits[a] to the Model Data.

Sample	Window Width (Å)	Fit	N		O		F
			CN[b]	R(Å)	CN	R(Å)	
FE3HBPZ	0.80 - 2.00	4.2-1	6.7	1.94			0.48
		4.2-2			5.4	1.92	0.64
FEACAC	0.70 - 2.15	4.2-3	7.3	2.02			0.72
		4.2-4			6.0	1.99	0.25
FECHEL	0.75 - 2.15	4.2-5	5.9	2.03			0.80
		4.2-6			4.9	2.00	0.41
		4.2-7	4.2	2.08			0.42
			4.4	1.98			
		4.2-8			0.9	2.08	0.37
					4.5	1.99	
		4.2-9	0.7	2.15	4.9	1.99	0.37
		4.2-10	0.96	1.95	4.6	2.01	0.38
FEDIPIC	0.85 - 2.10	4.2-11	5.3	2.04			0.90
		4.2-12			4.5	2.01	0.43
		4.2-13	0.8	2.51			0.32
			5.2	2.04			
		4.2-14			3.5	2.04	0.27
					2.0	1.95	
		4.2-15	2.2	2.11	4.0	1.98	0.28

Table 4.2. continued

Sample	Window Width (Å)	Fit	N		O		F
			CN[b]	R(Å)	CN	R(Å)	
FEDIPIC cont.		4.2-16	1.2	1.93	4.6	2.02	0.27
FESALMP0	0.95 - 2.30	4.2-17	1.8	2.02			1.25
		4.2-18			1.7	2.00	1.08
		4.2-19	3.8	2.13			0.30
			3.5	1.96			
		4.2-20			2.7	2.10	0.38
					2.5	1.93	
		4.2-21	3.3	2.14	2.8	1.95	0.36
		4.2-22	3.0	1.94	3.0	2.08	0.30
FEHBPZOH	0.85 - 2.10	4.2-23	4.3	2.04			0.95
		4.2-24			3.7	2.02	0.59
		4.2-25	3.4	1.97			0.33
			4.6	2.10			
		4.2-26			1.9	1.94	0.29
					3.4	2.06	
		4.2-27	2.9	2.13	3.8	1.98	0.27
		4.2-28	2.2	1.95	4.2	2.05	0.27

Table 4.2. continued

Sample	Window Width (Å)	Fit	N		O		F
			CN[b]	R(Å)	CN	R(Å)	
FEHBPZO[c]	1.2 - 2.15	4.2-29	3.7	2.12			0.62
		4.2-30			3.0	2.10	0.66
		4.2-31	1.4	2.24	3.4	2.07	0.15
					0.99	1.78	
		4.2-32	2.3	2.07	2.3	2.16	0.12
					0.95	1.79	
FE2CO2[c]	1.1 - 2.15	4.2-33	4.4	2.09			0.54
		4.2-34			3.6	2.06	0.48
		4.2-35			3.7	2.08	0.21
					1.2	1.95	
					0.8	1.72	
		4.2-36	3.4	2.14	2.6	1.99	0.18
					0.8	1.72	
FE3BIPHME[c]	1.2 - 2.15	4.2-37	4.2	2.11			0.55
		4.2-38			3.3	2.09	0.70
		4.2-39	0.7	2.27	3.8	2.08	0.17
					1.0	1.78	
		4.2-40	4.0	2.09	1.6	2.16	0.12
					0.9	1.80	

Table 4.2. continued

Sample	Window Width (Å)	Fit	N		O		F
			CN[b]	R(Å)	CN	R(Å)	
FESALMP1	0.80 - 1.9	4.2-41	2.2	2.03			1.1
		4.2-42			1.9	2.01	0.96
		4.2-43	3.4	2.18			0.25
			4.1	2.00			
		4.2-44			3.1	1.98	0.25
					2.4	2.16	
		4.2-45	3.0	2.19	3.3	1.99	0.25
		4.2-46	3.7	1.99	2.7	2.13	0.23
FESALMP2	0.80 - 2.20	4.2-47	4.0	2.14			0.88
		4.2-48			3.5	2.11	0.60
		4.2-49	3.5	2.23			0.33
			4.6	2.09			
		4.2-50			3.5	2.08	0.26
					1.9	2.21	
		4.2-51	2.1	2.26	4.0	2.09	0.26
		4.2-52	3.3	2.08	3.0	2.17	0.31

[a]Fitting range $k = 4 - 12$ Å^{-1}. Errors are estimated to be about $\pm$ 0.03 Å for distances and 25% for coordination numbers.[8] [b]CN = coordination number. [c]Fits to the data without the inclusion of the short Fe-O contribution resulted in negative coordination numbers.

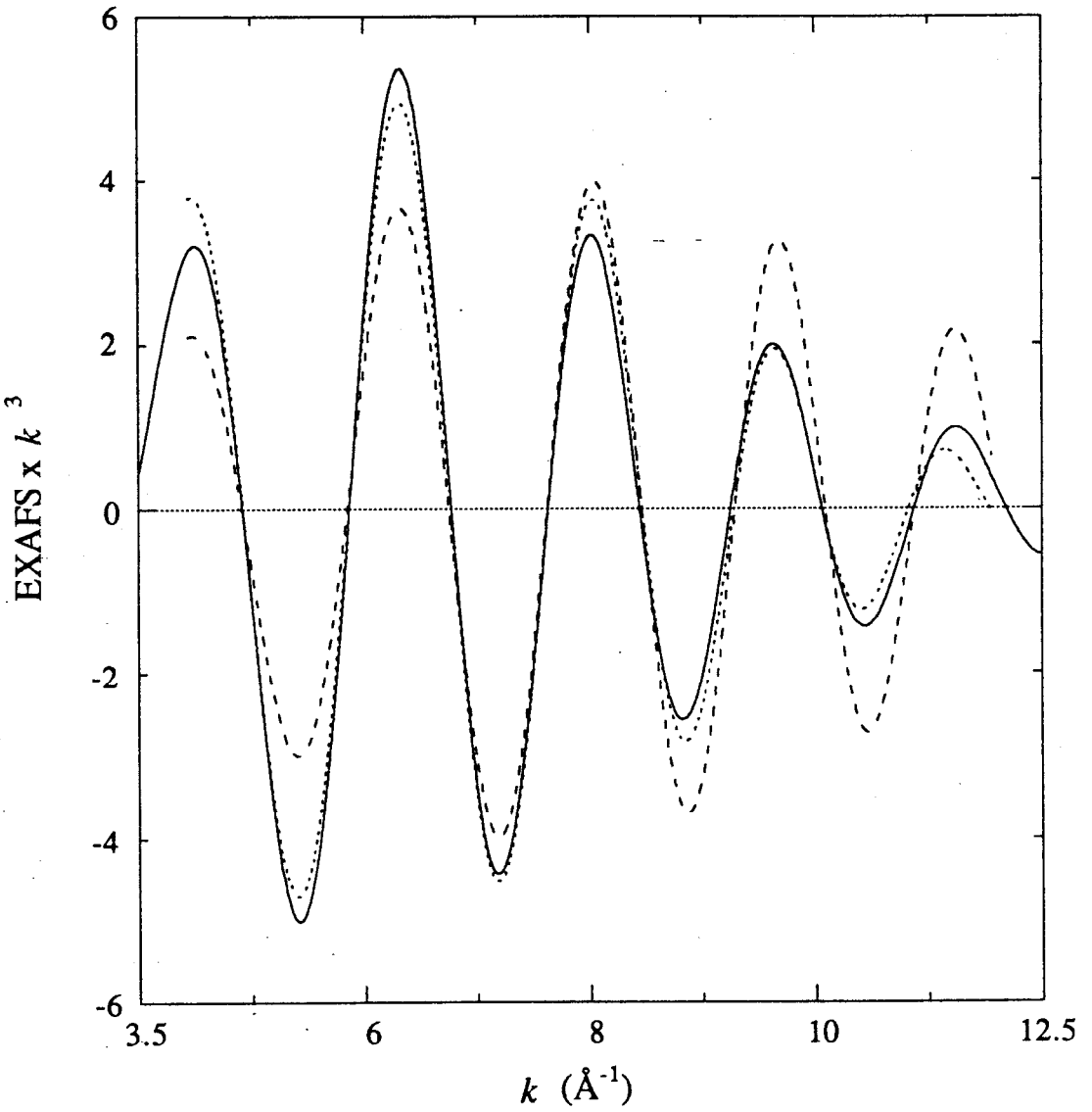

Figure 4.7. Fits to the first shell data of **FEHBPZOH**. The solid line is the data, the dashed line is the fit to the data with only N (Table 4.2, fit 4.2-23), and the dotted line is the fit to the data with N and O (Table 4.2, fit 4.2-27). Note the improvement in the fit in the high k region with the addition of a second contribution.

two contributions. Attempts to fit the data with N and O only, without the short Fe-O contribution resulted in negative or unreasonably high coordination numbers. However, the addition of a short Fe-O contribution resulted in a total coordination number of ~ 6 with a fit function of 0.12 - 0.15 for **FEHBPZO** (Table 4.2, fit 4.2-31 and 4.2-32). For the fits to the **FEHBPZO** data with a single N or O contribution, the coordination number was ~ 3 and the fit function was 0.62 - 0.66 (Table 4.2, fit 4.2-29 and 4.2-30). As noted before in fits to the MMO hydroxylase data (see Chapters 2 and 3), two minima were found for the N/O fits to the data, depending on the relative initial Fe-N and Fe-O distances used in the fits. This arises from the correlation of the amplitude and phase functions which describe the Fe-N and Fe-O interactions over the range of data available. The satisfactory results obtained by the two N and two O fits to the mixed N/O dimers reflects the similar backscattering strength of N and O atoms. The distance distribution rather than the atom type appears to be determining factor in the number of contributions required to fit the data.

Dimers with different numbers of N and O atoms were fit to determine if the fitting technique could discriminate between different ratios of N and O atoms in the first shell. Both **FECHEL** and **FEDIPIC** have 5 O and 1 N in the first coordination sphere, and good fits to the data were obtained with approximately 1 N at 1.93-1.95 Å and 4.6 O at 2.01-2.02 Å (Table 4.2, fits 4.2-10 and 4.2-16). The results of the fits agree with the crystallographic distances and coordination numbers (Table 4.1), however the result assigns the wrong atom type to the short distance. The 1.9 Å distance should be an oxygen atom, and the Fe-N distance should be 2.057 Å for **FECHEL** and 2.070 Å for **FEDIPIC**. Attempts to obtain a fit with a single short O contribution and 5 N contributions at the longer distance were unsuccesful, and in fits to the data with two O contributions (Table 4.2, fit 4.2-8 and 4.2-14), the lower contribution corresponded to the longer distance instead of to the shorter distance. The O-only fits to the data gave a satisfactory result as well (Table 4.2, fit 4.2-6 and 4.2-12). **FESALMP0** is coordinated by 4 O atoms at an average distance of 1.98 Å and 2 N atoms at an average distance of 2.15 Å (Table 4.1), but the best fits corresponded to either 3.3 N at 2.14 Å and 2.8 O at 1.95 Å (Table 4.2, fit 4.2-21) or 3.0 N at 1.94 Å and 3.0 O at 2.08 Å (Table 4.2, fit 4.2-22). The distances are within the expected 0.03 Å error for the crystallographic data based on atom type, but the coordination numbers are inaccurate. These results suggests that the relative numbers of N and O atoms cannot be reliably determined from the fits.

The model **FE2CO2** has an all O environment with a single oxygen atom at 1.795 Å and the remaining oxygen atoms at an average distance of 2.06 Å. The most reasonable fit to the data suggests that the non-oxo-bridge ligands correspond to a distribution of 1.2 O at 1.95 Å and 3.7 O at 2.08 Å (Table 4.2, fit 4.2-35), however there is no Fe-O distance at

1.95 Å according to the crystal structure. The coordination-weighted average distance for this fit, 4.9 O at 2.05 Å, is in good agreement with the crystallographic data. The coordination-weighted average distances for fits to the model compounds are listed in Table 4.3 along with the average distance calculated from the crystallographic data. There is excellent agreement between the crystallographic average and the EXAFS average for all of the model compounds. This illustrates that accurate information can be obtained by considering the coordination-weighted average distance from the fit results, even if the individual contributions are not accurate.

Fits were also done to the semimet and diferrous model compounds with the SALMP ligand, **FESALMP1** and **FESALMP2** and the results are also presented in Table 4.2 with the coordination-weighted averages given in Table 4.3. For the corresponding diferric model, **FESALMP0**, the average first shell distance from the crystal structure was 6 N/O at 2.03 Å and the average based on the EXAFS analysis was 6.1 N/O at 2.05 Å (Table 4.2, fit 4.2-21). The result of fits to the semimet data was 6.3 N/O at 2.09 Å (Table 4.2, fit 4.2-45), which agrees quite well with the crystallographic average of 6 N/O at 2.08 Å. For the reduced data, the average coordination was found to be 6.1 N/O at 2.15 Å (Table 4.2, fit 4.2-51), also in good agreement with the crystallographic data (6 N/O at 2.13 Å). The average distance in the first coordination sphere increases by 0.05 Å going from the diferric to the semimet oxidation state (2.03 to 2.08 Å) and by another 0.05 Å upon reduction to the diferrous state (to 2.13 Å) according to the crystal structures. The fit results reflect this trend, with the average distance increasing by 0.04 Å between the diferric and semimet states, and by an additional 0.04 Å to the diferrous state. The parameters used for the first shell fits, and the method of considering the coordination-weighted average of the fit result, therefore accurately reflect the increase in the Fe-ligand distances which occurs upon reduction of the diiron site.

4.3.2. The Dependence of Second Shell Fits on Choice of Model Compound

4.3.2.1. Investigation with Model Data. The model compounds chosen to test the transferability of the Fe-Fe parameters and the results of the fits to the second shell model data are listed in Table 4.4. Parameters were extracted from two diferric dibridged models (3.063 Å and 3.078 Å Fe-Fe distance), three diferric tribridged models (3.439 Å, 3.143 Å, and 3.20 Å Fe-Fe distance) and a diferrous dibridged model (3.20 Å Fe-Fe distance) and used in fits to each other as well as to other models. In every case, two minima separated by approximately 0.4 Å were found in fits to the second shell data,

Table 4.3. A Comparison of the Average First Shell Distances by EXAFS and Crystallography.

	Average First Shell Coordination	
Sample	from EXAFS analysis[a]	from crystal structure
FE3HBPZ	6.7 N at 1.94 Å	6 N at 1.95 Å
FEACAC	6.0 O at 1.99 Å	6 O at 1.99 Å
FECHEL	5.6 N/O at 2.01 Å	6 N/O at 2.02 Å
FEDIPIC	6.2 N/O at 2.03 Å	6 N/O at 2.03 Å
FESALMP0	6.1 N/O at 2.05 Å	6 N/O at 2.03 Å
FEHBPZOH	6.7 N/O at 2.04 Å	6 N/O at 2.04 Å
FEHBPZO	4.8 N/O at 2.11 Å; 1 O at 1.78 Å	5 N/O at 2.11 Å; 1 O at 1.79 Å
FE2CO2	4.9 O at 2.04 Å; 0.8 O at 1.72 Å	5 O at 2.06 Å; 1 O at 1.79 Å
FE3BIPHME	4.5 N/O at 2.11 Å; 1 O at 1.78 Å	5 N/O at 2.10 Å; 1 O at 1.79 Å
FESALMP1	6.3 N/O at 2.09 Å	6 N/O at 2.08 Å
FESALMP2	6.1 N/O at 2.15 Å	6 N/O at 2.13 Å

[a]The average distance reported is for the minimum corresponding to $R_N > R_O$. For **FE2CO2**, the all oxygen fit is reported.

Table 4.4. Fits to Second Shell Model Data. The samples fit are listed across the top of the table and the para listed down the side of the table.

Sample:	FESALMP0			FECHEL			FE
Fe-Fe distance (Å):	3.063			3.078			3
Window (Å):	2.20 - 3.45			2.55 - 3.20			2.5
Fe-Fe parameters	Fe	R (Å)	F	Fe	R (Å)	F	Fe
FESALMP0				0.4	3.07	0.29	0.4
3.063 Å				0.3	3.44	0.56	0.4
FECHEL	1.9	3.07	0.65				1.0
3.078 Å	0.7	3.44	1.4				0.4
FEHBPZO	1.1	3.06	0.47	0.4	3.07	0.42	0.5
3.145 Å	1.1	3.43	1.1	0.5	3.43	0.47	0.6
FE3BIPHME	1.5	3.07	0.83	0.8	3.09	0.31	0.9
3.200 Å	1.0	3.41	1.3	0.6	3.41	0.58	0.7
FESALMP2	1.1	3.10	0.36	0.5	3.10	0.27	0.5
3.202 Å	0.7	3.49	1.28	0.3	3.48	0.60	0.4
FEHBPZOH	1.0	3.06	1.1	0.3	3.07	0.63	0.3
3.439 Å	1.9	3.44	0.31	0.8	3.44	0.31	0.8

Table 4.4. continued

Sample:	FESALMP1			FEHBPZO			FE2CO2		
Fe-Fe distance (Å):	3.099			3.145			3.174		
Window (Å):	2.20 - 3.55			2.00 - 3.30			2.50 - 3.35		
Fe-Fe parameters	Fe	R (Å)	F	Fe	R (Å)	F	Fe	R (Å)	F
FESALMP0	1.0	3.08	0.31	0.7	3.15	0.37	1.0	3.15	0.57
3.063 Å	0.6	3.46	1.3	0.4	3.52	1.0	0.7	3.51	1.2
FECHEL	1.8	3.08	0.84	1.4	3.16	0.67	2.1	3.16	0.39
3.078 Å	0.4	3.47	1.4	0.4	3.48	1.1	1.0	3.49	1.4
FEHBPZO	1.2	3.07	0.38				1.1	3.15	0.71
3.145 Å	0.9	3.45	1.2				1.2	3.49	1.0
FE3BIPHME	1.2	3.11	0.42	0.9	3.19	0.48	1.9	3.17	0.47
3.200 Å	0.5	3.51	1.4	0.3	3.56	1.1	1.6	3.48	1.1
FESALMP2	1.5	3.08	0.95	1.3	3.16	0.63	1.2	3.19	0.62
3.202 Å	0.7	3.41	1.4	0.8	3.48	0.99	0.8	3.54	1.3
FEHBPZOH	1.1	3.07	0.99	1.0	3.15	0.69	0.8	3.16	1.27
3.439 Å	1.8	3.45	0.51	1.3	3.53	0.54	1.8	3.52	0.66

Table 4.4. continued

Sample:	**FE3BIPHME**			**FESALMP2**			**FEHBPZOH**		
	3.200			3.202			3.439		
Window (Å):	2.35 - 3.40			2.35 - 3.35			2.05 - 3.35		
Fe-Fe parameters	Fe	R (Å)	F	Fe	R (Å)	F	Fe	R (Å)	F
FESALMP0	0.4	3.19	0.42	0.8	3.17	0.27	0.7	3.07	0.32
3.063 Å	0.3	3.54	0.61	0.5	3.55	0.98	0.6	3.45	0.83
FECHEL	1.0	3.19	0.32	1.6	3.18	0.44	1.4	3.08	0.52
3.078 Å	0.5	3.52	0.67	0.3	3.52	1.1	0.7	3.45	1.0
FEHBPZO	0.5	3.19	0.43	0.9	3.16	0.46	0.8	3.06	0.60
3.145 Å	0.5	3.53	0.55	0.8	3.54	0.86	1.0	3.43	0.69
FE3BIPHME				1.1	3.18	0.70	1.0	3.08	0.78
3.200 Å				0.7	3.51	1.1	0.9	3.42	0.97
FESALMP2	0.5	3.22	0.47				0.9	3.10	0.45
3.202 Å	0.4	3.51	1.4				0.7	3.49	0.90
FEHBPZOH	0.4	3.22	0.63	0.7	3.15	0.89			
3.439 Å	0.8	3.56	0.48	1.5	3.54	0.35			

similar to the trend seen in second shell fits to the MMO hydroxylase data (see Chapters 2 and 3). The Fe-Fe distances were consistently longer by 0.03 - 0.08 Å for the fit results using the diferrous **FESALMP2** parameters to fit the diferric model data, except for **FE3BIPHME** which has the same Fe-Fe distance as **FESALMP2** (3.2 Å). A distance within 0.05 Å of the correct Fe-Fe distance was found for all of the samples, however in some cases the coordination number was off by a factor of two (Table 4.4). Using **FECHEL** parameters in fits to **FESALMP0**, which has a much more intense second shell peak relative to the first shell peak than **FECHEL** (Figure 4.4a and 4.4c), the coordination number was 1.9. In fits to **FEDIPIC** with the **FECHEL** parameters (which have similar intensity second shell peaks, Figure 4.4a and 4.4b), a coordination number of 1 was found. Similarly, in fits to **FECHEL** with **FESALMP0** parameters, the coordination was 0.4 Fe, half of the correct amount. The inaccuracy of the amplitude parameters reflects the relative weakness of the Fe-Fe contribution to the data (relative to the strength of the first shell contribution) in some models compared to others (see Figure 4.2). The enhanced amplitude of the second shell peaks in some models over others will be discussed below.

Of the two minima found during the fitting proceedure, the better fit to the data corresponded in every case to the minimum with the Fe-Fe distance closer to that of the model from which the parameters were obtained. This result was independent of the number and types of bridges in the iron center as well as the oxidation state of the diiron center. **FESALMP0** has a dialkoxo-bridged center with an Fe-Fe distance of 3.06 Å. Using the **FESALMP0** parameters in fits to **FEHBPZOH** data, a tribridged diferric center with a hydroxo-bridge and a 3.44 Å Fe-Fe distance, the best fit to the data corresponded to 0.7 Fe at 3.065 Å (Figure 4.8a). In addition, a fit of 0.6 Fe at 3.45 Å was found, but the fit was much worse than the fit at the shorter distance (Figure 4.8a). Likewise, use of the **FEHBPZOH** Fe-Fe parameters in fits to the **FESALMP0** data resulted in a better fit at 3.44 Å than at the correct distance of 3.06 Å (Figure 4.8b). Using the parameters from **FE3BIPHME**, a tribridged center with an oxo-bridge and a 3.20 Å Fe-Fe distance, in fits to **FEHBPZOH**, fits at 3.08 Å and 3.43 Å were obtained with the better fit corresponding to the shorter distance (Figure 4.8c). The overall worse fit function with the **FESALMP0** parameters reflects the difference in the appearance of the second

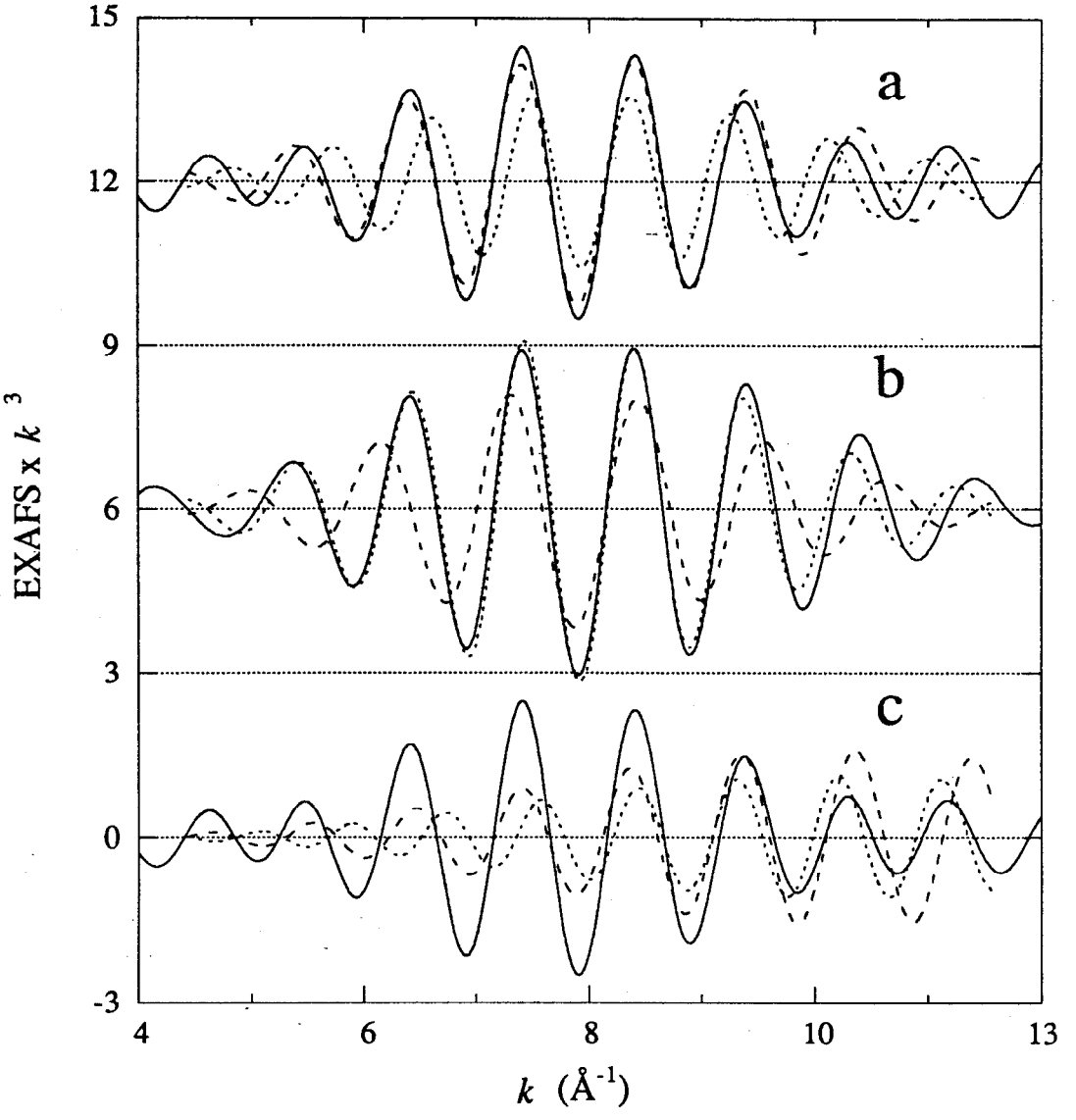

Figure 4.8. Comparison of the model-dependent fits to the second shell data (Table 4.4). The solid line is the data, the dashed line is the fit to the data with a short Fe contribution and the dotted line is the fit to the data with a long Fe contribution. (a) Fit to **FEHBPZOH** with **FESALMP0** Fe parameters. (b) Fit to **FESALMP0** with **FEHBPZOH** Fe parameters. (c) Fit to **FEHBPZOH** with **FE3BIPHME** Fe parameters.

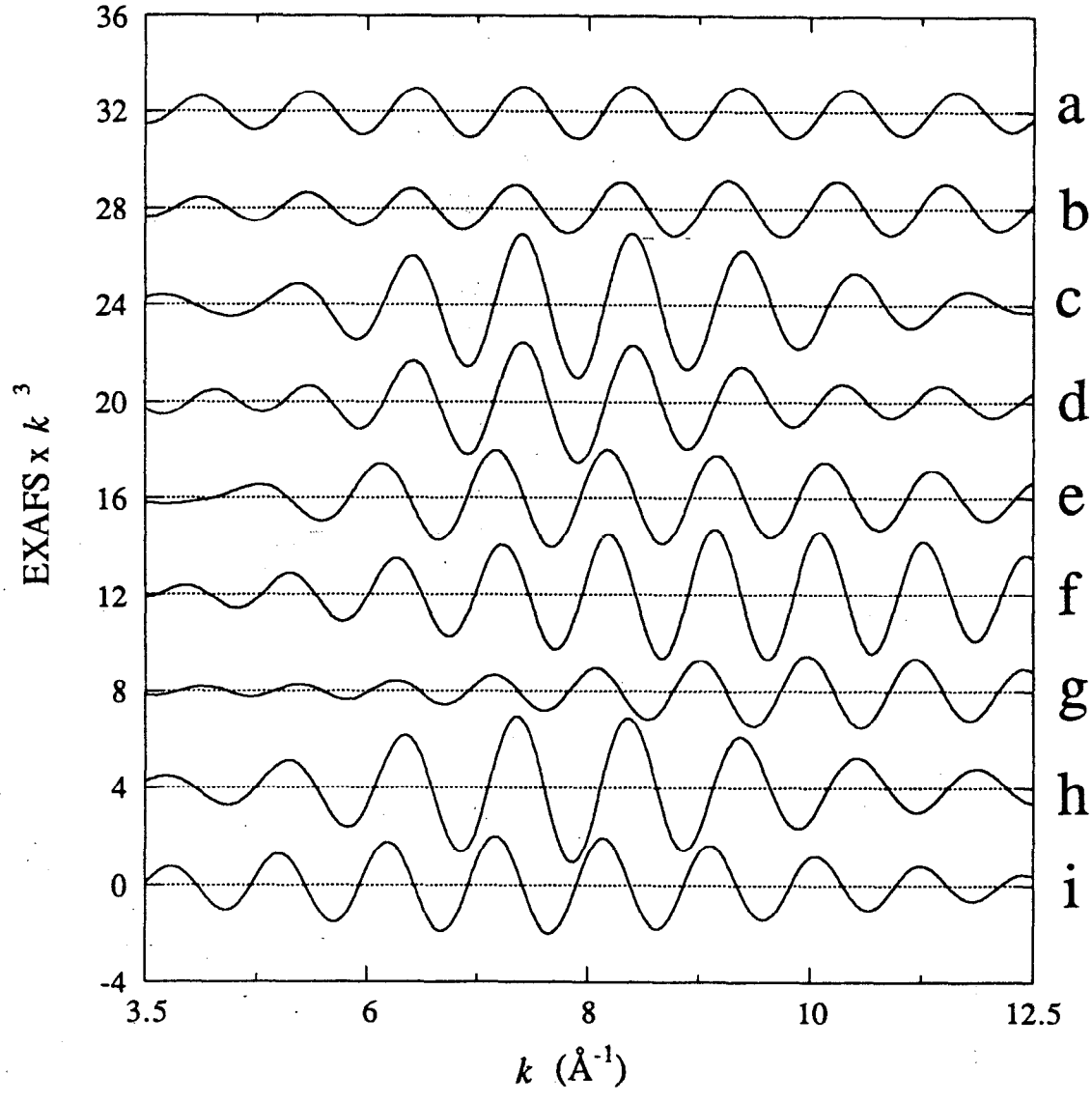

Figure 4.9. Comparison of the filtered second shell data of iron dimers. The windows used to isolate the data from the Fourier transforms are given in Table 4.4. (a) **FECHEL**, (b) **FEDIPICE**, (c) **FESALMP0**, (d) **FEHBPZOH**, (e) **FEHBPZO**, (f) **FE2CO2**, (g) **FE3BIHME**, (h) **FESALMP1**, (i) **FESALMP2**.

different for each sample, however there does not seem to be any correspondence to the shape of the amplitude envelope with either Fe-Fe distance or bridging geometry. The data for **FEHBPZO**, **FEHBPZOH**, and **FESALMP0** (tribridge oxo, 3.14 Å Fe-Fe; tribridge hydroxyo, 3.43 Å Fe-Fe; dibridge alkoxo, 3.06 Å Fe-Fe, respectively) reach a maximum at around 8 $Å^{-1}$ and dampen out at both ends of the data range (Figure 4.9e, 4.9d and 4.9c, respectively). For **FE3BIPHME**, another tribridge oxo compound like **FEHBPZO**, the data are damped in the low *k* region and reach a maximum above 9 $Å^{-1}$ (Figure 4.9g), while for **FECHEL**, which has an Fe-Fe distance similar to that of **FESALMP0**, the data reach a maximum at 8 $Å^{-1}$, but do not dampen out over the data range (Figure 4.9a). In addition, the amplitude is not as great for the **FECHEL** data as for the **FESALMP0** data (Figure 4.9a and 4.9c).

Both **FE3BIPHME** and **FESALMP2** have Fe-Fe distances of 3.2 Å, however **FE3BIPHME** is a diferric tribridged compound with an oxo bridge, while **FESALMP2** is a dibridged diferrous compound. The second shell data for **FESALMP2** (Figure 4.9i) does not resemble the **FE3BIPHME** second shell data (Figure 4.9g). Using these parameters in fits to **FE2CO2**, a 3.185 Å Fe-Fe distance was obtained with the **FESALMP2** parameters, and a 3.165 Å Fe-Fe distance with the **FE3BIPHME** parameters (Table 4.4). For both fits, the distance is within 0.01 Å of the correct distance of 3.17 Å, however the fit to the data is better with the **FE3BIPHME** parameters than with the **FESALMP2** parameters because the amplitude envelope of the second shell **FE3BIPHME** data and **FE2CO2** data resemble each other (Figure 4.10). The only advantage of making a choice of a model compound based on the shape of the second shell data is a purely cosmetic one. Not surprisingly, better fits to any set of data correspond to the use of parameters from a model with a similarly shaped amplitude envelope, however the same two minima were found using any set of Fe parameters in fits to any data set. Additionally, the shape of the second shell amplitude envelope for **FE3BIPHME** and **FE2CO2**, suggests that the second shell data has more than a single contribution of atoms.

4.3.2.2. Correlations with Second Shell Low-Z Atoms. Previous investigations of the hydroxylase data revealed a strong correlation of the second shell low-Z and Fe parameters which impacted both the distances and coordination numbers. To test whether this fitting approach can distinguish between an Fe-Fe interaction and an Fe-C interaction at approximately the same distance, as is the case for the structurally characterized $Fe_2(OR)_2$ iron center, a second shell low-Z contribution was added to some of the iron fits in Table 4.4 for **FECHEL** and **FESALMP0**. Specifically, a carbon contribution was added to the fits of **FECHEL** with **FESALMP0** parameters, and to fits of **FESALMP0** with **FECHEL** parameters. These models have similar bridging

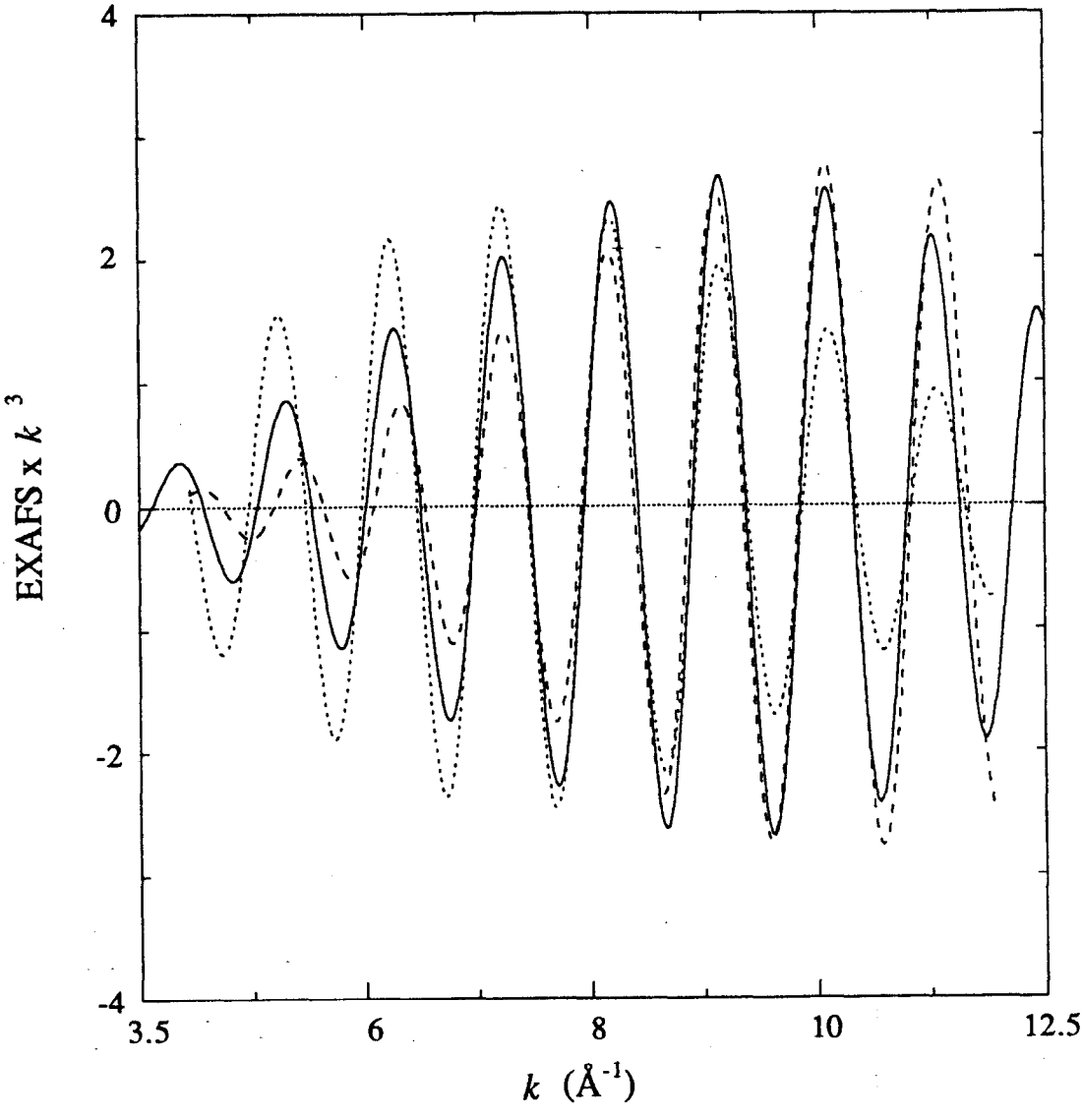

Figure 4.10. Comparison of fits to the second shell data of **FE2CO2** (Table 4.4). The solid line is the data, the dashed line is the fit with **FE3BIPHME** Fe parameters and the dotted line is the fit with **FESALMP2** Fe parameters.

environments and Fe-Fe distances (3.08 and 3.06 Å, respectively), but the second shell peaks in the Fourier transforms have different intensities (Figure 4.9a and 4.9c). The difference in the amplitudes of the second shell contributions should provide insight into the interference between low-Z and metal contributions which may contribute to the enhancement or reduction of the second shell peak in the Fourier transforms. In addition, a C contribution was added to fits to the second shell data of **FEHBPZOH** with **FECHEL** and **FESALMP0** parameters, and to fits to **FECHEL** and **FESALMP0** data with **FEHBPZOH** parameters to explore the effect the addition of another contribution has on the model dependent results of second shell fits. The results are presented inTable 4.5.

The second shell data for the three models were first fit with only a second shell C contribution from $Fe(acac)_3$. As noted before in fits to the hydroxylase data (Chapters 2 and 3), two minima were found, separated by 0.4 Å at the same distances as the Fe-only fits to the data (Table 4.5, fits 4.5-1, 4.5-2, 4.5-9, 4.5-10, 4.5-17 and 4.5-18, compare with Table 4.4). The better fit to the data corresponded to the shorter Fe-C distance, similar to what was seen for the hydroxylase data. The distance of the short C fit for **FECHEL** is slightly long and it should be pointed out that there are no atoms 3.4 Å away from the iron site according to the crystal structure. In general, the distances for the short C minima were slightly longer than the crystallographically determined distances, and the coordination numbers were inaccurate as well for **FEHBPZOH** and **FESALMP0**. For example, in the second shell of **FEHBPZOH**, there is a cluster of 6 N and 4 C atoms from the pyrazole rings between 3.0 and 3.05 Å, however the fit to the data with the C parameters resulted in a coordination number of 5.6 C at 3.06 Å (Table 4.5, fit 4.5-17). For **FESALMP0**, the coordination numbers of the low-Z contribution were high. According to the crystal structure, there are 6 C at 3.04 Å and 5 N/C at 3.45 Å, but the fits determine 8.2 C at 3.07 Å or 7.5 C at 3.43 Å, with the longer fit being considerably worse (Table 4.5, fit 4.5-9 and 4.5-10). To properly fit the second shell data, three contributions should be included, consisting of two C and one Fe wave, however, such a fit would be unreasonable to try due to the correlation of the C and Fe parameters and the ability of the C contribution to mimic the Fe contribution.

In general, the addition of C to the Fe contribution improved the quality of the fits, resulting in lower values of the fit function F by as much as a factor of 2. The bias of the best fit for the Fe-Fe distance of the model from which the parameters were derived was maintained in the Fe + C fits to the data. The overall best fit using the **FEHBPZOH** parameters in fits to **FECHEL** and **FESALMP0** corresponded to the 3.4 Å Fe minimum (Table 4.5, fit 4.5-5 and 4.5-13). The Fe contribution remained about the same for both samples (relative to the Fe-only fits, see Table 4.4), but the coordination number of C

Table 4.5. Fits to Second Shell Model Data with Fe and C.[a]

Sample[b] (Window Width (Å))	Fe-Fe Parameters	Fit	Fe		C	
			CN[c]	R(Å)	CN	R(Å)
FECHEL		4.5-1			3.5	3.08
(2.55 - 3.45)		4.5-2			3.8	3.43
	FEHBPZOH	4.5-3	0.2	2.91	4.1	3.08
		4.5-4	0.2	3.05	3.5	3.44
		4.5-5	0.7	3.44	0.8	3.42
	FESALMP0	4.5-6	0.4	3.01	3.6	3.14
		4.5-7	0.4	3.07	1.1	3.44
		4.5-8	0.2	3.41	3.2	3.09
FESALMP0		4.5-9			8.2	3.07
(2.20 - 3.45)		4.5-10			7.5	3.43
	FEHBPZOH	4.5-11	0.4	2.96	8.7	3.08
		4.5-12	0.8	3.05	6.3	3.44
		4.5-13	2.0	3.45	3.3	3.34
	FECHEL	4.5-14	1.0	3.09	5.2	3.05
		4.5-15	1.8	3.07	0.9	3.49
		4.5-16	0.6	3.42	8.2	3.07

Table 4.5. continued

Sample[b] (Window Width (Å))	Fe-Fe Parameters	Fit	Fe		C		F
			CN[c]	R(Å)	CN	R(Å)	
FEHBPZOH		4.5-17			5.6	3.06	0.64
(2.05 - 3.35)		4.5-18			6.1	3.44	0.79
	FECHEL	4.5-19	1.2	3.10	3.3	3.02	0.30
		4.5-20	0.7	3.44	5.5	3.07	0.52
	FESALMP0	4.5-21	0.8	3.08	2.4	2.95	0.15
		4.5-22	0.4	3.45	4.5	3.06	0.47

[a]Fitting range $k = 4 - 12$ Å^{-1}. Errors are estimated to be about $\pm$ 0.03 Å for distances and 25% for coordination numbers.[8] [b]The Fe only fits are presented in Table 4.4. [c]CN = coordination number.

decreased from 3.8 to 0.8 (Table 4.5, fit 4.5-5) for **FECHEL**. Both the C coordination number and distance decreased for **FESALMP0**, from 7.5 C at 3.43 Å (fit 4.5-10) to 3.3 C at 3.34 Å (fit 4.5-13). Fits to the data consisting of a long Fe and a short C contribution resulted in negative coordination numbers. The addition of C to the short Fe distance resulted in a small decrease in the Fe distance and both the Fe and C coordination number (Table 4.5, fit 4.5-3 and 4.5-4 for **FECHEL** and 4.5-11 and 4.5-12 for **FESALMP0**). The C contribution for these fits was dominant over the Fe contribution.

Using the **FECHEL** and **FESALMP0** parameters in Fe + C fits to the **FEHBPZOH** data, the best fit corresponded to the shorter Fe-Fe distance (Table 4.5, fits 4.5-19 and 4.5-21). The C coordination number and distance decreased for the short Fe/short C fit to the data (fits 4.5-19 and 4.5-21) while the Fe distance increased by about 0.01 - 0.02 Å. Addition of C to the long Fe distance resulted in a decrease in the coordination number from 0.6 Fe to 0.4 Fe for the fits with **FESALMP0** (Table 4.5, fit 4.5-22), while the Fe contribution for the fits with **FECHEL** stayed the same (Table 4.5, fit 4.5-20). Fits to the **FEHBPZOH** data with Fe and a long C contribution resulted in negative coordination numbers.

The results of the Fe + C fits for **FECHEL** and **FESALMP0** using **FESALMP0** and **FECHEL** parameters, respectively, also showed correlation effects. The coordination number of Fe stayed at 0.4 for the short Fe fits to **FECHEL** with **FESALMP0** parameters, but the Fe distance decreased to 3.01 Å from 3.07 Å with the addition of a short C contribution (Table 4.5, fit 4.5-6), while the C distance increased from 3.08 Å to 3.14 Å. In the short Fe/short C fit to **FESALMP0** with **FECHEL** parameters, the Fe coordination number decreased from 1.9 to 1.0 and the distance increased 0.02 Å (Table 4.5, fit 4.5-14), while the C coordination decreased from 8.2 to 5.2. This fit agrees with the distribution of atoms in the second shell of **FESALMP0**, but the Fe-Fe distance is slightly long. The fits to the data with the 3.4 Å Fe contribution and a short C contribution resulted in little or no difference in the C coordination number and distance, but the Fe coordination number and distance decreased slightly (Table 4.5, fits 4.5-8 and 4.5-16). The overall best fits to the data were for the short Fe/short C fit to the data. Fits to the data with a long Fe and long C contribution resulted in negative coordination numbers.

4.3.2.3. Investigation with Hydroxylase Data. The parameters from the various models were used in fits to the second shell data of the hydroxylase component of MMO from *Methylococcus capsulatus* (Bath) in its oxidized and semimet state (**EXAFS5** and **EXAFS2**, respectively). The results using **FEHBPZOH** and **FEHBPZO** parameters have been briefly reported (Chapter 2 and ref. 2a) but are included here in detail. Two minima were found in every case, and the better fit to the data corresponded to

the minimum with the Fe-Fe distance close to that of the model compound from which the parameters were obtained (Table 4.6). In addition, the coordination number for Fe was closer to 1 for the short Fe minimum than for the long Fe minimum except for the fits with **FE3BIPHME** and **FEHBPZOH** parameters, for which the coordination number was closer to 1 for both Fe minima. In general, the short Fe minimum was strongly preferred over the longer Fe minimum, except for the fits with **FEHBPZOH**, which are biased for the longer Fe minimum. It is interesting to note that while the long Fe minimum varies from 3.38 to 3.46 Å (0.08 Å) for **EXAFS5** and 3.35 to 3.43 Å (0.08 Å) for **EXAFS2**, the short Fe minima varies by only 0.05 Å. In addition, in every case, the two minima found were on the order of 3.0 Å and 3.4 Å even with the 3.2 Å parameters from **FE3BIPHME**, whereas use of the **FE3BIPHME** fits to the diferric **FEHBPZO** and semimet **FESALMP1** resulted in minima greater than 3.1 and 3.5 Å. This result strongly supports the previous conclusion that the second shell contributions to the data occur at 3.0 and 3.4 Å. A comparison of the fits to the data for **EXAFS5** with the **FESALMP0** parameters and **FEHBPZOH** parameters is presented in Figure 4.11.

4.4. Discussion

4.4.1. Interpretation of First Shell Fits

The EXAFS technique has long been recognized as being able to accurately determine the first shell coordination of an absorbing atom. The model compounds investigated in this paper were all octahedrally coordinated, but had different numbers of N and O atoms coordinating the Fe atoms as well as different numbers and types of bridges between the Fe atoms. For the monomeric compounds, which contain a shell of nearly equidistant N or O atoms, the data could be adequately described by a single contribution at the correct distance (Table 4.2, **FE3HBPZ** and **FEACAC**). Fits to the iron dimer data with a single N or O contribution resulted in low coordination numbers, although the distance was generally close to the average first shell distance from the crystal structure (excluding the oxo-bridge distance in the average distance). Instead, two contributions at different distances were required to adequately fit the data in the absence of an oxo-bridge, and three contributions if an oxo-bridge was present (the third contribution representing the oxo-bridge itself).

The fit results did not correspond to the crystallographic information based on the numbers of N or O atoms in the first shell, but instead seemed to reflect the distribution of atoms in the first shell based on the distance from the iron atom. The distortion of the iron

Table 4.6. Fits to Second Shell Hydroxylase Data.

Sample:	**EXAFS5** (diferric)			**EXAFS2** (semimet)		
Window (Å):	2.15 - 3.20			2.20 - 3.40		
Fe-Fe parameters:	Fe	R (Å)	F	Fe	R (Å)	F
FESALMP0	0.6	3.04	0.23	0.6	3.04	0.42
3.063 Å	0.3	3.41	0.86	0.3	3.40	0.99
FECHEL	1.0	3.05	0.47	1.3	3.04	0.58
3.078 Å	0.2	3.38	0.92	0.3	3.35	1.04
FEHBPZO	0.8	3.03	0.22	0.8	3.03	0.26
3.145 Å	0.5	3.41	0.81	0.5	3.39	0.95
FE3BIPHME	1.0	3.05	0.52	1.2	3.04	0.43
3.200 Å	0.6	3.37	0.85	0.8	3.35	0.93
FESALMP2	0.8	3.08	0.25	0.8	3.07	0.5
3.202 Å	0.2	3.46	0.90	0.2	3.43	1.0
FEHBPZOH	0.7	3.04	0.65	0.8	3.04	0.73
3.439 Å	1.1	3.42	0.40	1.1	3.41	0.61

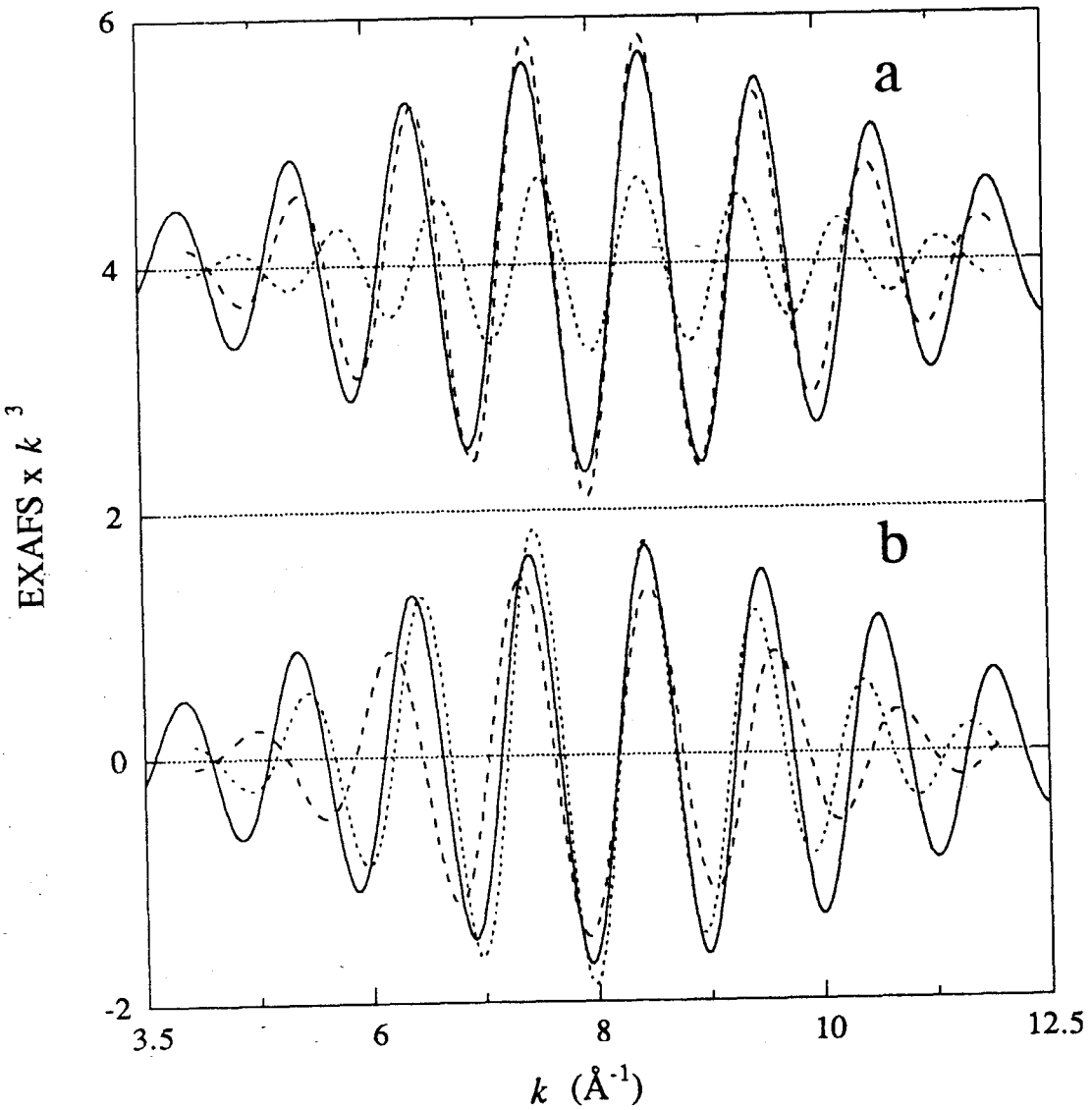

Figure 4.11. Fits to the oxidized hydroxylase data (Table 4.5). The solid line is the data, the dashed line is the fit to the data with a short Fe contribution and the dotted line is the fit to the data with a long Fe contribution. (a) Fit to **EXAFS5** data with **FESALMP0** Fe parameters. (b) Fits to **EXAFS5** data with **FEHBPZOH** data.

site from octahedral symmetry imposed by the bridging and ligand geometries, and the mixture of N and O ligation results in a range of first shell distances. In the oxo-bridged models, the bond lengths range from ~1.8 Å for the oxo-bridge Fe-O distance to over 2.1 Å for the atom coordinated in a position *trans* to the oxo bridge (see Table 4.1). The relationship governing the resolution of distances as determined by the EXAFS technique as a function of the range of data available is given by $\Delta k\, \Delta R = \pi/2$ where Δk is the range of data ($Å^{-1}$) and ΔR is the corresponding limit on the resolution of the distances determined in the fitting technique (Å). For data to k = 12.5 $Å^{-1}$, the corresponding resolution of bond lengths is 0.126 Å. This explains the sensitivity of the EXAFS technique to the presence of the 1.8 Å Fe-O distance of the oxo-bridge, which is ~ 0.2 Å shorter than the average bond length of the rest of the atoms. In the model compounds investigated in this study, the range of distances is close to this resolution limit, and although two contributions are required to fit the data, the correct individual contributions cannot be determined due to the limited range of data used for these investigations. In the first shell of **FESALMP0**, the distribution of atoms can be divided into two sets, corresponding to 3 atoms at an average distance of 1.95 Å and 3 atoms at an average distance of 2.11 Å which differ by 0.16 Å (Table 4.1). The fits to the data (Table 4.2, fits 4.2-21 and 4.2-22) correspond quite well to this interpretation of the crystal structure data. In **FECHEL**, the range of distances in the first coordination sphere is 0.126 Å with a single O atom at 1.97 Å and 5 atoms at an average distance of 2.05 Å. The fit to the data reflects this distance distribution (Table 4.2, fit 4.2-10) although N corresponded to the short distance contribution. The first shell fit results thus seem to reflect the distribution of atoms based on their average distance from the iron atom, rather than the contribution of a specific atom type at a given distance.

It was only with the information provided by the crystal structure that the individual contributions based on the fit results could be interpreted for some of the models discussed here. For an unknown structure, such an interpretation would not be possible. The inability of this approach to accurately determine the numbers of N and O atoms reflects in part the similar backscattering strength of these atoms. The approach taken in the curve-fitting technique employed here assumes that the Debye-Waller factors for the experimentally derived first shell Fe-N and Fe-O parameters are transferable to the model compounds, however this is not necessarily true. Further investigation of the first shell fits using fixed, correct coordination numbers and allowing the distance and Debye-Waller factor to float would provide additional insight into the ability of the curve-fitting technique to resolve individual contributions to the first shell data. In addition, more than one fit minimum was found, depending on the relative initial distances of the N and O

contributions. The shorter distance was sometimes conserved in the two minima, but the longer distance sometimes changed by more than 0.1 Å which is greater than the expected distance error for the EXAFS technique (± 0.03 Å).[8] This suggests that the individual contributions should not be interpreted as giving accurate information about the distance distribution of atoms in the first coordination sphere for the range of data investigated. Data to a higher *k* range would provide more accurate and reliable distance information.

The most reliable way to use the results of fits to the first shell data is to consider the coordination-weighted average distance information. For all of the model compounds, the coordination-weighted average of both fit minima falls within the expected error for both the coordination number and distance for the EXAFS technique.[8] This has been the proceedure used to interpret the results for the hydroxylase data (Chapters 2 and 3). It has generally been assumed that the average distance corresponds to the relative numbers of N and O in the first coordination sphere:[12] in addition, the average first shell distance reflects the presence of an oxo-bridge in the center. The presence of an oxo-bridge tends to distort the iron site and results in longer first shell distances, and therefore a longer average distance, than non-oxo-bridged models. This is seen clearly by comparing the average first shell distances for **FEHBPZO** and **FEHBPZOH** excluding the shortest bridging distance. **FEHBPZO** and **FEHBPZOH** both are coordinated by 3 O and 3 N atoms and the primary difference in their structure is the presence of the oxo-bridge in **FEHBPZO**. The average first shell distance in **FEHBPZO** (excluding the oxo-bridge) is 2.12 Å, whereas in **FEHBPZOH**, the average distance is 2.06 Å (excluding the hydroxo-bridge). If the bridging distance is included, the average for **FEHBPZO** decreases to 2.06 Å and to 2.04 Å for **FEHBPZOH**. The average distances in the first coordination sphere for all atoms for a variety of multiply-bridged ferric iron dimers with N and O coordination are listed in Table 4.7 and presented graphically in Figure 4.12. In general, the average first shell distance does tend to increase as the number of N atoms relative to O atoms increases, and for the same N and O ligation, the average first shell distance will be longer if an oxo bridge is present.

4.4.2. Model-Dependent Results of Second Shell Fits

4.4.2.1. Model Compounds. It has previously been pointed out that care must be taken when choosing a model compound to mimic the second shell interaction of an unknown compound, and one of the criterion suggested was that the irons in the model have similar bridging oxygens to what is suspected in the unknown.[13] This does not seem to be the case for the model compounds discussed above. If it were true that the types of

Table 4.7. Average First Shell Distances as a Function of First Shell Ligation.

Sample	Ref.	Bridging Geometry	First Shell Ligation	R_{avg} (all)[a]	R_{avg} [b]
Non-oxo Bridged Models					
$[FeOH(H_2O)Chel]_2(H_2O)_4$	6a	dibridge, $(OH)_2$	5 O, 1 N	2.02 Å	2.04
$[Fe_2(salmp)_2]\cdot 2DMF$	6b	dibridge, $(OR)_2$	4 O, 2 N	2.03 Å	2.03
$[Fe_2OH(OAc)_2(HB(pz)_3)_2](ClO_4)$	6c	tribridge, $OH(OAc)_2$	3 O, 3 N	2.04 Å	2.06
Oxo-bridged Models					
$[Fe_2O(OAc)_2\{[OP(OEt)_2]_3Co(C_5H_5)\}_2]$	6e	tribridge, $O(OAc)_2$	6 O	2.02 Å	2.06
$[Fe_2O(O_2CH)_4(BIPhMe)_2](CH_3OH)$	6f	tribridge, $O(O_2CH)_2$	4 O, 2 N	2.05 Å	2.10
$[Fe_2O(OAc)_2(HB(pz)_3)_2]$	6d	tribridge, $O(OAc)_2$	3 O, 3 N	2.06 Å	2.11
$[Fe_2O(OAc)TPA]$	11	dibridge, O(OAc)	4 N, 2 O	2.07 Å	2.12

[a]The distance reported is the average distance over all first shell bonds. [b]The distance reported is the average over all atoms except the shortest bridging atom. For example, the Fe-O_{oxo} bond length was excluded for this average for the oxo-bridged models.

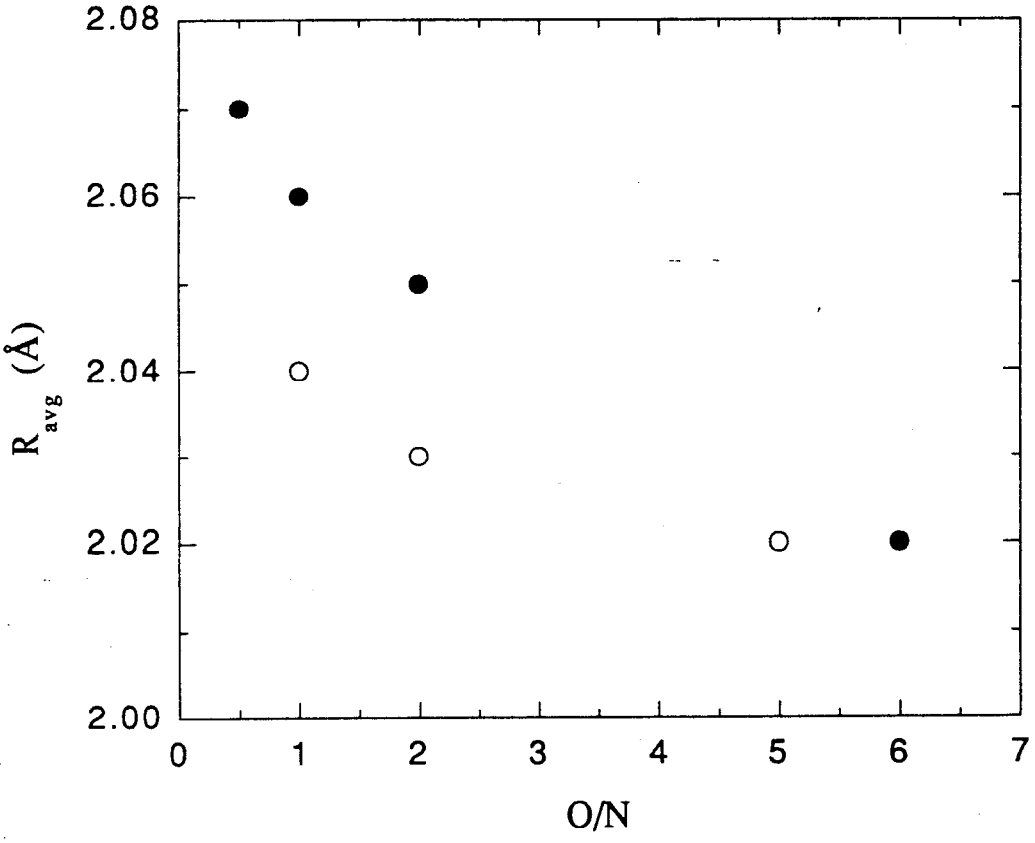

Figure 4.12. Comparison of the average first shell distance with the numbers of O to N atoms coordinating the iron atoms (Table 4.7). The solid circles are the oxo-bridged model data and the open circles are the non-oxo-bridged model data.

bridges determined the choice of an appropriate model, then the tribridged models with an oxo-bridge should be poor choices for the dihydroxo and dialkoxo models, however the fits do not support this hypothesis (Table 4.4). The parameters from both **FEHBPZO** and **FE3BIPHME** adequately fit the dialkoxo model **FESALMP0** and the dihydroxo models **FECHEL** and **FEDIPIC** at the correct distance (the coordination numbers are low for fits to **FECHEL** and **FEDIPIC** with the **FEHBPZO** parameters). Likewise, the **FESALMP0** and **FECHEL** parameters adequately fit the tribridged **FEHBPZO** and **FE3BIPHME** second shell data.

None of the models tested gave satisfactory fits to the **FEHBPZOH** second shell data at the correct 3.4 Å Fe-Fe distance. The correct distance was found in every case, but the better fit corresponded to the shorter distance minimum. All of the models with the exception of **FEHBPZOH** have Fe-Fe distances of 3.2 Å or less. Using the **FEHBPZOH** Fe-Fe parameters in fits to the other models, the better fit occured in every case at a distance on the order of 3.4 Å or longer. These results clearly demonstrate that fits to the second shell data are strongly dependent on the compound chosen to model the Fe-Fe interaction. In particular, *the bias favors the Fe-Fe distance of the model rather than the number or types of bridges in the diiron center.*[14]

One would also expect, if similar bridging geometry determined an appropriate model choice, that the dihydroxo-bridged models **FECHEL** and **FEDIPIC** would be excellent models for dialkoxo-bridged **FESALMP0**, all of which have Fe-Fe distances between 3.1 and 3.0 Å and Fe-O_{br}-Fe angles around 100°. Although the distance information obtained is reasonable in cross-fits between these models, the coordination numbers are off by a factor of two. Inspection of the Fourier transforms shows that the second shell peak in **FEDIPIC** and **FECHEL** is much less intense relative to the first shell peak compared to the Fourier transform of **FESALMP0**. This would lead to different amplitude functions and therefore incorrect coordination numbers for the cross fits. Similar differences in amplitude functions have been noted in fits to iron dimers and has been attributed to multiple scattering contributions to the data arising from the focusing effect of the intervening oxo-bridge, however this effect was determined to be a factor only if the Fe-O-Fe bridging angle were greater than 150°.[15] In addition to the focusing effect for models with angles greated than 150°, the various multiple scattering pathways would not be resolveable in the Fourier transform of the data which would also lead to a broadening of the second shell contribution. For **FESALMP0**, and the other models investigated in this paper, multiple scattering contributions involving the Fe_2O core should not interfere with the second shell data.

The various contributions from the multiple scattering pathways should be resolved in the data of **FESALMP0**, however the second shell peak (Figure 4.5c) is rather broad. The presence of rigid groups such as imidazole also contribute strongly to outer shell data resulting in strong peaks in Fourier transforms.[16] It is interesting to note that a recent multiple scattering analysis of $Fe(acac)_3$[17] has revealed that there is a very strong contribution to the second shell data from a multiple scattering pathway involving the Fe-O-C unit (Fe-O-C angle 129.3°). This demonstrates that $Fe(acac)_3$ is not a good choice as a model for the single-scattering Fe-C parameters. This kind of geometry may be similar to ligation of metal sites in proteins by carboxylate groups and so may similarly contribute to the data. It would be interesting to investigate the angular dependence of multiple scattering contributions from various chelating groups. Clearly, an understanding of the relationship between the geometries of the ligands coordinating diiron centers and the multiple scattering pathways which contribute significantly to the second shell data of dinuclear non-heme iron models and protein systems needs to be developed. The determination of the multiple pathways which contribute to the second shell data of model compounds investigated for this paper would provide a great deal of insight into the active site structures of the hydroxylase of MMO, uteroferrin, ribonucleotide reductase and hemerythrin.

The distances of the Fe-Fe contributions in **FECHEL** (3.08 Å) **FEHBPZOH** (3.44 Å) are well resolved from the contributions of second shell low-Z atoms (2.9 Å for **FECHEL** and between 3.0 and 3.05 Å for **FEHBPZOH**). Fits to the second shell data should therefore lead to well defined minima corresponding to the Fe and the low-Z atom contribution (modeled as C), however this was not the case. As seen before in fits to the hydroxylase data, the second shell Fe and C parameters were strongly correlated, with the Fe and C distances and coordination numbers changing for the Fe + C fits from the values obtained in the Fe-only and C-only fits to the data. The model bias held in the Fe + C fits to the data as well, with the best fit corresponding to the iron distance closest to the Fe distance of the model used for Fe parameters. This certainly impacted the results of the fits to **FEHBPZOH**, as none of the other models are adequate models of this compound. However, a reasonable fit was obtained for **FESALMP0** using **FECHEL** Fe parameters and a short C contribution. The difference between the Fe and C shells in **FESALMP0** is less than 0.1 Å. Given the general trends seen in the Fe + C fits to the second shell data, it is not entirely clear if this result reflects the quality of the **FECHEL** parameters in fits of this kind, or if it is simply coincidental.

Moreover, the best fit to the data corresponded to the minimum in which both the Fe-C and Fe-Fe distance were closest to the Fe-Fe distance of the parameter model. In general, the second shell low-Z contribution did not model the total low-Z atom

contribution to the data at a given distance, nor did the Fe + C fits agree with the crystal structure data (with the exception noted above). The use, and the interpretation of results from the use, of $Fe(acac)_3$ (and therefore other metal$(acac)_3$ compounds) as a model of the single scattering Fe-C second shell contribution should be reexamined in light of the multiple scattering analysis discussed above.

4.4.2.2. The Hydroxylse Active Site. In the earlier studies of the hydroxylase active site, the 3.4 Å minimum was assigned as the Fe contribution and the 3.0 Å mimimum was assigned as the low-Z atom contribution due to the presence of clusters of low-Z atoms at ~ 3.0 Å in model compounds and a recognition that low-Z atoms located at more than 3.0 Å would not contribute strongly to the EXAFS due to the increased disorder of three-bond Fe-C distances (see Chapter 2). The fits to the second shell data with the various model compounds done for this work consistently resulted in a 3.0 Å minimum and a 3.4 Å minimum, supporting the interpretation that there are contributions to the second shell data at those distances, however it is not as easy to dismiss the 3.0 Å minimum as the iron contribution in light of the strong preference for that distance over the longer distance in fits using the $Fe_2(OR)_2$ model parameters.

The lack of evidence of an oxo-bridge in the diferric iron center was used as the basis for the choice of the hydroxo-bridged diferric model **FEHBPZOH** as the model of the Fe-Fe interaction for the hydroxylase data over the oxo-bridged model **FEHBPZO**. The choice of model compound based on the lack of the presence of an oxo-bridge in the MMO center is certainly a valid one, but it is not clear how to choose between two models with different bridging environments and Fe-Fe distances, but each of which lacks an oxo-bridge. Such a choice is represented by **FEHBPZOH** (tribridge, Fe-Fe 3.44 Å) and **FESALMP0** (dibridge, Fe-Fe 3.06 Å).[18] Based on the results of fits to the hydroxylase data with **FESALMP0** parameters, one would conclude that the Fe-Fe distance in the oxidized hydroxylase is 3.04 Å, but with **FEHBPZOH** parameters, the data suggest that the correct Fe-Fe distance is 3.42 Å.

If the diiron center in the hydroxylase were a dibridged center similar to that in the **FESALMP** model compounds, then it would be expected that in the diferrous form of the hydroxylase, the Fe-Fe distance would be on the order of 3.2 Å. For such a compact dinuclear iron site, it would be reasonable to expect to see the Fe-Fe interaction in the Fourier transform, similar to that which is seen in the diferrous **FESALMP2** data (Figure 4.5e). For the diferrous protein data, however, no Fe-Fe interaction is seen in the Fourier transform (see Figure 2.2 in Chapter 2) suggesting that the Fe-Fe distance in the diferrous form of the hydroxylase is longer than 3.2 Å. This in turn suggests that the Fe-Fe distance in the diferric form is longer than 3.0 Å, supporting the assignment of the 3.4 Å minimum

as the Fe contribution. Another possibility, however, is that the Fe distance in the hydroxylase is on the order of 3.0 Å and that upon reduction to the diferrous state, a major rearrangement in the bridging ligands occurs, resulting in an Fe-Fe distance in the diferrous state that is longer than what can be detected with EXAFS. Such a rearrangement may involve a shift in the coordinating mode of carboxylate groups ligating the iron center.[19]

Although the only known diferric model with a 3.4 Å Fe-Fe distance is the tribridged **FEHBPZOH**, the possibility that the hydroxylase is dibridged cannot be eliminated. While the dibridged **FESALMP** models exhibit different magnetic behaviour from the MMO hydroxylase (being ferromagnetic,[6b] whereas MMO is antiferromagnetic[2]) which eliminates them as models for the hydroxylase, the other dibridged models (**FECHEL, FEDIPIC, FEPIC**) are antiferromagnetically coupled. The only dibridged model with a 3.4 Å Fe-Fe distance is $[Fe_2O(TPA)_2PHT]$[11] which has a (μ-oxo)(μ-carboxylato) core (see footnote 14). Since it was possible to synthesize the hydroxo-bridged derivative of the (μ-oxo)bis(μ-carboxylato) model $[Fe_2O(OAc)_2(HB(pz)_3)_2]$,[6c] a model with a (μ-hydroxo)(μ-carboxylato) core may also be possible to synthesize which would have a longer Fe-Fe distance and should exhibit magnetic behaviour similar to that of the hydroxylase active site.

4.4.2.3. Survey of Other Second Shell Analysis Methods. A variety of other techniques have been used to determine the Fe-Fe distances in dinuclear iron centers. The ratio method has been used to determine the Fe-Fe distances in various forms of hemerythrin[13,20] in which the amplitude and phase parameters of structurally characterized models are compared the the amplitude and phase parameters of the unknown. The earlier results[20] determined with this method have been corrected[13] based on an evaluation of the model compounds employed, and a set of criteria have been described by the authors as the basis for determining the appropriate model to use in the determination of the correct Fe-Fe distance.[13] In the earlier work, the long Fe-Fe distances obtained for oxy- and methemerythrin (3.59 and 3.49 Å respectively) were obtained with the use of a 3.3 Å Fe-Fe model.[20a] Using data between 5 and 12 $Å^{-1}$ to eliminate low-Z atom interference, the early results were reevaluted using the tribridged oxo-bridged dimer **FEHBPZO** which is known based by comparison with the crystal structure to be very similar to the active site of hemerythrin.[21] A distance of 3.24 Å was obtained for oxyhemerythrin, in good agreement with the crystal structure (the Fe-Fe distance in the model is 3.14 Å, see Table 4.1).

The discrepancy between the earlier and later results was attributed to the dissimilarity of the bridging groups in the 3.3 Å Fe model to those in hemerythrin, as well as to the inclusion of low *k* data in the earlier analysis, which would have a strong

contributions from second shell low-Z scatterers.[22] Although the the use of the 3.14 Å model could be justified based on the known structure of the protein, there was an indication that the results of this analysis may also be model-dependent. The authors repeated the fits using the 3.30 Å Fe-Fe model and the new protocol and stated that the use of a 3.30 Å Fe-Fe model in fits to the protein data *resulted in consistently longer Fe-Fe distances* by about 0.2 Å than the results obtained by the use of the 3.14 Å Fe-Fe model.[13]

A second method employed in the determination of second shell Fe-Fe distances is the FABM (fine adjustment based on models) method which uses empirically adjusted theoretical parameters.[12,23] In this approach, fits to a model compound are done with the correct distance information and theoretical parameters, while adjusting both an amplitude reduction factor (A) and shell-specific energy shift (ΔE) during the fitting proceedure[12,23a] or just an amplitude factor.[23b,23c] These parameters are then used in non-linear least-squares fits to the data using the theoretical parameters and allowing the distance and coordination number (or Debye-Waller factor) to vary. Different values of A and ΔE were obtained in references 12 and 23a, so there is some dependence of these parameters on the model employed.[24] The dependence of the values of A and ΔE on the model compound, and the dependence of the results using the different A and ΔE sets has not been explored. Reliable Fe-Fe distances were obtained in tests on model compounds,[12,23a] but in some cases more than one Fe minima was found, similar to results reported here (see Table II in reference 12). It would be informative to explore the range of applicability and any limitations of this approach.

4.5. Conclusions

These studies have demonstrated the utility of the EXAFS technique in determining the average first shell coordination of iron atoms in non-heme dinuclear iron centers. The distances obtained with these fits for a variety of model compounds were accurate to within 0.03 Å and the total coordination number to within 10 %. The sensitivity of this technique to the presence or absence of a short μ-oxo bridge was once again demonstrated. The exact numbers of N and O atoms ligated to the iron center could not be directly determined. The average first shell distance as determined by EXAFS analysis was found to correlate with both the relative numbers of N and O atoms and the presence of an oxo-bridge in the iron center (for mixed N and O ligation).

The non-linear least-squares curve-fitting method using Fe-Fe parameters derived from model compounds has proven to be extremely model-dependent. The other techniques used for the analysis of second shell data also seem to be susceptible to model

dependence, although this has not yet been throughly tested. Unlike the conclusion reached from the ratio method of determining Fe-Fe distances,[13] these studies show that *the bias seen reflects the Fe-Fe distance of the model compound from which the parameters were obtained, and is independent of the number or nature of bridges in the diiron center except as those factors determine the Fe-Fe distance.* A strong correlation between the second shell Fe and C parameters was also observed for the di- and tribridged models tested, impacting both the coordination numbers and the distances of the Fe and C contributions. These results illustrate that care must be taken in the analysis and interpretation of the second shell data for dinuclear iron systems. Similar caution should be used in the interpretation of fits for other dimetallic systems as well.

The method employed in fits to the second shell dinuclear iron data assumes that the strongest contribution to the second shell EXAFS will be the single-scattering event between the two iron atoms, however multiple scattering contributions could be contributing as well. Multiple scattering pathways involving the Fe_2O core should not impact the second shell data of the models investigated here.[15] Rigid coordinating groups such as imidazole also have an effect on second shell data.[16] It has recently been discovered that for monomeric $Fe(acac)_3$, multiple scattering along the Fe-O-C path contibutes significantly to the second shell amplitude, suggesting that other pathways may be important. The pathways which contribute strongly to the second shell EXAFS need to be determined before the second shell data for dinuclear iron systems can be completely understood. An understanding of the multiple scattering contributions and the developement of a protocol for properly accounting for both the multiple and single scattering interactions will be an important step in the reliable application of the EXAFS technique to second shell data in dinuclear metalloprotein systems. Finally, with the emergence of the theoretical fitting codes FEFF[25] and GNXAS,[26] a systematic investigation of theoretical fitting approaches to the complicated systems discussed in this paper can be done and compared to the results obtained from the use of empirically derived amplitude and phase parameters presented here.

4.6. Acknowledgements

The data were collected at the Stanford Synchrotron Radiation Laboratory and the National Synchrotron Light Source, Brookhaven National Laboratory, which are supported by the Department of Energy, Office of Basic Energy Sciences, Division of Chemical Sciences and Division of Materials Sciences. SSRL is also supported by the National Institutes of Health, Biomedical Resource Technology Program, Division of Research

Resources (RR-01209) and the Department of Energy, Office of Health and Environmental Research. Grant support was provided by the National Science Foundation (CHE 91-21576 to KOH). The author wishes to thank Profs. Stephen Lippard and Richard Holm for providing model compounds.

4.7. References and Notes

1. Cramer, S. P. *X-Ray Absorption: Principles, Applications, Techniques of EXAFS, SEXAFS and XANES*; John Wiley and Sons, Inc.: New York, 1988; pp 257-320.

2. (a) DeWitt, J. G.; Bentsen, J. G.; Rosenzweig, A. C.; Hedman, B.; Green, J.; Pilkington, S.; Papaefthymiou, G. C.; Dalton, H. J.; Hodgson, K. O.; Lippard, S. J. *J. Am. Chem. Soc.* **1991**, *113*, 9219-9235. (b) Ericson, A.; Hedman, B.; Hodgson, K. O.; Green, J.; Dalton, H.; Bentsen, J. G.; Beer, R. H.; Lippard, S. J. *J. Am. Chem. Soc.* **1988**, *110*, 2330-2332.

3. Hedman, B.; Co, M. S.; Armstrong, W. H.; Hodgson, K. O.; Lippard, S. J. *Inorg. Chem.* **1986**, *25*, 3708-3711.

4. Vaarkamp, M.; Dring, I.; Oldman, R. J.; Stern, E. A.; Koningsberger, D. C. *Proc. XAFS VII*, Kobe, Japan; August 1992, in press.

5. Scott, R. A.; Eidsness, M. K. *Comments Inorg. Chem.* **1988**, *7*, 235-267.

6. (a) Thich, J. A.; Ou, C. C.; Powers, D.; Vasilou, B.; Mastropaolo, D.; Potenza, J. A.; Schugar, H. J. *J. Am. Chem. Soc.* **1976**, *98*, 1425-1433. (b) Snyder, B. S.; Patterson, G. S.; Abrahamson, A. J.; Holm, R. H. *J. Am. Chem. Soc.* **1989**, *111*, 5214-5223. (c) Tolman, W. B.; Bino, A.; Lippard, S. J. *J. Am. Chem. Soc.* **1989**, *111*, 8522-8523. (d) Armstrong, W. H.; Lippard, S. J. *J. Am. Chem. Soc.* **1984**, *106*, 4632-4633. (e) Armstrong, W. H.; Spool, A.; Papaefthymiou, G. C.; Frankel, R. B.; Lippard, S. J. *J. Am. Chem. Soc.* **1984**, *106*, 3653-3667. (f) Feng, X.; Bott, S. G.; Lippard, S. J. *J. Am. Chem. Soc.* **1989**, *111*, 8046-8047. (g) Armstrong, W. H.; Lippard, S. J. unpublished results (h) Iball, J.; Morgan, C. H. *Acta Cryst.* **1976**, *23*, 239-244. (i) Roof, Jr., R. B. *Acta Cryst.* **1956**, *9*, 781-786.

7. Scott, R. A.; Hahn, J. E.; Doniach, S. ; Freeman, H. C.; Hodgson, K. O. *J. Am. Chem. Soc.* **1982**, *104*, 5364-5369.

8. (a) Cramer, S. P.; Hodgson, K. O.; Stiefel, E. I.; Newton, W. E. *J. Am. Chem. Soc.* **1978**, *100*, 2748-2761. (b) Cramer, S. P.; Hodgson, K. O. *Prog. Inorg. Chem.* **1979**, *15*, 1-39. (c) Scott, R. A. *Methods Enzymol.* **1985**, *117*, 414-459.

9. Johansson, L. *Chem. Scr.* **1976**, *9*, 30-35. The crystal structure of the perchlorate salt has not been determined, but the $[Fe(phenanthroline)_3]^{2-}$ complex structure can be assumed to be identical with that of the corresponding iodide salt (Johansson, L.; Molund, M.; Oskarsson, Å. *Inorg. Chim. Acta* **1978**, *31*, 117-123).

10. Kurtz, D. M. Jr. *Chem. Rev.* **1990**, *90*, 585-606.

11. (a) Norman, R. E.; Yan, S.; Que, L. Jr.; Backes, G.; Ling, J.; Sanders-Loehr, J.; Zhang, J. H.; O'Connor, C. J. *J. Am. Chem. Soc.* **1990**, *112*, 1554-1562. (b) Norman, R. E.; Holz, R. C.; M'enage, S.; O'Connor, C. J.; Zhang, J. H.; Que, L. Jr. *Inorg. Chem.* **1990**, *29*, 4629-4637.

12. Scarrow, R. C.; Maroney, M. J.; Palmer, S. M.; Que, L. Jr.; Row, A. L.; Salowe, S. P.; Stubbe, J. *J. Am. Chem. Soc.* **1987**, *109*, 7857-7864.

13. Zhang, K.; Stern, E. A.; Ellis, F.; Sanders-Loehr, J.; Shiemke, A. *Biochemistry* **1988**, *27*, 7470-7479.

14. It should be noted that there is a series of dibridged (μ-oxo)(μ-carboxylato) model compounds which have Fe-Fe distances from 3.1 to 3.4 Å (ref. 11). These compounds were synthesized and EXAFS data were collected on them twice, however incorrect structural information resulted from fits to the data, so these models were not included in this study. Although the information to date strongly points to a bias based on distance rather than bridging atom type, the inclusion of the model with the 3.4 Å Fe-Fe distance would certainly complete the investigation.

15. Co, M. S.; Hendrickson, W. A.; Hodgson, K. O.; Doniach, S. *J. Am. Chem. Soc.* **1983**, *105*, 1144-1150.

16. (a) Co, M. S.; Scott, R. A.; Hodgson, K. O. *J. Am. Chem. Soc.* **1981**, *103*, 986-988. (b) Hasnain, S. S., Ed. *Synchrotron Radiation and Biophysics*; Ellis Horwood Ltd.; Chichester, 1990; Chapters 3 and 4.

17. Westre, T. E.; Di Cicco, A.; Filipponi, A.; Natoli, C. R.; Solomon, E. I.; Hedman, B.; Hodgson, K. O. to be submitted

18. **FECHEL** also meets the criterion of a lack of an oxo-bridge, but the difference in the relative intensites of the second shell peaks in **FECHEL** and **EXAFS5** and **EXAFS2** (see Figure 4.5) suggests that **FECHEL** will not model the amplitude correctly, which is supported by the fits to the hydroxylase data.

19. Rardin, R. L.; Tolman, W. B.; Lippard, S. J. *New J. Chem.* **1991**, *15*, 417-430.

20. (a) Elam, W. T.; Stern, E. A.; McCallum, J. D.; Sanders-Loehr, J. *J. Am. Chem. Soc.* **1982**, *104*, 6369-6373. (b) Elam, W. T.; Stern, E. A.; McCallum, J. D.; Sanders-Loehr, J. *J. Am.Chem. Soc.* **1983**, *105*, 1919-1923.

21. Stenkamp, R. E.; Sieker, L. C.; Jensen, L. H.; McCallum, J. D.; Sanders-Loehr, J. *Proc. Natl. Acad. Sci. USA* **1985**, *82*, 713-716.

22. The use of high *k* data may not eliminate the second shell low-Z atom contribution as the ability of groups of low-Z atoms to mimic a second shell metal contribution has been noted by us (ref. 2) and others (ref. 5).

23. (a) True, A. E.; Scarrow, R. C.; Holz, R. C.; Que, L. Jr. *Inorg. Biochem.* **1991**, *43*, 545 and personal communication. (b) Kauzlarich, S. M.; Teo, B. K.; Zirino, T.; Burman, S.; Davis, J. C.; Averill, B. A. *Inorg. Chem.* **1986**, *25*, 2781-2785. (c) Prince, R. C.; George, G. N.; Savas, J. C.; Cramer, S. P.; Patel, R. N. *Biochim. Biophys. Acta* **1988**, *952*, 220-229.

24. The values of A and ΔE were obtained by fitting the difference of the second shell data for **FEHBPZOH** and **FEHBPZO** in ref. 12. The model employed in determining the values of A and ΔE in ref. 23a was not discussed.

25. Mustre de Leon, J.; Rehr, J. J.; Zabinsky, S. I.; Albers, R. C. *Phys. Rev. B* **1991**, *44*, 4146.

26. Filipponi, A.; Di Cicco, A.; Tyson, T. A.; Natoli, C. R. *Solid State Comm.* **1991**, *78*, 265.